STRUCTURAL ANALYSIS OF MORPHING CONTROL SURFACES

A THESIS SUBMITTED TO
THE GRADUATE SCHOOL OF NATURAL AND APPLIED SCIENCES
OF
MIDDLE EAST TECHNICAL UNIVERSITY

BY

HARUN TIRAŞ

IN PARTIAL FULFILLMENT OF THE REQUIREMENTS
FOR
THE DEGREE OF MASTER OF SCIENCE
IN
AEROSPACE ENGINEERING

FEBRUARY 2017

Approval of the thesis:

STRUCTURAL ANALYSIS OF MORPHING CONTROL SURFACES

submitted by **HARUN TIRAŞ** in partial fulfillment of the requirements for the degree of **Master of Science in Aerospace Engineering Department, Middle East Technical University** by,

Prof. Dr. Gülbin Dural Ünver   _____
Dean, Graduate School of **Natural and Applied Sciences**

Prof. Dr. Ozan Tekinalp   _____
Head of Department, **Aerospace Engineering**

Prof. Dr. Yavuz Yaman   _____
Supervisor, **Aerospace Engineering Dept., METU**

Examining Committee Members:

Prof. Dr. Serkan Özgen   _____
Aerospace Engineering Dept., METU

Prof. Dr. Yavuz Yaman   _____
Aerospace Engineering Dept., METU

Assoc. Prof. Dr. Erdem Acar   _____
Mechanical Engineering Dept., TOBB-ETU

Asst. Prof. Dr. Ercan Gürses   _____
Aerospace Engineering Dept., METU

Asst. Prof. Dr. Gökhan Özgen   _____
Mechanical Engineering Dept., METU

Date: *03.02.2017*

I hereby declare that all the information in this document has been obtained and presented in accordance with academic rules and ethical conduct. I also declare that, as required by these rules and conduct, I have fully cited and referenced all material and results that are not original to this work.

Name, Last Name : Harun Tıraş

Signature   :

ABSTRACT

STRUCTURAL ANALYSIS OF MORPHING CONTROL SURFACES

Tıraş, Harun

M.S., Department of Aerospace Engineering

Supervisor : Prof. Dr. Yavuz Yaman

February 2017, 134 pages

In this thesis, design and analysis of a hybrid trailing edge control surface is performed. Only camber motion and twisting motion of the trailing edge control surface are considered. There are four control surface configurations that are analyzed. For the first configuration, servo actuators actuating the control surface are inside the control surface volume and control surface is without pre-twist. For the second case, the control surface is pre-twisted and actuators are inside the control surface volume. For the third case, servo actuators actuating the control surface are inside the torque box volume and control surface is without pre-twist. For the final case, the control surface is pre-twist but actuators are inside the torque box volume. The proper servo actuator selections for all of the configurations are done by considering the available volumes of the control surface volume and torque box volume. The downward deflection limits of the trailing edge control are determined for all of the configurations. The advantages and disadvantages of all configurations are explained. The CAD model of the control surface is created by using CATIA V5-6R2012 package software and finite element analyses are done by using ANSYS Workbench v14.0 package software.

ÖZ

BÜYÜK ORANDA ŞEKİL DEĞİŞTİREBİLEN KONTROL YÜZEYLERİNİN YAPISAL ANALİZİ

Tıraş, Harun

Yüksek Lisans, Havacılık ve Uzay Mühendisliği Bölümü

Tez Yöneticisi   : Prof. Dr. Yavuz Yaman

Şubat 2017, 134 sayfa

Bu tezde, hibrid firar kenarlı kontrol yüzeyinin tasarımı ve analizi gerçekleştirilmiştir. Firar kenarı kontrol yüzeyinin sadece kambur hareketi ve burulma hareketi incelenmiştir. Analiz edilen dört kontrol yüzeyi konfigürasyonu bulunmaktadır. İlk konfigürasyonda, kontrol yüzeyini hareket ettiren servo aktüatörleri kontrol yüzeyinin içinde bulunmaktadır ve kontrol yüzeyinde ön kambur bulunmamaktadır. İkinci konfigürasyonda ise, kontrol yüzeyi ön kamburludur ve servo aktüatörleri kontrol yüzeyinin içinde bulunmaktadır. Üçüncü konfigürasyonda ise kontrol yüzeyini hareket ettiren servo aktüatörler tork kutusunun içinde bulunmaktadır ve kontrol yüzeyi ön kambursuzdur. Son konfigürasyonda ise kontrol yüzeyi ön kambursuz olup, servo aktüatörler tork kutusunun içinde bulunmaktadır. Tüm konfigürasyonlarda, düzgün servo aktüatör seçimi, kontrol yüzeyi hacmi ve tork kutusu hacmi hesaba katılarak yapılmıştır. Tüm konfigürasyonlarda aşağı sapma limiti belirlenmiştir. Tüm konfigürasyonların avantajları ve dezavantajları açıklanmıştır. Kontrol yüzeyinin CAD modeli CATIA V5-6R2012 paket programı kullanılarak çizilmiştir ve sonlu elemanlar analizi ise ANSYS Workbench v14.0 paket programı kullanılarak yapılmıştır.

TABLE OF CONTENTS

LIST OF TABLES

LIST OF FIGURES

FIGURES

xv

LIST OF ABBREVIATIONS

CHANGE	Combined morphing assessment software using flight envelope data and mission based morphing wing prototype development
FEA	Finite Element Analysis
FEM	Finite Element Model
LaRC	Langley Research Center
L/D	Lift to Drag Ratio
METU	Middle East Technical University
NASA	National Aeronautics and Space Administration
TAI	Turkish Aerospace Industries
TUBİTAK	The Scientific and Technological Research Council of Turkey
UAV	Unmanned Aerial Vehicle

CHAPTER 1

INTRODUCTION

1.1 Objective of the Study

Generally, aircraft spend lots of their flight hours in a specific flight phase and conventional aircraft are designed for that specific flight phase. But other than that phase, their configuration is not the optimum one. By the help of the recent technologies in smart materials and advances in servo actuators and mechanisms, unconventional aircraft are getting more popular. These aircraft enable optimum performance at each of their missions. This can be done by changing the configuration of the aircraft at each of its flight phases. This configuration changing phenomenon is called as "morphing". Therefore, it decreases the fuel consumption rate and increase aircraft' flight envelope limit.

In this thesis, a new concept morphing hybrid trailing edge control surface mechanism is introduced. This control surface is a hingeless trailing edge mechanism connected to the wing which enables the air flows around it smoothly. The camber motion of this mechanism is investigated.

The study was conducted within the scope of the CHANGE Project (**C**ombined morp**H**ing **A**ssessment software usi**NG** flight **E**nvelope data and mission based morphing prototype wing development) which is a project of 7th Framework Programme of European Commission.

1.2 Layout of Thesis

In chapter 1, the topic is introduced. The objective of the study is explained. The differences between the conventional and unconventional aircraft are mentioned. The layout and limitations of the study is clarified.

In chapter 2, literature review is done. History of the morphing concept is explained. Several aircraft that have the morphing capability are presented. Then, the types of the morphing aircraft are introduced with examples.

In chapter 3, the interior design of the hybrid trailing edge control surface is explained. The baseline and target airfoil NACA profiles are mentioned. The dimensions of the control surface are shown. The parts of the control surface are introduced and also the used materials and their properties are presented. Finally, servo actuator selection procedures and selected servo actuators are given.

In chapter 4, the finite element modeling of the hybrid trailing edge control surface is explained. First of all, structural parts of the finite element model are presented. Then, the connection types between the structures are defined. After that, the meshing procedure is applied. The convergence study for meshing is performed in order to select the optimum mesh size. Then, proper boundary conditions and loading are applied. Finally, the analysis type is selected.

In chapter 5, structural analyses of the hybrid trailing edge control surface with the actuators inside the control surface volume in in-vacuo condition are performed. The camber motion of the control surface is examined. After proving the control surface is capable of morphing from NACA 6510 to NACA 9510 profile, the limits of downward deflection is searched.

In chapter 6, structural analyses of the hybrid trailing edge control surface with the actuators inside the torque box volume in in-vacuo condition are performed. The camber motions of this configuration are examined. The limits of the camber motion are searched.

In chapter 7, the conclusion part is given. Some general conclusions are made and recommendations for the future studies are listed.

1.3 Limitations of the Thesis

The limitations of the thesis are listed below

- Only camber motion of the hybrid trailing edge control surface is considered.
- Structural analyses are performed in in-vacuo condition only.
- Battery selection and cabling are not considered.
- Inertial loads due to maneuvers are not considered.
- The design of the connectors (bolts, nuts or glue strength) is not considered.

CHAPTER 2

LITERATURE REVIEW

2.1 Introduction

The innovations of the energy-saving economy in the aircraft industry lead to a new concept: morphing wing technology which can be defined as changing the wing shape to achieve better performance. However, it is researched by not only the private aircraft industry but also military/government institutions since this technology allows the aircraft to perform different missions or flight phases more efficiently in terms of aerodynamic performance. The morphing of the wings changes the design characteristics (e.g. span, chord, thickness, wetted area and aspect ratio) of the aircraft. As a result, an aircraft which has the ability of morphing its wings could perform many different missions including loiter, reconnaissance, attack more efficiently etc. instead of a group of aircraft that each one is specialized in one of these missions.

Implementing the morphing concept has some disadvantages such as increasing cost, complexity and weight of the added actuator system. But by the help of the recent developments in smart materials [1] and developments in actuators, these effects can be decreases or eliminated.

The utilization of morphing concept is getting popular. There are many recent studies use this concept in order to improve aircrafts' performance. The research project "Aeroservoelastic Analysis of the Effects of Camber and Twist on Tactical UAV Mission-adaptive Wings", supported by Turkish Scientific and Technological Research Council through TUBITAK/107M103 Programme, was successfully completed. In this project, the camber and twist of a mission-adaptive UAV wing is controlled by a guiding slide mechanism and a servo actuators [2]. The control

surfaces of the morphing concept are designed as open trailing edge surface in order to eliminate high skin stresses [3], [4]. The conceptual design of the mechanism is shown in Figure 1 and the placement of the morphing mechanism on the wing structure is shown in Figure 2 [5].
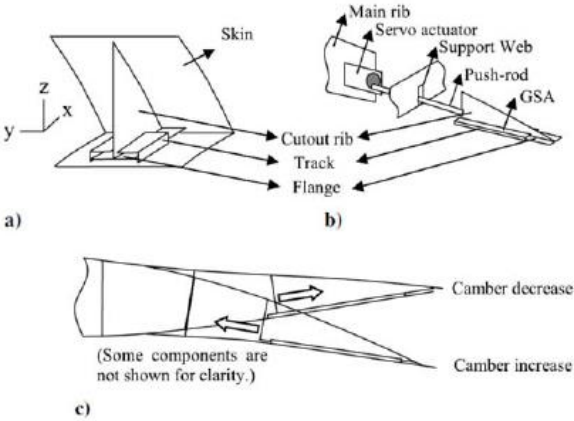
Figure 1: The Adaptive Camber Concept Developed by METU Researchers [5]
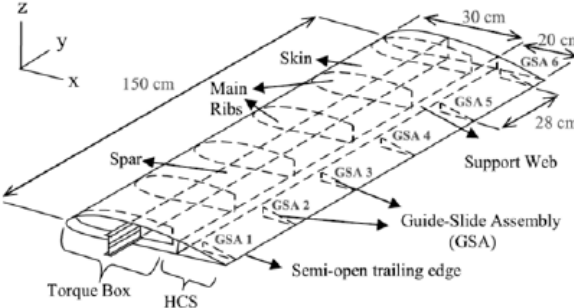
Figure 2: Placement of the Adaptive Camber Guide-Slide Assembly on the Trailing Edge of the Wing Structure [5]

Another research project is the CHANGE Project "**C**ombined Morp**H**ing **A**ssessment Software Usi**NG** Flight **E**nvelope Data and Mission Based Morphing Prototype Wing Development" supported by the European Community's Seventh Framework Programme (FP7). The main aim of the project is to design and

manufacture an UAV wing that integrates up to four different morphing mechanisms into a single wing and demonstrate the ability of this wing to fly [6].

Aerodynamic optimization of morphing wings under performance and geometric constraints are studied in the Ph. D. thesis of Körpe [7]. 3-D panel method and 2-D boundary layer solver are developed to perform aerodynamic optimization and lift and drag values are obtained. The results show that remarkable drag reductions were occurred as expected in the case of a morphing wing. However, planform morphing drag reductions are significantly higher than the airfoil shape morphing.

The determination of optimum number of servo actuators in a morphing control surface is studied by Arslan. et. al. [8]. They used total of six servo actuators initially then performed an optimization study in order to reduce the servo actuators which leads to weight reduction.

The effect of locations of the servo actuators on the control surface performance is examined by Arslan. et. al. [9]. They use three configurations, each of which has different number of servo actuators and different locations of servo actuators. They compare the results by considering the weight and torque requirements of servo actuators.

The investigation of morphing performance by comparing the target morphing profile and reached morphing profile is studied by Arslan. et. al. [10]. In this study, they aimed to morph a hybrid trailing edge control surface from NACA 6510 profile to NACA 2510, NACA 3510 and NACA 8510 profile. Then they compare the morphed control surface how close it is to the target NACA profiles.

The effects of different compliant materials on the morphing performance are examined by Yaman. et. al. [11]. In this study, they performed parametric study. Different number of servo actuators, various geometrical shapes and different types of materials are used and the optimum configuration is selected by considering all of the parameters mentioned above.

Structural meshing of the morphing geometry in the finite element analysis is studied by Yaman. et. al. [11]. In this study, they use different size of meshing

elements. Then they compare the results for these mesh sizes and select the optimum mesh size by considering also analysis time.

The implementation of morphing concept is not limited to the main wing. Oktay. et. al. [12] try to increase the flight performance of an UAV by using active morphing on both main wing and horizontal wing of the aircraft. For this purposes, optimum values of the UAV and its autopilot parameters are determined by using stochastic optimization. The designed UAV has the ability of wing extension and horizontal tail extension as shown in Figure 3.
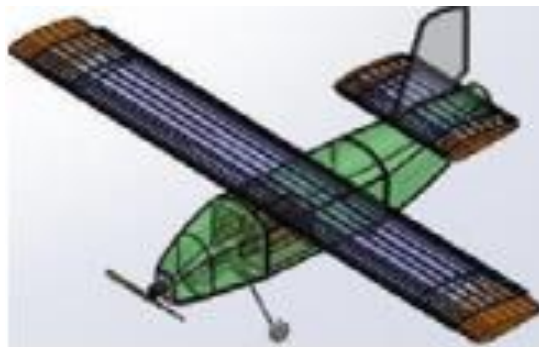
Figure 3: Main Wing Extension and Horizontal Wing Extension of the
Designed UAV

2.2 History of the Morphing Wings

The nature inspires many engineering ideas and concepts. By implementing these inspirations in the field of technology and applying reverse engineering, humans have found answers for many problems since mankind has existed.

Since the sources of inspiration of aircraft are birds, aircraft should look more like birds in order to have more efficient aerodynamic performance. To do so by applying biomimetic approaches in aviation, morphing concept is raised.

Although the morphing technologies are rather a new research area in aerospace, the morphing concept in airplanes dates back to 1903 when the Wright Brothers first flied a powered heavier than air flying machine. A technique called

wing warping was used to twist the wingtips of the flexible wings by using pulleys and cables [13]. In Figure 4, a diagram of the wing warping technique which was used for the lateral (roll) control for a fixed wing aircraft is shown.
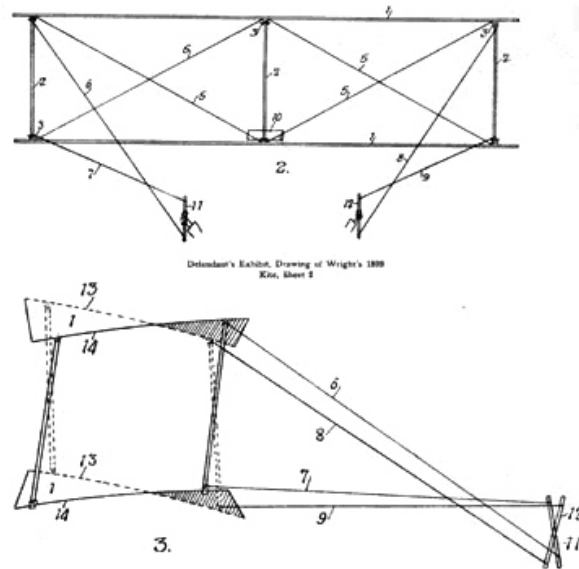
Figure 4: Diagram of the Wright Brothers' 1899 Kite [14].

Morphing aircraft are also called as variable geometry or polymorphous aircraft [15]. There are historically many landmarks on the evolution of this subject.

In July1915, Edson Fessenden Gallaudet, a pioneer in the field of aviation, was granted a patent for a "variable skewed" wing. An improved wing construction and control mechanism were invented for this wing. The operator of the aircraft could control the angular position of the wings as a whole, adapt them to changing conditions, particularly speed changes, and warp the wings by varying the angular position between the inner and outer portions of the wing to provide lateral stability [16].

In 1931, Geoffrey T. R. Hill developed Pterodactyl IV, whose wings have variable sweep properties in a small range of angles in order to provide longitudinal trim in flight in the absence of any horizontal stabilizer [17] as shown in Figure 5.

Figure 5: Westland Pterodactyl IV Variable Sweep Wing [17]

In 1931, Ivan Makhonine, an expatriate aircraft designer from the Soviet Union, designed and flew a variable geometry research aircraft named as the telescoping wing Makhonine MAK-10 in France. The innovation in MAK-10 was a telescopic wing which increased the wing span by 8 m (26 ft 3 in) from passing the high speed configuration to take-off condition and vice versa [18]. The retracted and extended versions of the Mak-10 aircraft are shown in Figure 6 and Figure 7.

Figure 6: Mak-10 with Wings almost completely Retracted [18]

Figure 7: Mak-10 with Wings completely Extended [18]

In November 1940, Nikitin – Shevchenko from USSR, designed and manufactured the IS-1 which was a polymorphic fighter that is, it could morph from monoplane to biplane configuration and vice versa in the air shown in Figure 8.

Figure 8: IS-1 Fighter

In 1964, North American XB-70 Supersonic Bomber was developed and rolled out for the United States Air Force Strategic Air Command [19]. Three dimensional wing morphing was used in that design as shown in Figure 9 and Figure 10.

Figure 9: XB-70 Supersonic Bomber with Extended Wingtips [19]

Figure 10: XB-70 Supersonic Bomber with Folding Wingtips [18]

In December 1964, General Dynamics developed and flew F-111 Aardvark supersonic, all-weather attack aircraft. F-111 had variable geometry wings and its wing sweep varied between 16 to 72.5 degrees shown in Figure 11.
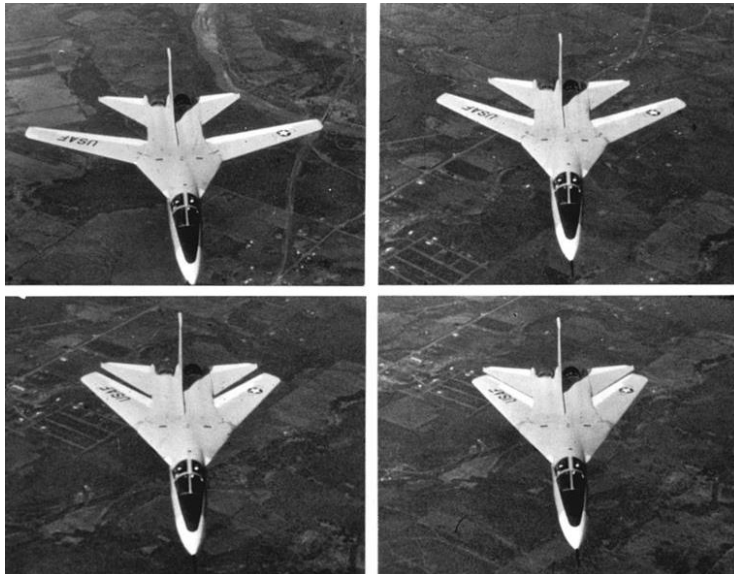
Figure 11: Four Photo Series Showing the F-111A Wing Sweep Sequence [20]

In 1975, German FS-29 Glider was built and flew by using the telescopic variable span wing to improve soaring performance. With full extension wings and

with fully retracted wings, FS-29 had both good soaring/slow speed and good cruising/high-speed features. The retracted and fully extended view of the FS-29 is shown in Figure 12.
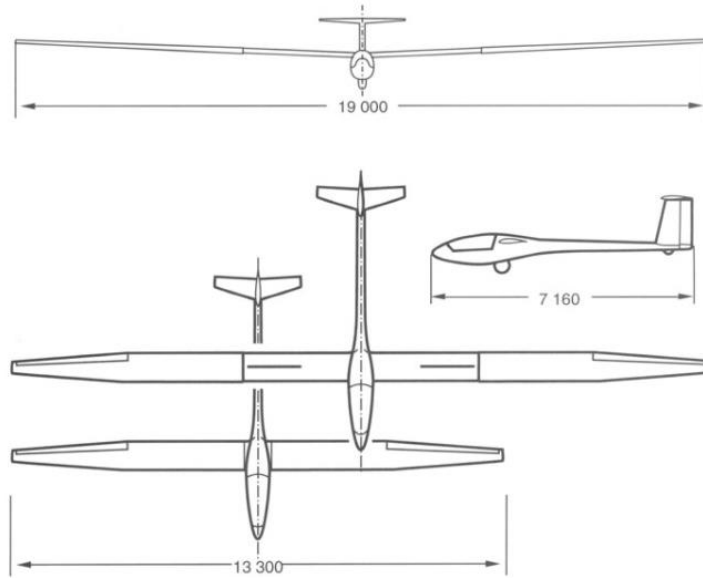
Figure 12: FS-29 Glider Planform Geometry

The morphing aircraft concept was revived at NASA/LaRC in the mid 1990's and continues today as part of NASA's Breakthrough Vehicle Technologies Project [18].

Brief photographic review of representative vehicles with shape changing wings are shown in Table 1, Table 2, Table 3 and Table 4 [19].

Table 1: Historical Examples of Vehicles with Shape Changing Wings –
Experimental Manned Aircraft [19]

Year/Ref	Organization/Vehicle	Shape Change Description	Photo
1903	Wright Flier	Twist Angle	
1951	Bell-X5	Sweep Angle	
1964	North American Aviation XB-70	Wing Span	
1984	Grumman X-29	Passive Bend-Twist Angle	
1986	AFTI F-111 MAW	Camber, Sweep Angle	
2002	Boeing X-53 AAW	Wing Twist Angle	

Table 2: Historical Examples of Vehicles with Shape Changing Wings -
Production Manned Aircraft [19]

Year/Ref	Organization/Vehicle	Shape Change Description	Photo
1955	Vought F8U Crusader	Wing Incidence Angle	
1964	General Dynamics F-111	Sweep Angle	
1970	Grumman F-14	Sweep Angle	
1974	Rockwell/Boeing B-1	Sweep Angle	

Table 3: Historical Examples of Vehicles with Shape Changing Wings -
Production Unmanned Air Vehicles [19]

Year/Ref	Organization/Vehicle	Shape Change Description	Photo
2010	Prioria Maveric	Passive Twist Angle	

Table 4: Historical Examples of Vehicles with Shape Changing Wings -
Experimental Unmanned Air Vehicles [19]

Year/Ref	Organization/Vehicle	Shape Change Description	Photo
1983	NASA HİMAT	Camber, Aeroelastic Tailoring	
2001	NASA I2000	Inflatable-Wing Span/Area	
2002	NextGen MFX-2	Sliding Skin Span/Wing Area	
2002	Lockheed Martin Agile Hunter	Folding Wing Span/Area	
2002	Raytheon UAV	Wing Span/Area	
2003	Virginia Tech Betamax	Wing Span/Area	
2003	Aerovisions Droid	Wing Span/Area	
2006	University of Florida Urban Stunt Plane	Wing Dihedral/Twist Angle	
2007	University of Florida Ebony Thunder	Wing Sweep/Twist Angle	
2008	Wageningen University Roboswift	Wing Sweep Angle	
2010	Aerovironment Nano Air Vehicle	Flapping Dihedral Angle	

2.3 Types of Morphing Wings

According to [21], morphing concept can be divided into three. These are the planform alteration, out-of-plane transformation and airfoil adjustment. The organization of the morphing types can be seen in Figure 13.
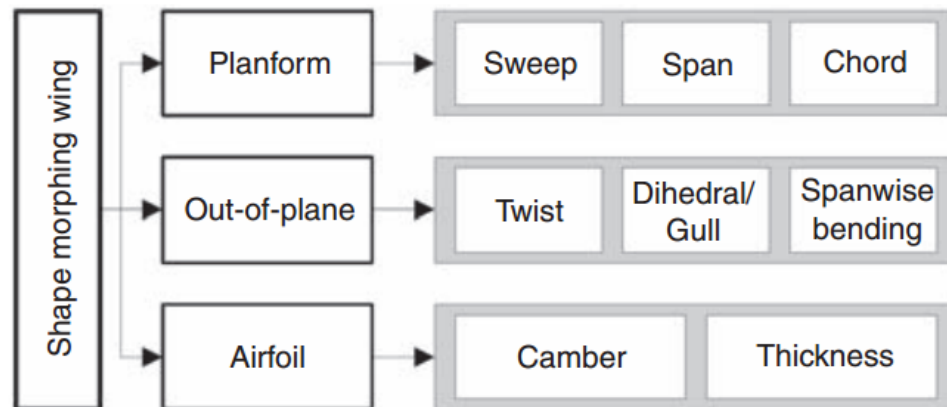
Figure 13: Types of Morphing

Sweep morphing: This type of morphing is used by many of the military aircraft such as Mig-23, Tornado, Su-22 etc. [21]. It enables the aircraft to shorten the take-off distance, increase load carry capability and attain low drag at high speed.

Span morphing: High aspect ratio aircraft are suitable for long range, loiter mission but their maneuver behavior is not good. On the other hand, low aspect ratio aircraft are faster than the high aspect ratio aircraft, and they are more maneuverable than the high aspect ratio counterpart. But they lack aerodynamic efficiency [22]. Span morphing concept allows one aircraft to have both high and low aspect ratio capability.

Chord morphing: This morphing type is used extensively in helicopter industry. It increases the lift of the air vehicle significantly. Khoshlahjeh et al. examined this type of morphing on a helicopter blade [23]. They increase the chord length of the airfoil %20 and they observe that using such a morphing mechanism

enables helicopter to increase in gross weight capability up to 1200 [lb] and reduction of power required up to 15.3 %.

Twist morphing: This type of morphing is used to increase the roll performance of the aircraft. Miller tested this type of morphing and observed that using twist morphing enables aircraft to roll at a dynamic pressure whereas at the same dynamic pressure, control surface reversal is obtained in conventional case [24].

Dihedral/gull morphing: This type of morphing is used in order to increase the performance and enhance flight characteristics of the aircraft. Shelton et. al. use this type of morphing on their UAV and observe that low speed performance of the aircraft is increased and the range, endurance and maneuverability of the aircraft is also increased [25].

Span-wise bending: Sofla et al. uses this concept in a UAV and observes the power consumption rate of that UAV [26]. The results indicate benefits of this type of morphing.

Camber morphing: The main purpose of this type morphing is to change the airfoil profile and increase the L/D ratio [27].

Thickness morphing: This type of morphing is used in order to reduce the drag of the aircraft. Gano and Renaud developed an UAV which can increase its efficiency by changing its airfoil thickness [28].

CHAPTER 3

INTERIOR DESIGN OF THE HYBRID TRAILING EDGE CONTROL SURFACE

3.1 Introduction

In this chapter, the interior design of hybrid trailing edge control surface is explained. First of all, the airfoil profile of the hybrid trailing edge control surface is mentioned. Then, dimensions of the control surface are shown. After that, the control surface parts are introduced. The material properties of each control surface parts are also given in that sub-section. Later, the selected servo actuators are presented. Finally, discussion and conclusion parts are given.

3.2 Control Surface Profile

For the CHANGE Project, the unconventional wing has been optimized for each of its flight phases. Therefore, the wing changes its airfoil profile in order to get the optimum shape for each of its flight phases. For landing and loiter mission, the optimum airfoil shape is determined as NACA 6510 profile. For take-off mission, the optimum airfoil shape is determined as NACA 3510 profile. And for high speed dash mission, the optimum airfoil profile is determined as NACA 2510 profile. All of the three NACA profiles used in CHANGE project are drawn on top of each other and shown in Figure 14.
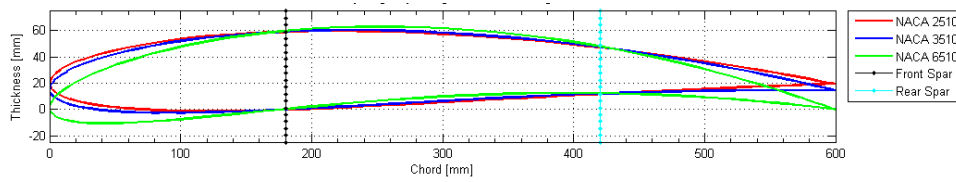
Figure 14: CHANGE Morphing NACA Profiles

Since the designed UAV spends most of its flight hour during the loiter mission, the baseline airfoil profile of the unconventional wing is decided as the NACA 6510 profile, which is suitable one for loiter mission Therefore, in the analyses, the undeformed airfoil shape is taken as NACA 6510 profile and other profiles are tried to be achieved by applying loading to NACA 6510 profile. Although the hybrid trailing edge control surface is capable of both cambering and decambering [29], only the camber capability of the trailing edge control surface of the wing from its baseline NACA profile is examined in this thesis.

In any emergency condition, the designed UAV may need extra lift and this can be achieved by deflecting its control surface beyond NACA 6510 airfoil profile. The primary aim of this thesis is to examine the downward deflection limits of the hybrid trailing edge control surface beyond NACA 6510 airfoil profile. Therefore, the downward deflection capability of the airfoil profile from NACA 6510 to NACA 9510 is tested. If the control surface is capable of morphing to this value, further deflection of the control surface will also be studied. Since the NACA 9510 airfoil profile is the end of NACA 4 digit series, further downward deflection will be studied in terms of tip downward displacement only. The schematic representation of further deflection of the control surface is shown in Figure 15.
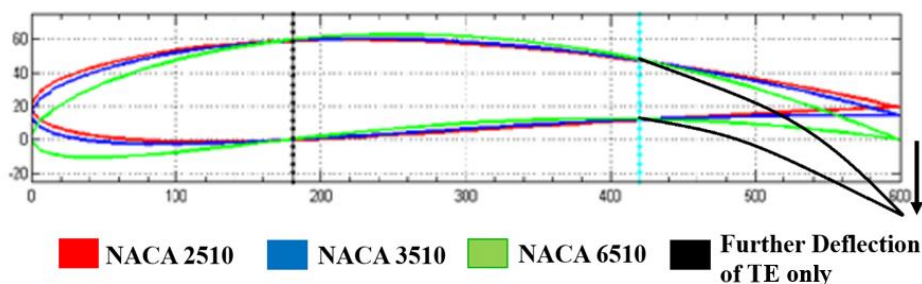
Figure 15: Deflection Limits of the Control Surface

20

3.3 Dimensions of the Control Surface

There are basically four types of wing configurations used in this thesis. These are:

- Control surface without pre-twist configuration and having the actuators inside the control surface volume, called as Design 1
- Control surface with pre-twist configuration and having the actuators inside the control surface volume, called as Design 2
- Control surface without pre-twist configuration and having the actuators inside the torque box volume, called as Design 3
- Control surface with pre-twist configuration and having the actuators inside the torque box volume, called as Design 4

The full assemblies of these configurations are shown in Figure 16, Figure 17, Figure 18 and Figure 19 respectively.
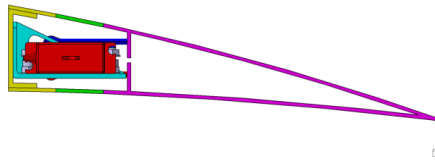
Figure 16: Design 1
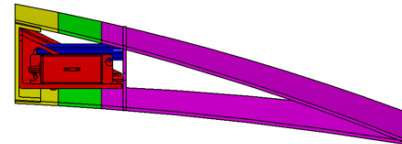
Figure 17: Design 2

Figure 18: Design 3
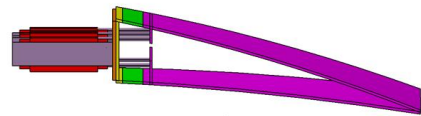
Figure 19: Design 4

The interior designs of these configurations are similar to each other. So the interior design chapter is explained based on Design 1. But, the differences between the control surface configurations are also specified.

The location of the hybrid trailing edge control surface on the wing and dimensions are given in Figure 20, Figure 21 and Figure 22. In Figure 20, the baseline wing and trailing edge control surface are shown. The baseline wing has a NACA 6510 profile along its span. The span of the wing is 2000 [mm]. The trailing edge control surface starts at 100 [mm] from the root of the wing. Also 5 [mm] clearance is left from inboard and outboard of the hybrid trailing edge control surface shown in Figure 21.
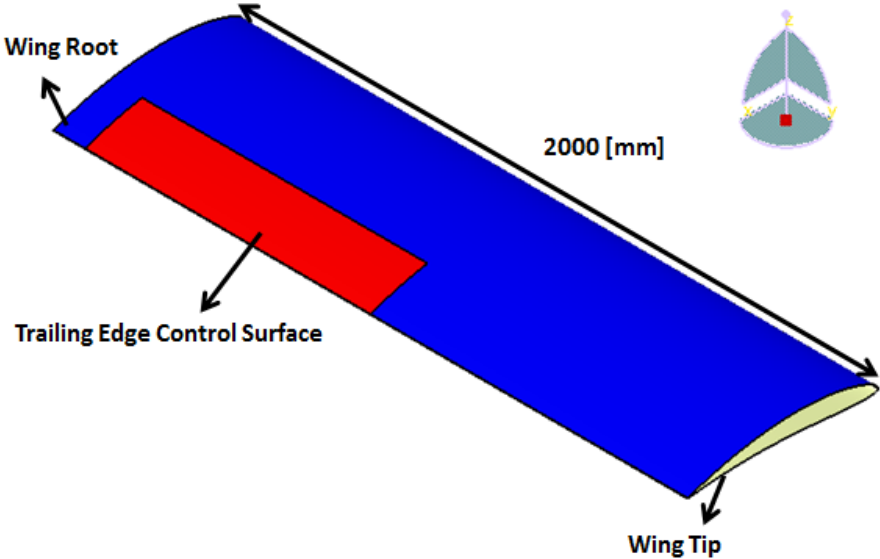
Figure 20: Baseline Wing with Trailing Edge Control Surface
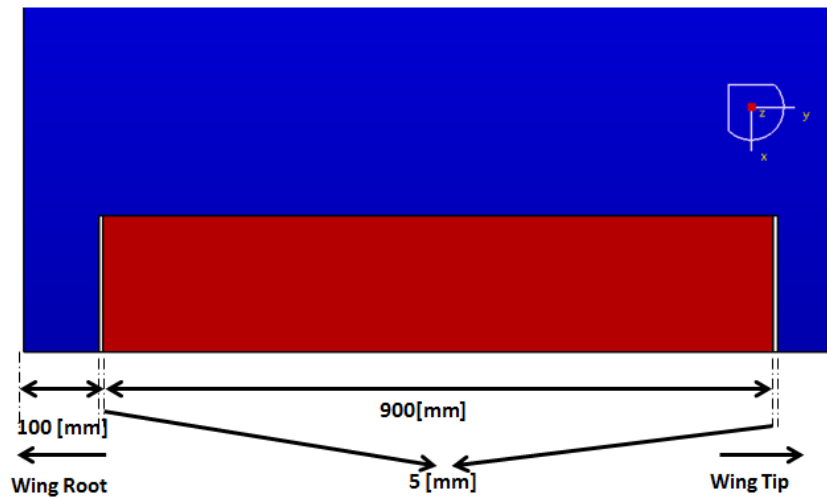
Figure 21: Dimension of the Control Surface – Top View

The length of hybrid trailing edge control surface in chord-wise direction is 180 [mm] which is 30% chord of the wing shown in Figure 22.
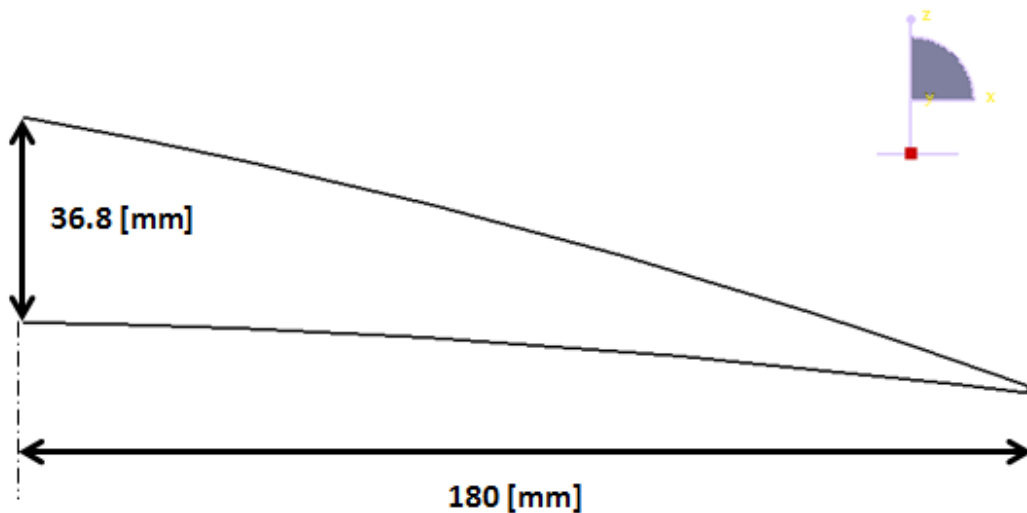
Figure 22: Dimensions of the Control Surface without Pre-Twist – Side View

For the pre-twisted configuration, it has a pre-twist of approximately 5 [deg] along its span and incidence angle of 1.9 [deg] at the root. All the other dimensions are same with the configuration explained above. The side view of the pre-twisted configuration is shown in Figure 23.
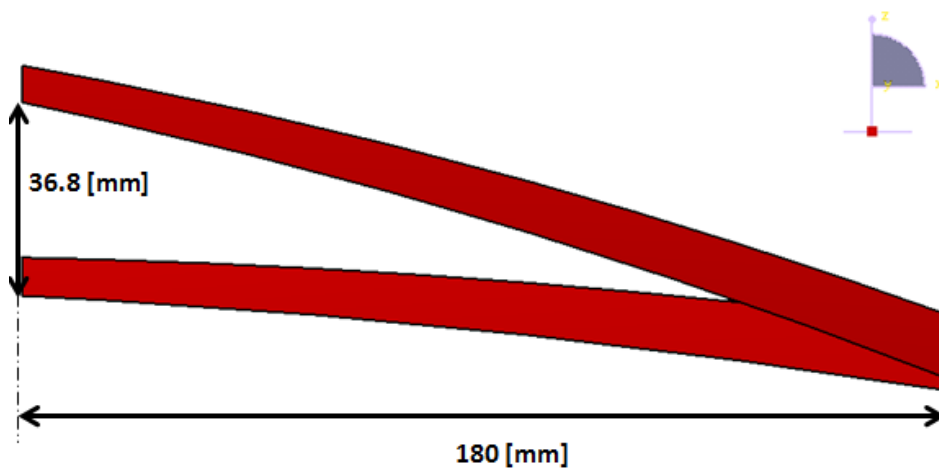
Figure 23: Dimensions of the Control Surface with Pre-Twist – Side View

3.4 Parts of the Control Surface

The designed hybrid trailing edge control surface is an unconventional type such that there is no hinge between the control surface and the wing. Instead, the control surface is directly connected to the wing with no gap. This results in reduction of aerodynamic noise and increase in the aerodynamic performance of the aircraft [30].

The interior design of the hybrid trailing edge control surface consists of three parts which are shown in Figure 24.
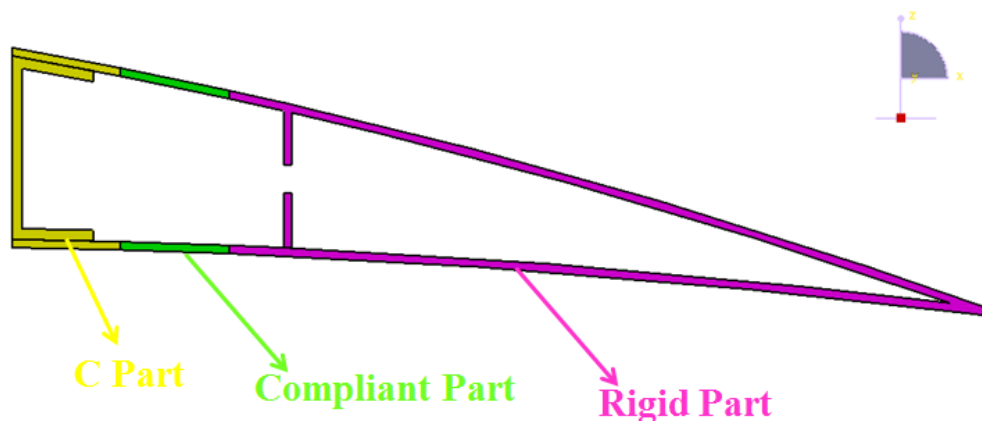
Figure 24: Parts of the Hybrid Trailing Edge Control Surface

24

3.4.1 C Part

C part consists of two parts. These are the interior c-bar section and outer skin section. Both sections are made of aluminum alloy. The properties of the material are given in Table 5.

Table 5: The Properties of Aluminum Alloy

Density	2770 [kg/m3]
Young's Modulus	71 [GPa]
Poisson Ratio	0.33
Tensile Yield Strength	280 [MPa]
Tensile Ultimate Strength	310 [MPa]

Interior c-bar section is used for connecting the control surface to the wing rear spar. It is connected to the rear spar with bolts and nuts.

The outer skin of the C part is connected to the interior c-bar section with bolts and nuts. For maintenance purposes, one must remove the outer skin of the C part and can reach the interior structures. The allowable maintenance space of the control surface is given in Figure 25.
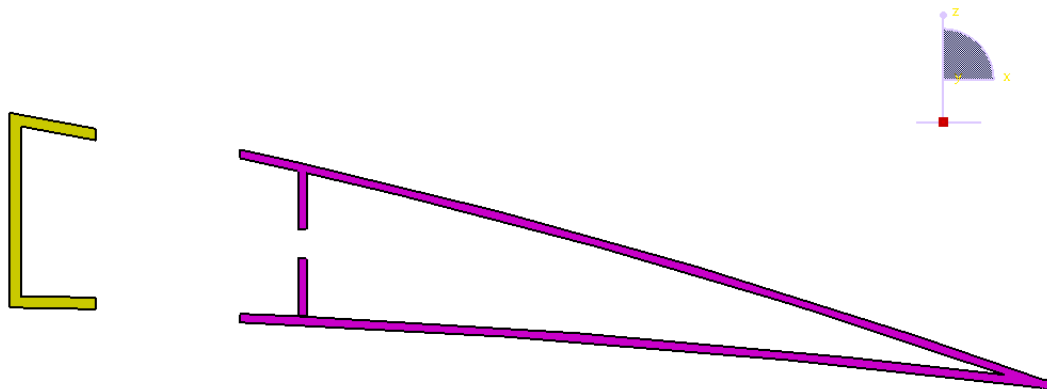
Figure 25: Side View of the Trailing Edge Control Surface with Allowable Maintenance Space

Assembling/disassembling of the control surface from the wing can be achieved again by removing the outer skin of the C part first and then unscrewing the bolts-nuts of interior c-bar section.

3.4.2 Compliant Part

Compliant part is the material between C part and Rigid part. It is rubber like soft material and it can withstand large strains. Since it is very soft material, it must always be in tension during the analyses. For the downward deflection of the control surface, the compliant material at the lower surface may tend to be in compression easily. The designer must be aware of this. Otherwise there may be undesirable hump on it which can disrupt the flow around it.

For the analyses, Neoprene Rubber is used as compliant material. The properties of the material are taken from ANSYS Workbench v14.0 package software material library except for the density of the material. The properties taken from ANSYS are given in Figure 26.
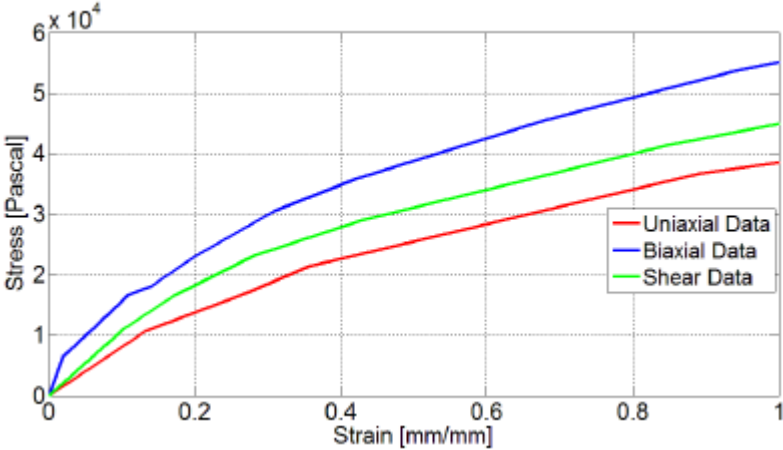
Figure 26: Neoprene Rubber Experimental Test Data

Density of the Neoprene Rubber is taken as 1250 [kg/m**3] [31]

26

3.4.3 Rigid Part

This component of the control surface is named as "Rigid Part" because this part is exposed to very low deformations when compared to the compliant part. Instead, significant amount of rigid body motion is observed for this part. The vertical components of rigid part are called as transmission part and shown in Figure 27.
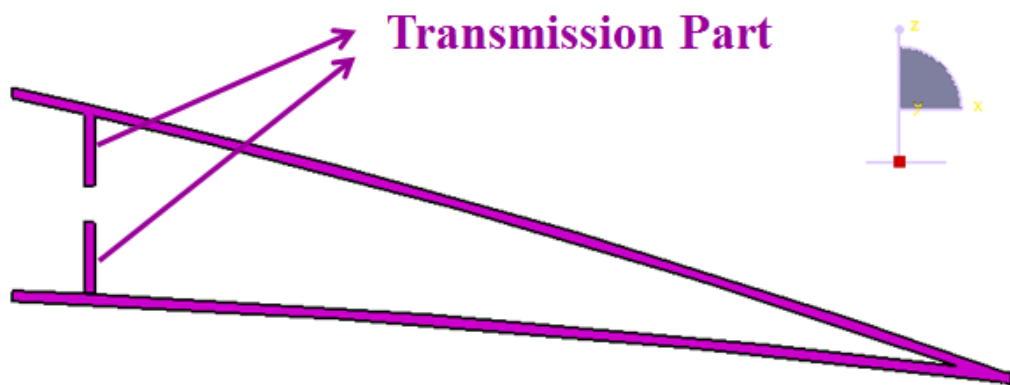
Figure 27: Side View of Rigid Part

Transmission parts are used to transmit the loads come from the servo actuators to the rigid part.

The rigid part is called as open cell type. In other words, there is a gap between the lower and upper transmission parts. So there are two load paths in the model. One of which uses the upper transmission part and the other uses the lower transmission part.

The material of the rigid part is taken as aluminum. This makes the production of the rigid part easier when compared to using composite materials. But some weight increment is expected since composite materials can be used here and composite's densities are less than the aluminum used [29].

The CAD model of the Design 2 is shown in Figure 28. The difference between this configuration and Design 1 is only the pre-twist property. Other than the pre-twist, all the structures and their dimensions are the same.
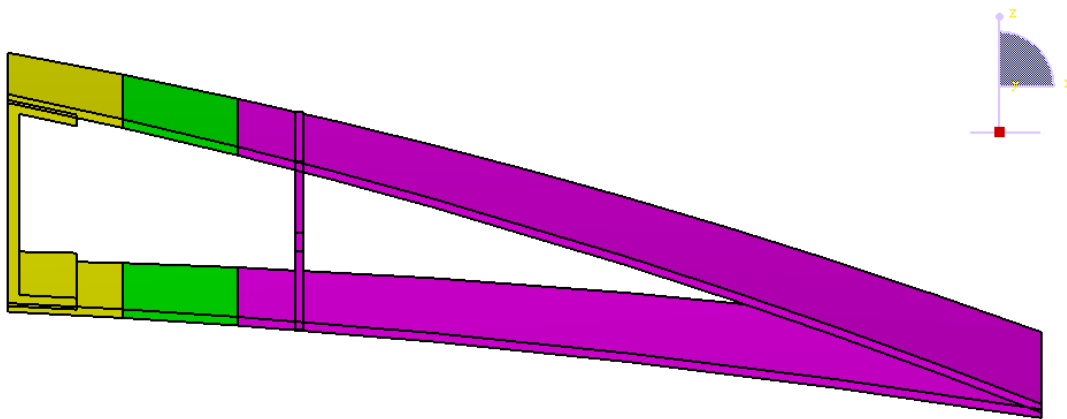
Figure 28: Control Surface with Pre-Twist Configuration, Actuators are inside the Control Surface Volume

When the servo actuators are put inside the torque box volume (Design 3 and Design 4), the length of the c bar and the length of the compliant part are shortened. Also the transmission parts are closer to the rear spar. These modifications are done in order to reduce the length of the transmission rods (explained in section 3.5). The CAD model of the Design 3 and Design 4 are shown in Figure 29 and Figure 30.

The difference between Design 3 and Design 4 is only the pre-twist property. Other than the pre-twist, all the structures and their dimensions are the same.
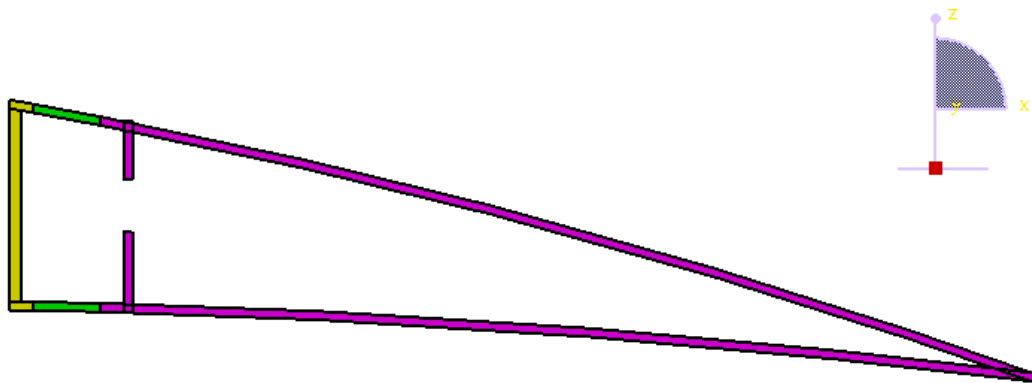
Figure 29: Control Surface without Pre-Twist Configuration, Actuators are inside the Torque Box Volume
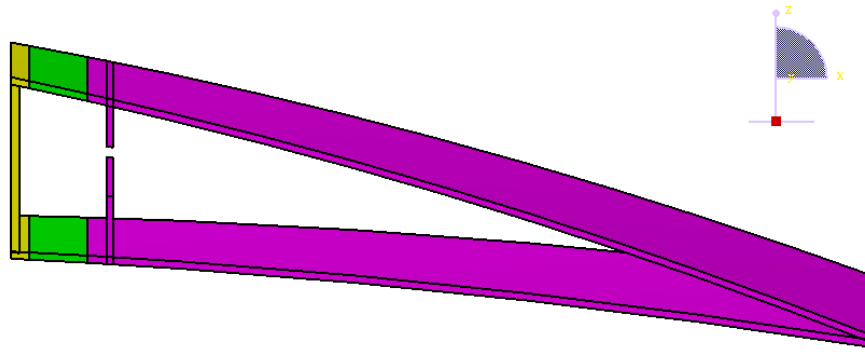
Figure 30: Control Surface with Pre-Twist Configuration, Actuators are
inside the Torque Box Volume

3.5 Servo Actuators

The motion of unconventional control surface is accomplished by using servo actuators. When the servo actuators are excited, their motion is transferred to the moment arm, actuator rod and finally to the transmission parts. Then the rigid part starts to do rigid body motion. This rigid body motion results in the compliant part to elongate. Finally, the control surface takes the desired shape. Since the upper and lower compliant materials must be in tension, at least one servo actuator is needed for each of the upper and lower surfaces. They can prevent or reduce compression of the compliant material. The desired motion of the control surface is obtained by using the differential displacement of upper and lower surface of the control surface. If the upper surface of the control surface extents more than the lower surface, the overall displacement is in downward direction. Similarly if the lower surface of the control surface extents more, then, an upward motion is observed. Since only the downward motion is considered in this thesis, more servo actuators are needed for the upper surface when compared the lower surfaces.

According to Tunçöz [29], if only the downward motion of the control surface is examined, the servo actuator configuration consisting of three actuators actuating the upper surface of the control surface and two actuators to actuate the lower surface of the control surface is the optimum servo configuration in terms of

lower reaction torques of the servo actuators and lower beam stress values of the moment arm and actuator rods. Since the scope of this thesis is only the downward deflection of the hybrid trailing edge control surface, Tunçöz's [29] suggestion is used.

Because of the geometrical shape of the airfoil used, the torque box volume is greater than the control surface volume. Therefore one can fit bigger servo actuators (stronger servo actuators) inside the torque box volume when compared to control surface volume. This results in higher camber deflection of the control surface. But if the torque box volume is planned to be occupied by other structures such as the telescoping wing rails etc., one can be forced to use the control surface volume for the home of servo actuators which reduces the size and torque capability of the servo actuators. In this thesis, servo actuators are placed both inside the torque box and inside the control surface volume.

When the actuators are placed in the control surface volume, they are connected to the C bar by using suitable fasteners. The configuration of servo actuators used in the control surface volume is shown in Figure 31. The span-wise orientations of servo actuators are also shown in Figure 31. These span-wise locations are also optimum locations for the downward deflection of the control surface [29].
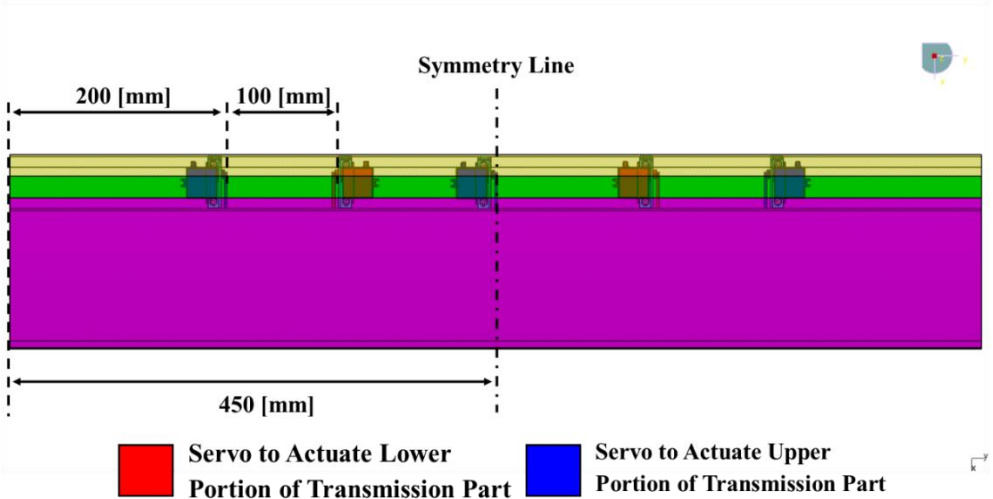
Figure 31: Servo Actuators inside the Control Surface Volume Configuration [29]

30

Servo actuator selection for the case of actuators inside the control surface is done by considering the available area inside the control surface volume. After searching on market, the servo actuator that can fit inside the control surface volume and has the maximum torque capacity is chosen. Volz DA 13-05-60 servo actuator [32] is suitable for these criteria. The model of the actuator is shown in Figure 32.
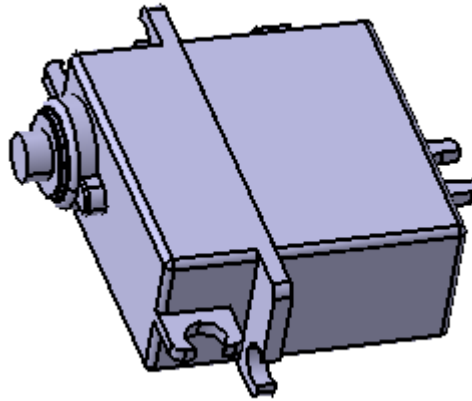
Figure 32: Volz DA 13-05-60 Servo Actuator

The properties of the selected servo actuator are given in Table 6.

Table 6: Technical Specification of Volz DA 13-05-60 Servo Actuator [32]

Supply Voltage	5.0 [V] DC
Peak Torque	600 [Nmm]
Operating Temperature	-35 ^{0}C to +70 ^{0}C
Mass	19 [g]
Case Dimension	28.4 mm x 38.0 mm x 13.3 mm

The moment arm of the selected servo actuator is given in Figure 33. In order to maximize the force given by the servo actuator, the middle hole of the moment arm is used.
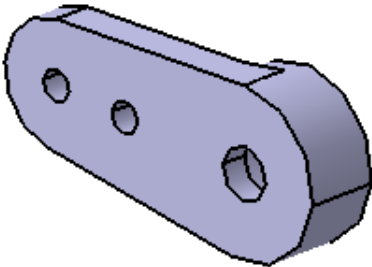
Figure 33: Servo Actuator Moment Arm Initial Model

The unnecessary part of the servo actuator moment arm is trimmed. The Final moment arm is shown in Figure 34.
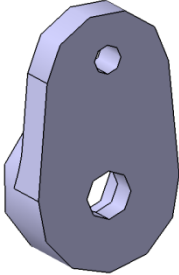
Figure 34: Servo Actuator Moment Arm Trimmed Model

Trimming the unnecessary part also enables some clearance between the lower surface and the moment arm. This is illustrated in Figure 35 and Figure 36.
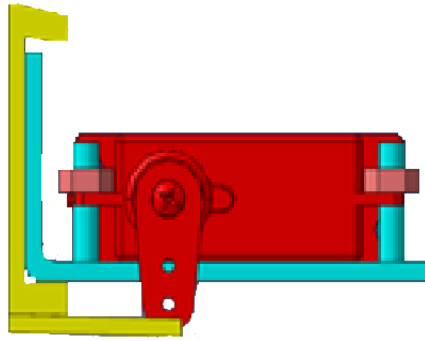
Figure 35: Moment Arm Initial Model
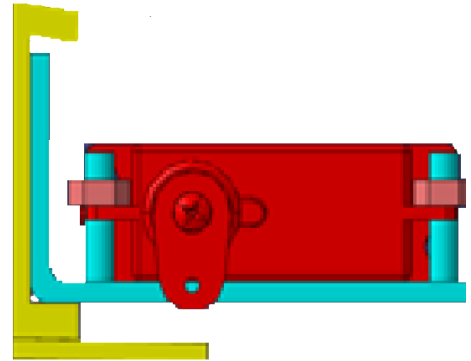
Figure 36: Moment Arm Final Model

The rod between the moment arm and transmission part is called as transmission rod shown in Figure 37. The length of this rod is taken as 34.5 [mm] and diameter of the circular cross section is taken as 2.5 [mm]. This rod transmits the torque of the actuator to the transmission part as an axial force.
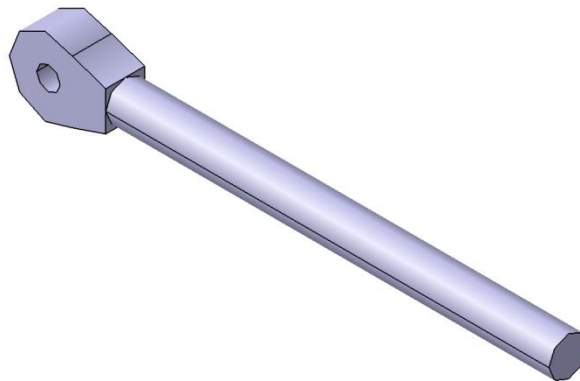
Figure 37: Transmission Rod

Servo actuators are connected to the C bar by using fasteners shown in Figure 38. These fasteners are made of aluminum.
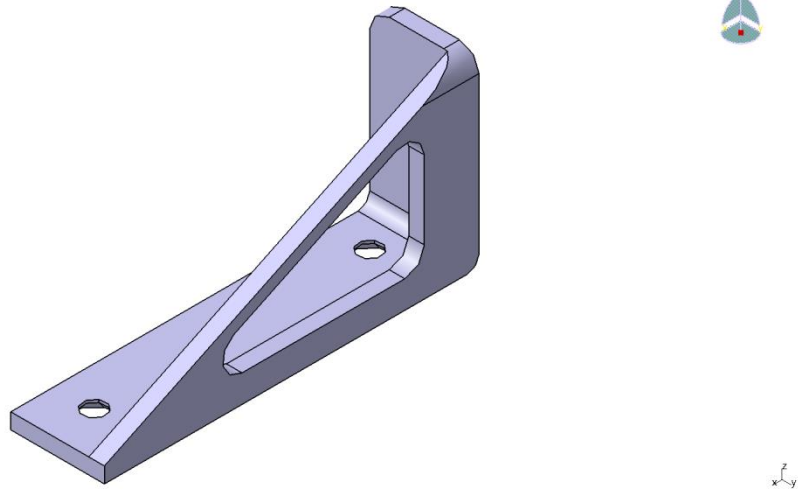
Figure 38: Servo Actuator Fastener

The volume of servo actuators prevent using bold-nut connection between the fasteners and c-bar. Therefore these two structures are glued to each other. In order to prevent sliding of the fastener on the C bar, female guides are opened on the c-bar as shown in Figure 39.
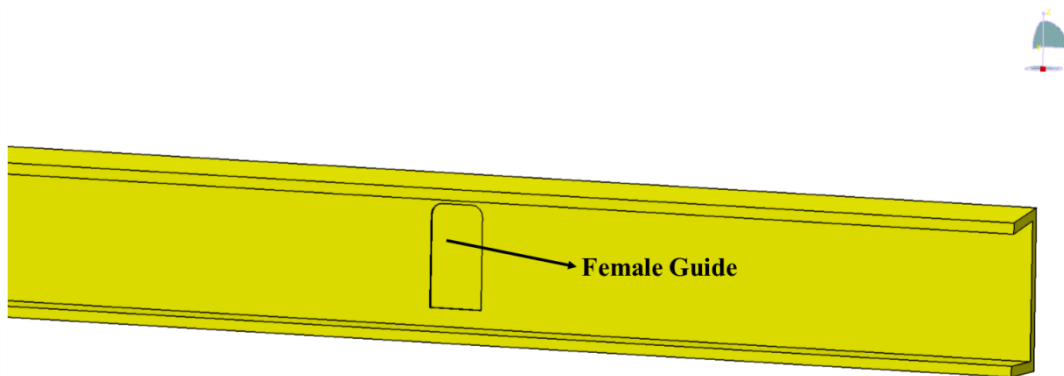
Figure 39: Female Guide of the C Bar

When the servo actuators are placed in the torque box volume, they are connected to the rear spar of the wing by using suitable fasteners. Since the volume of the torque box is greater than the volume of the control surface, bigger and powerful servo actuators are selected for this case. The selected servo actuator is shown in Figure 40.

Figure 40: Servo Actuator, Futaba S9156

The properties of the selected servo actuator is shown in Table 7.

Table 7: Technical Specification of Futaba S9156

Torque at 4.8 [V]:	19.6 [kg-cm]
Dimensions:	40 x 20 x 37 [mm]
Mass:	63 [g]

The selected servo actuator and the transmission rod are implemented to the designed assembly by using CATIA V5-6R2012 package software and are shown in Figure 41.
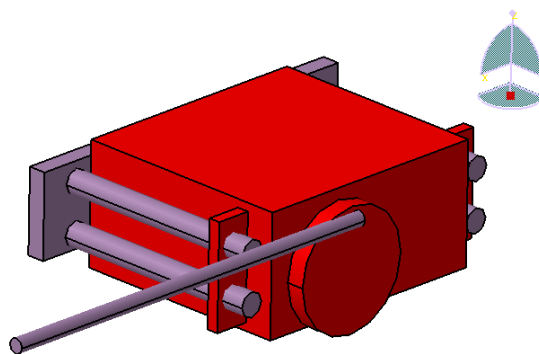
Figure 41: CAD Modelling of the Servo Actuator that is inside the Torque Box Volume

3.6 Discussion and Conclusion

In this chapter, the interior design of the hybrid trailing edge control surface is explained. The airfoil profile used, the dimensions and parts of the control surface are described. CAD drawings of the configurations are shown. Possible locations of servo actuators, advantages and disadvantages of these locations are specified. If the torque box volume is available for the servo actuators, more powerful servos can be used there. Otherwise comparatively small scaled servos are needed in the control surface volume. Servo actuators of the configurations are selected and presented.

CHAPTER 4

FINITE ELEMENT MODELING OF HYBRID TRAING EDGE CONTROL SURFACE

4.1 Introduction

In this chapter, the finite element modeling procedures of the hybrid trailing edge control surface are explained. All the control surface configurations are similar in terms of meshing, defining connections, applying boundary conditions and analysis type. Therefore the finite element modeling method is explained for design 1 only. The main idea of the method can be applied to other configurations.

The CAD drawings of the trailing edge control surface are obtained by using CATIA V5-6R2012 package software and finite element modeling is done by using ANSYS Workbench v14.0 program.

In the modeling process, proper material properties and connection types are assigned for each of the material used. The quality of the meshing is checked by applying mesh convergence analysis. After that necessary boundary conditions are considered and the loads are applied to the system. Finally, discussion and conclusion parts are given.

4.2 Finite Element Modeling of the Hybrid Trailing Edge Control Surface

4.2.1 Structural Parts of the Finite Element Model

Before starting the finite element modeling, the structures that are to be modeled and their modeling types are determined. Rigid part, transmission parts, compliant part and surface of the C part are modeled as surface bodies. The servo

actuator moment arm and transmission rods are modeled as line bodies. The C bar section is modeled as a solid body. The solid CAD model and the corresponding model to be used for the finite element model can be seen in Figure 42 and Figure 43.
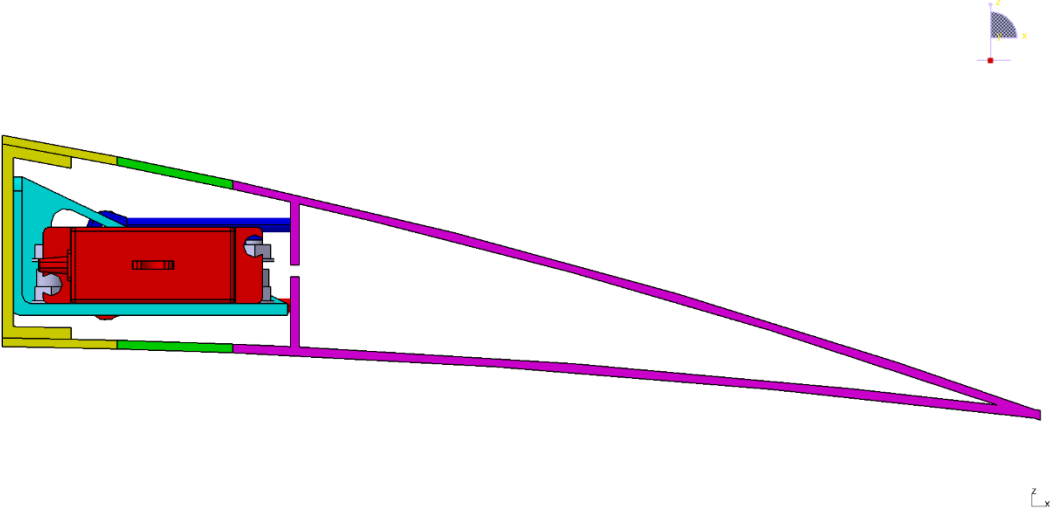
Figure 42: Solid CAD Model of the Hybrid Trailing Edge Control Surface with the Actuators inside the Control Surface Volume
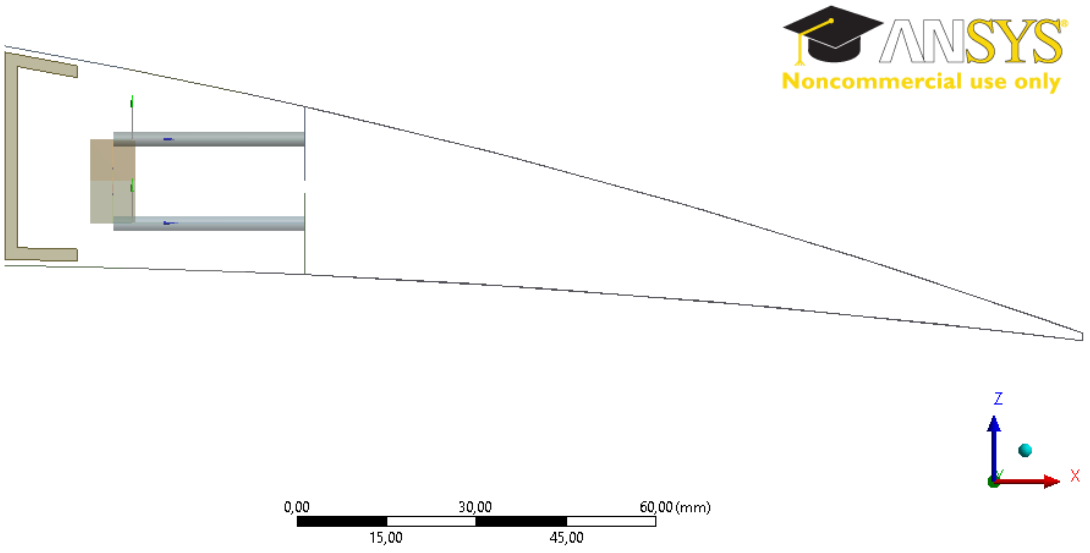
Figure 43: The CAD Model to be Used in Finite Element Model

The shell thicknesses of the all surfaces are taken as 1.5 [mm]. The diameter of the transmission rods are taken as 2.5 [mm]. Moment arm cross section is taken as

rectangular whose height is 7.4 [mm] and width is 1.9 [mm]. The moment arm and transmission rod models are shown in Figure 44.
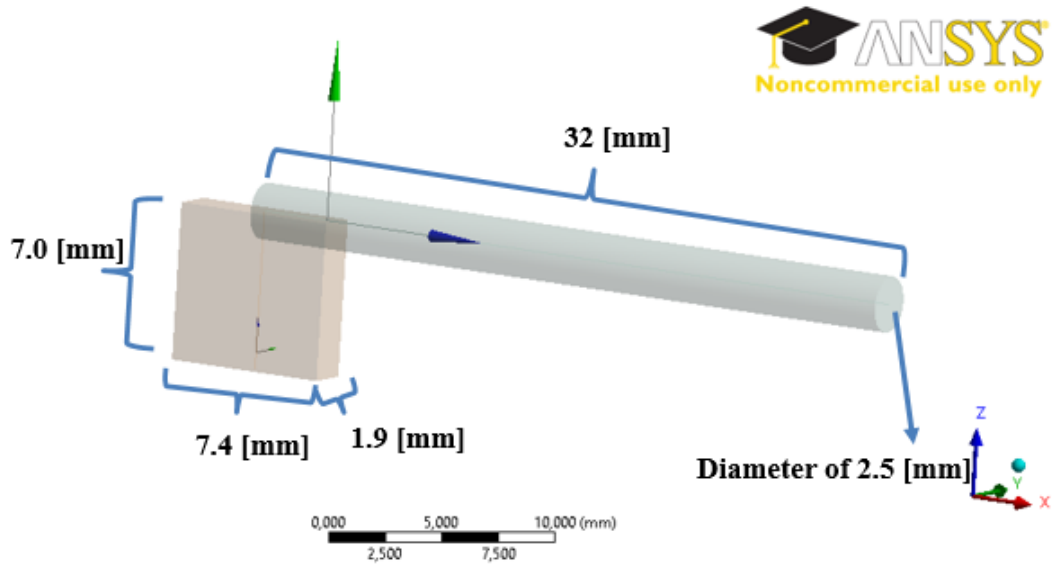
Figure 44: The Modeled Moment Arm and Transmission Rod

The dimensions of the c bar are given in Figure 45.
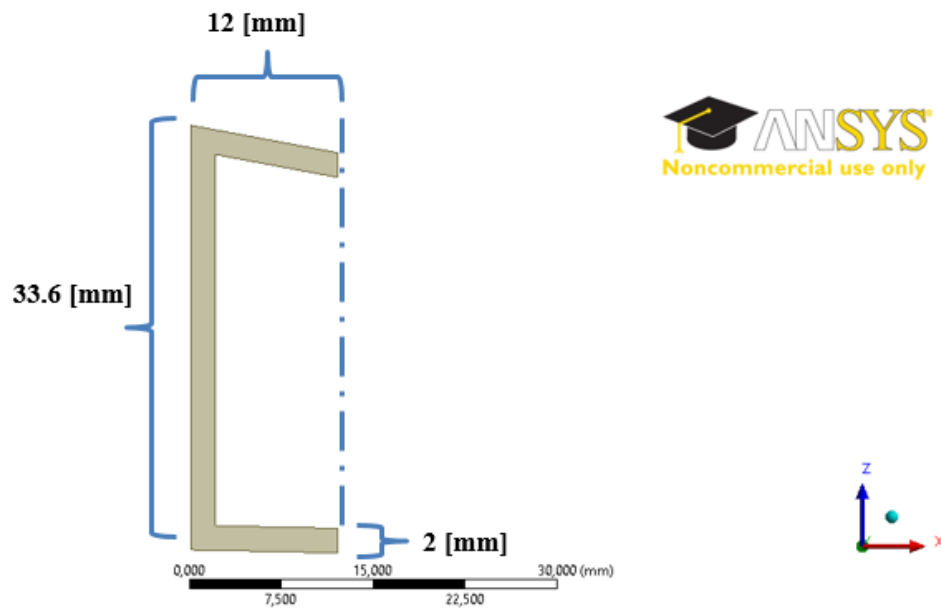
Figure 45: Dimension of the C Bar

4.2.2 Connection Types between the Structures

Some connections are applied to the model. These are:

- Bonded contact between the c bar and outer skin of the c part (shown in Figure 46)
- Bonded contact between transmission rods and transmission parts (shown in Figure 47).
- Hinge-like contact between the moment arm and transmission rod (shown in Figure 51).

Bonded contact means sliding and separation are not allowed between the connections during the analyses. In other words, for the bonded contact, three translational degrees of freedom and three rotational degrees of freedom are coupled for the nodes in the contact region. In reality, different connections may be possible but in theoretical analysis, a simplified fully bonded contact is selected.
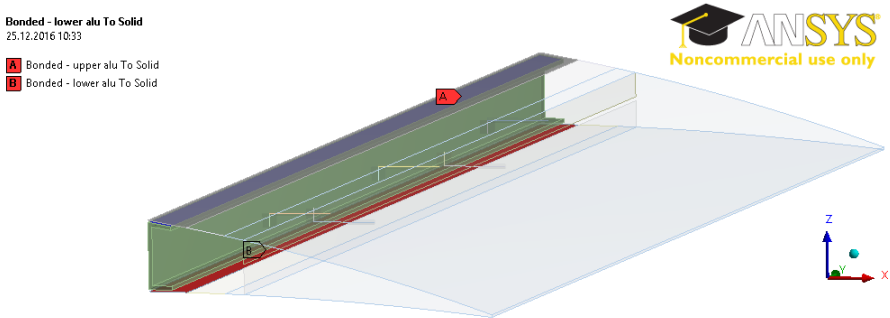
Figure 46: Bonded Contact between C Bar and Outer Skin of the C Part.
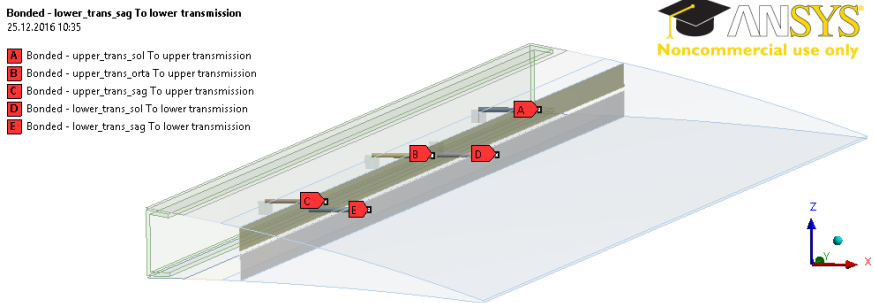
Figure 47: Bonded Contact between Transmission Rods and Transmission Parts

In Figure 46, blue region is the bonded contact between the c bar and upper skin part whereas the red region is the bonded contact between the c bar and lower skin part.

In Figure 47, Contacts A, B and C are between the upper transmission rods and the upper transmission part whereas contract D and E are between the lower transmission rods and the lower transmission part.

In ANSYS, there is an alternative way of using bonded contact which is defined as "joint". By using joints where possible, the designer can save computational time since using bonded contact takes much computational time with compared to using joint during the analyses. Using "Joint" option enables user to use "share topology" option which means combining the meshes of two different surfaces shown in Figure 48 and Figure 49. In Figure 48, one needs to define a contact between the two surfaces because contact meshes are not combined. Whereas, in Figure 49, contact meshes are combined and defining contact is not needed. Faster solution is reached for the second case.
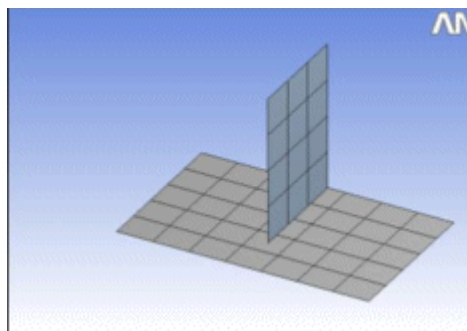
Figure 48: Meshing without Using Joint
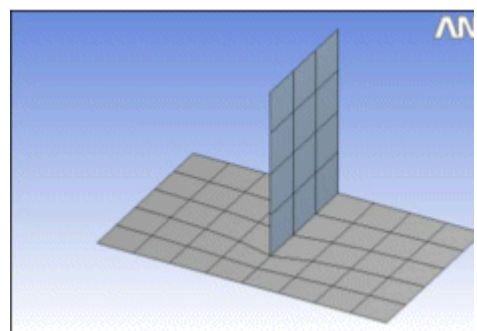
Figure 49: Meshing with Using Joint

The regions where the "joint" option is used are shown in Table 8.

Table 8: The Regions where the "Joint" Option are Used

Upper Compliant Skin **vs** Rigid Part
Lower Compliant Skin **vs** Rigid Part
Upper Transmission Part **vs** Rigid Part
Lower Transmission Part **vs** Rigid Part
Upper Skin Part of the C Part **vs** Upper Compliant Skin
Lower Skin Part of the C Part **vs** Upper Compliant Skin

The connection regions where the "joint" option is used are shown (green line) in Figure 50.
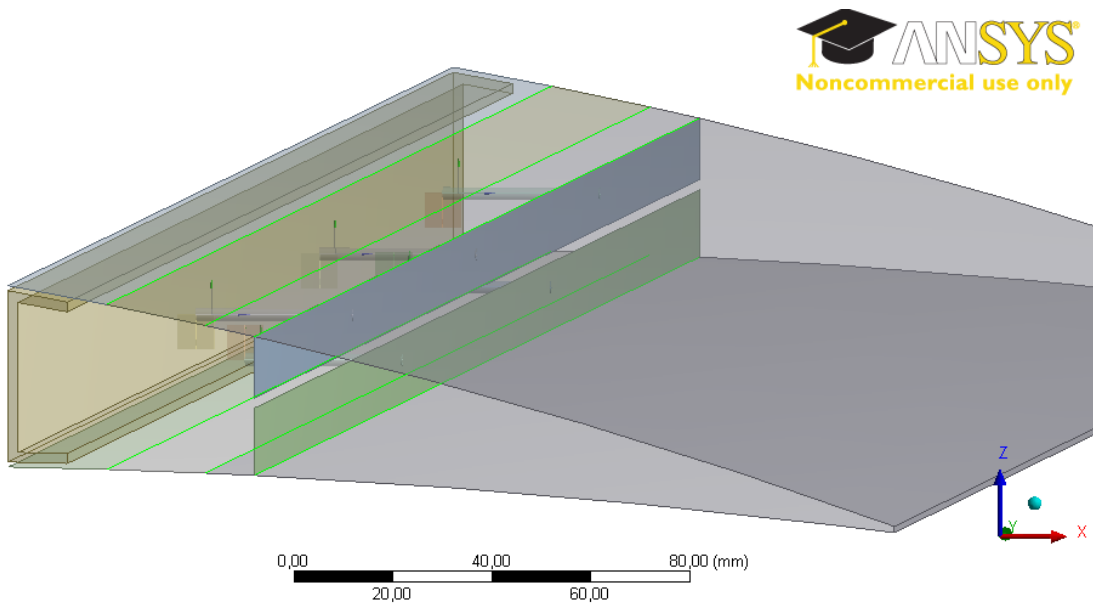
Figure 50: The Joint Lines (shown in Green)

Also note that, sometimes, using bolted contact may result in convergence problem during the analyses. Using "joint" option also eliminates some of the convergence problems result from the contacts.

Hinge-like contact is defined between the moment arm and transmission rod. This point is considered as a hinge such that the end node of the moment arm and the

end node of the transmission part are doing the same motion for x, y, z displacement and for x and z rotations. Only y rotational angle is set to free. In other words, around y axis, the rotational trend of the end node of the moment arm and end node of the transmission rod is independent of each other. This connection is shown in Figure 51. In reality, it is expected to exist some rotational stiffness around y axis at the connection point but in this thesis, this stiffness value is neglected and considered to be small.
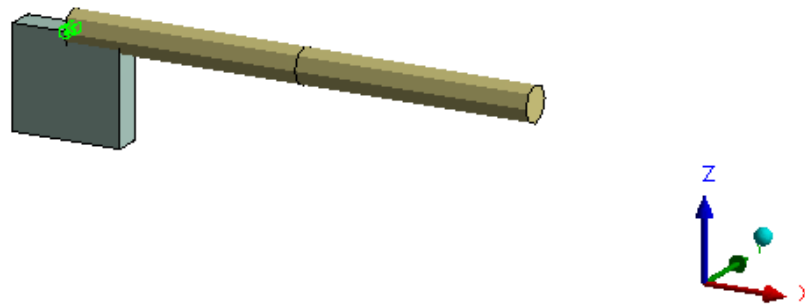
Figure 51: Hinge-like Contact between Moment Arm and Transmission Rod

4.2.3 Meshing of the Hybrid Trailing Edge Control Surface

Since shell 181 elements are appropriate for analyzing thin structures [33], for all the surface parts in the model, uniform quadrilateral four noded-shell 181 elements are used. These elements have six degrees of freedom with three translation and 3 rotations at its each node.

For the c-bar, solid 185 is used which has eight nodes each of which has three translational degrees of freedom [33]. The size of the elements are determined as 5 [mm].

For the beam elements in the model (moment arms and transmission rods), beam 188 elements are used which are linear, 2 node beam elements having six degree of freedom (three translation and three rotations) [33].

The element size of the rigid part is taken as 30 [mm] and the element size of the compliant part is taken as 10 [mm]. These magnitudes are determined from the mesh convergence analyses which are shown in Figure 52 and Figure 53.
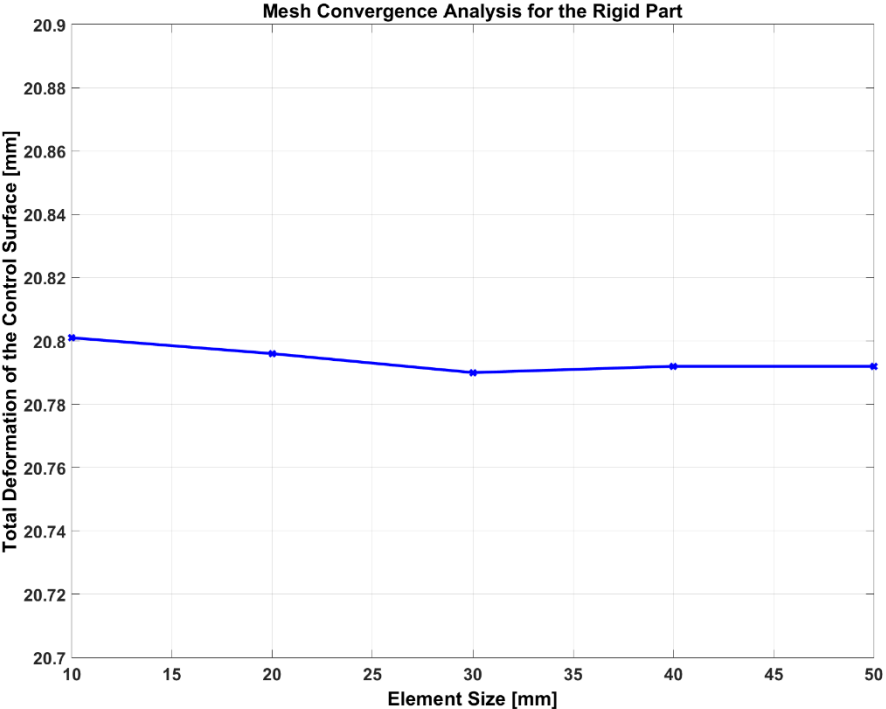
Figure 52: Mesh Convergence Analysis for the Rigid Part
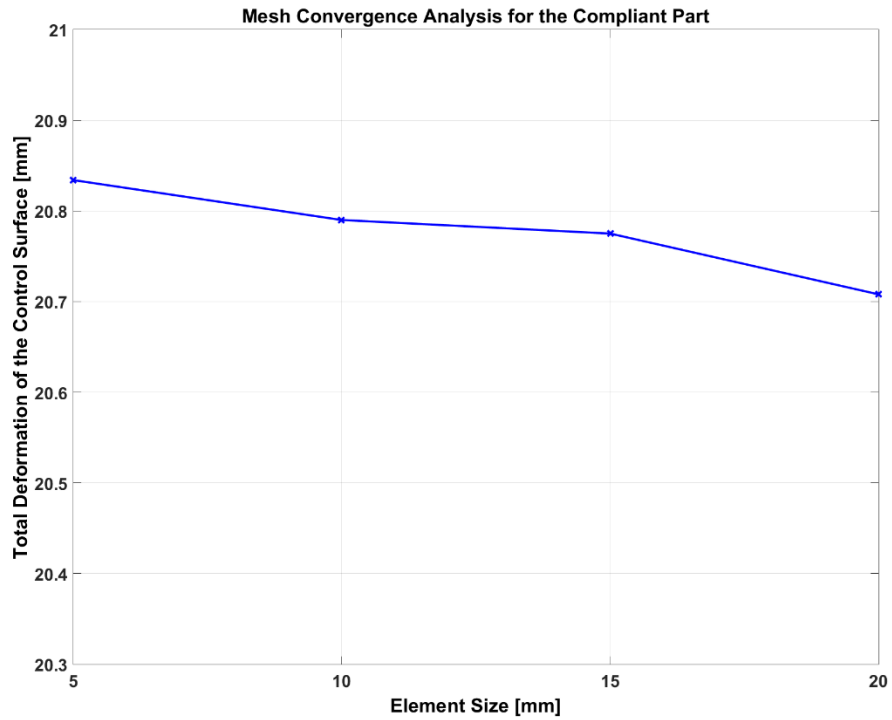
Figure 53: Mesh Convergence Analysis for the Compliant Part

For the mesh convergence analysis results of rigid part, taking the element size between 10 [mm] and 50[mm] changes the maximum total deformation magnitude of the control surface around 0.04%. Therefore, 30 [mm] element size of rigid part is selected by also considering the solution time.

Similarly, for the mesh convergence analysis results of compliant part, taking the element size between 5 [mm] and 20 [mm] changes the maximum total deformation magnitude of the control surface around 0.6%. Therefore, 10 [mm] element size of compliant part is selected by also considering the solution time.

The final meshed view of the control surface can be seen from the Figure 54 and Figure 55.
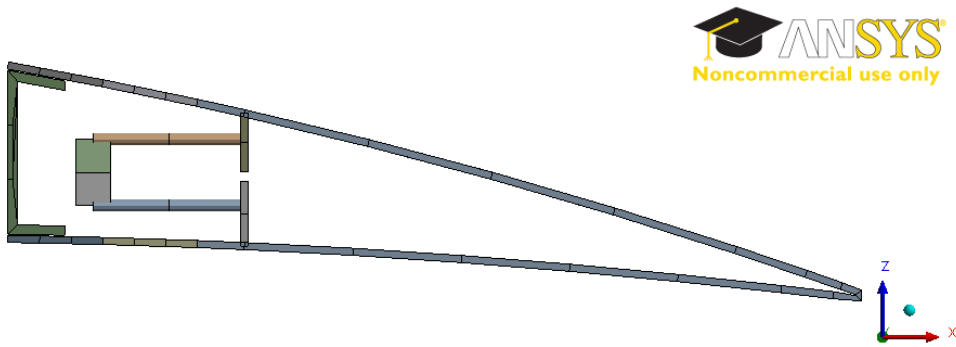
Figure 54: Side View of the Meshed Trailing Edge Control Surface
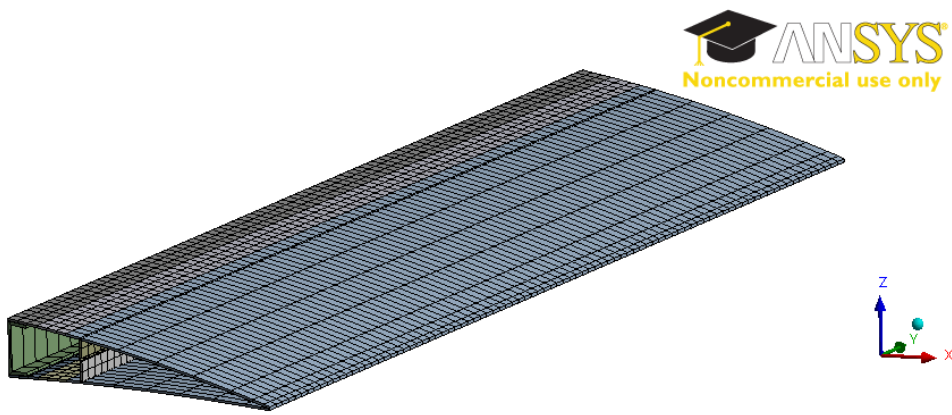
Figure 55: Isometric View of the Meshed Trailing Edge Control Surface

The meshed view of the moment arm and transmission rod combination can be seen in Figure 56.
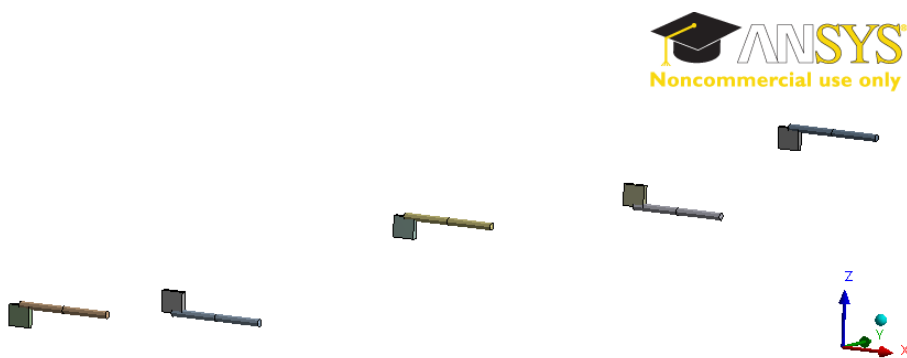
Figure 56: Finite Element Model of Moment Arm and Transmission Rods

4.2.4 Loading and Boundary Conditions

Since the scope of this thesis is structural analyses in in-vacuo condition, aerodynamic loading is not considered.

First of all, the gravity is considered in order to create inertial loading. And for that, the Standard Earth Gravity is taken as 9.8060 m/s^2 in –z direction shown in Figure 57.
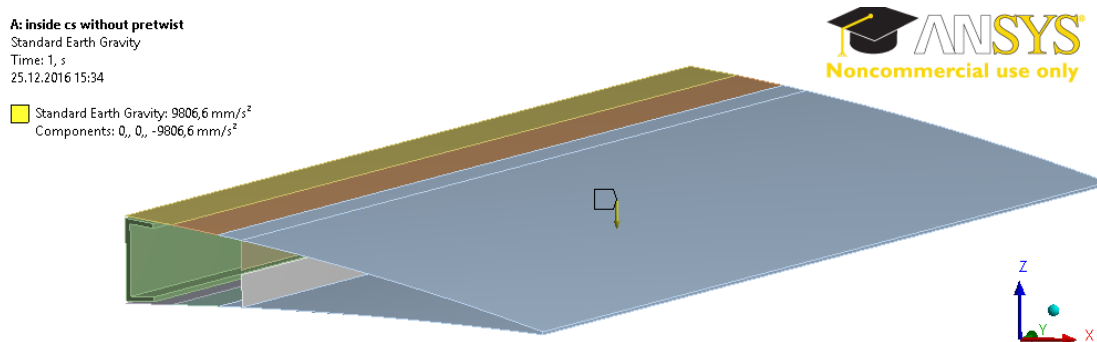
Figure 57: Appling Gravity to the Trailing Edge Control Surface

Then servo actuator loads are applied. Since servo actuators are assumed to be rigid, their locations are also assumed to be fixed during the analyses and for that servo actuators are not modeled.

In order to apply servo actuators loads properly, three translational degrees of freedom (x, y, and z) are set to zero and two of the three rotational degrees of freedom (x and z) are set to zero at the center of rotation of the servo actuator moment arm. Only rotation angles around y axis are defined for each servo actuator. This results in rotation of the moment arm around y axis and movement of the actuator rods. Finally this leads to deflection of the control surface.

In order to actuate the control surface, three angles around y axis are defined for three servo actuator moment arm that actuate the upper surface of the trailing edge control surface and two rotation angles around y axis are defined for two servo actuator moment arm that actuate the lower surface of the trailing edge control surface.

47

For the boundary conditions, only fix support boundary condition is applied at the surface of the c bar shown in Figure 58.
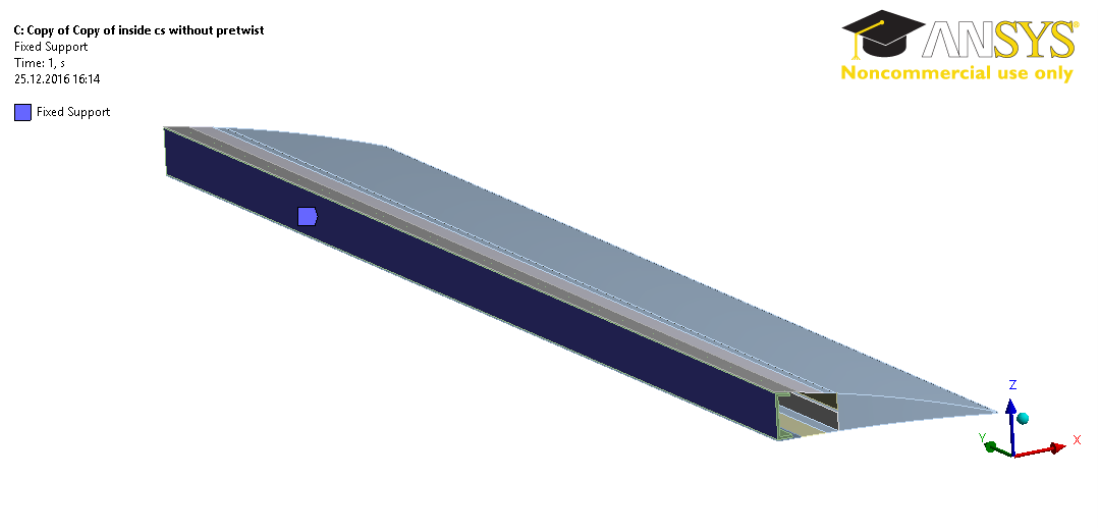
Figure 58: Fix Support Boundary Condition

4.2.5 Analysis Type

Since the designed control surface is capable of large deflection and also has a nonlinear material (neoprene rubber), the nonlinear module of ANSYS is used. Nonlinear module is used by activating the "large deflection" option of ANSYS. "Large deflection" option enables the solver to perform both geometric and material nonlinearity solutions.

4.3 Discussion and Conclusion

In this chapter, FEM of the hybrid trailing edge control surface is explained. Structural parts that are modeled with finite element are defined. The connection types between the structures are mentioned. The meshing procedures are explained. Then loading and boundary conditions are defined. Finally, analysis type is selected. There are more than one configuration that are structurally analyzed (Design 1, Design 2, Design 3 and Design 4). But they are very similar in term of finite element

modeling. The same procedure can be applied any other configuration that are analyzed in this thesis.

CHAPTER 5

STRUCTURAL ANALYSIS OF THE HYBRID TRAILING EDGE CONTROL SURFACE WITH THE ACTUATORS INSIDE THE CONTROL SURFACE VOLUME IN IN-VACUO CONDITION

5.1 Introduction

In this chapter, finite element analyses of the hybrid trailing edge control surface with the actuator inside the control surface volume are performed in in-vacuo condition. Both control surfaces with pre-twist and without pre-twist are analyzed. Static Structural module of ANSYS v14.0 program is used for finite element analyses. Only downward deflection of the control surface is examined. First of all, the downward deflection of the airfoil profile NACA 6510 to NACA 9510 profile is tested. If the trailing edge control surface is capable of this morphing, further deflection of the control surface is studied. The camber deflection limit of the control surface is determined. Finally, twist capability of the designed control surface is studied.

5.2 Control Surface without Pre-Twist Configuration

5.2.1 Downward Deflection of the Hybrid Trailing Edge Control Surface

In this section 6510. Therefore all the downward deflection analyses start from the baseline airfoil, downward deflection of the hybrid trailing edge control surface without pre-twist configuration is studied. The limit of the downward deflection is determined. The baseline airfoil profile is selected as NACA.

5.2.1.1 Deflection of NACA 6510 Profile by 15.2 [mm] in Transverse Direction

The undeformed, baseline airfoil profile NACA 6510 and deformed target airfoil profile NACA 9510 can be seen in Figure 59. In order to deflect the control surface from NACA 6510 to NACA 9510, around 15.2 [mm] tip deflection in z direction is needed.
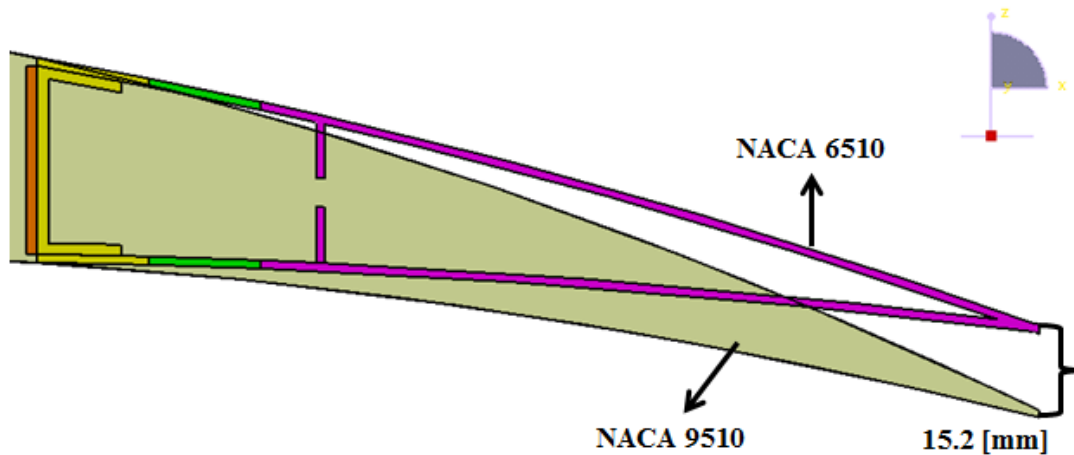
Figure 59: NACA 6510 and NACA 9510 Profiles

In order to deflect the tip of the hybrid trailing edge control surface 15.2 [mm] in vertical direction, rotation angles around y axis are defined +21.08 [deg] at the rotation center of the moment arms which actuate the upper part of the control surface and -12 [deg] rotation angles around y axis are defined at the center of the moment arms which actuate the lower part of the control surface.

The z directional displacement of the control surface is shown in Figure 60. Equivalent elastic stress and strain of the control surface are shown in Figure 61 and Figure 62 respectively. Maximum combined beam stress of the moment arms and transmission rods is given in Figure 63.
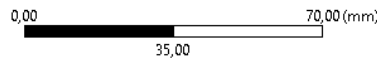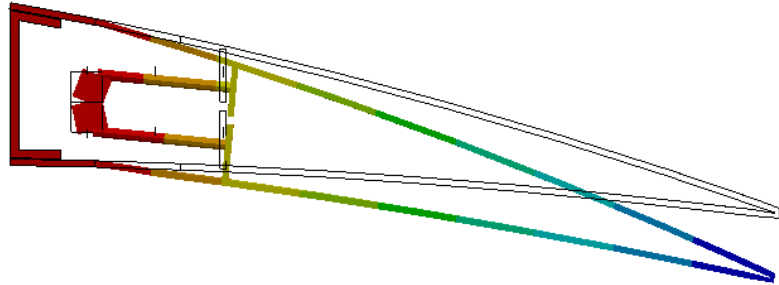
Figure 60: Z Directional Displacement Contours of the Control Surface –
15.2 [mm] Downward Deflected – Servo Actuators inside the Control Surface –
without Pre-Twist – Maximum 15.205 [mm]
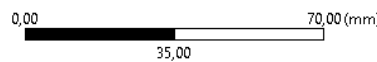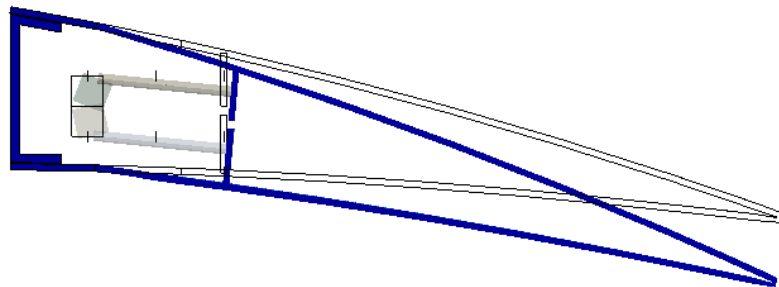
Figure 61: Equivalent Elastic Stress of the Control Surface 15.2 [mm]
Downward Deflected – Servo Actuators inside the Control Surface – without Pre-
Twist – Maximum 13.841 [MPa]
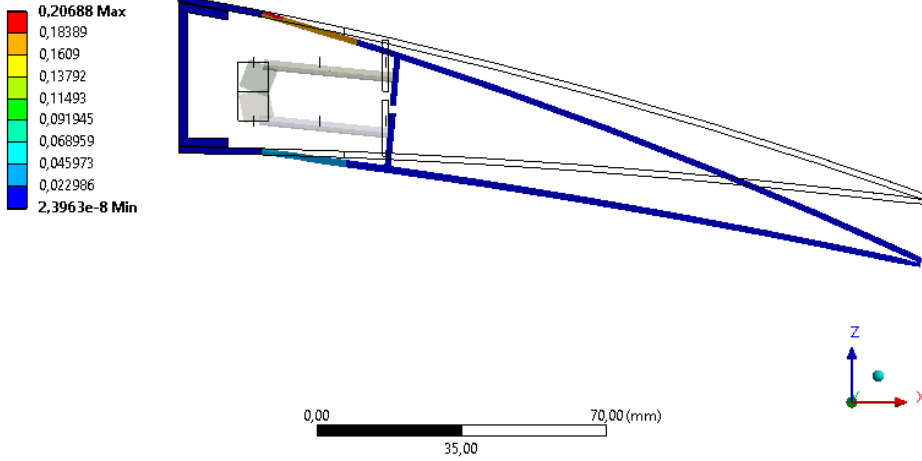
Figure 62: Equivalent Elastic Strain of the Control Surface 15.2 [mm] Downward Deflected – Servo Actuators inside the Control Surface – without Pre-Twist – Maximum 0.20688 [mm/mm]
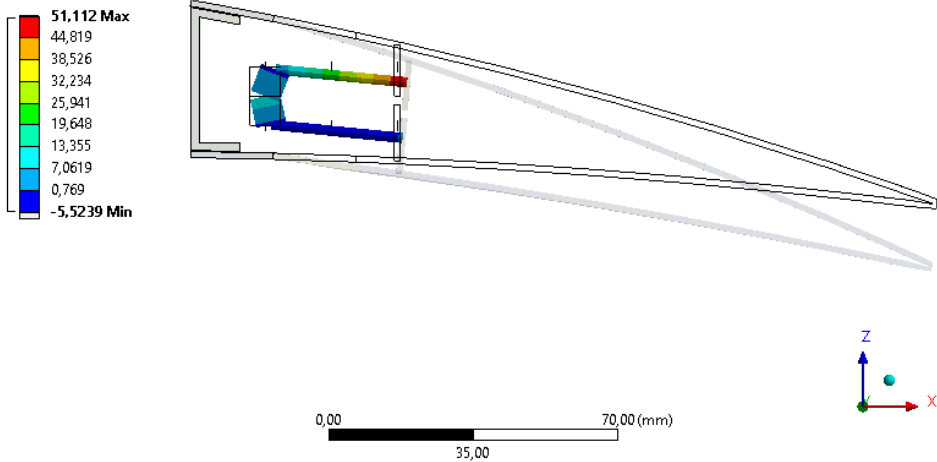
Figure 63: Maximum Combined Beam Stress of the Control Surface 15.2 [mm] Downward Deflected – Servo Actuators inside the Control Surface – without Pre-Twist – Maximum 51.112 [MPa]

Note that the maximum combined beam stress shown in Figure 63 is a combination of both axial and bending stress existing on the beams (moment arms and transmission rods). The maximum strain value (0.21 [mm/mm]) is reached for the compliant skin of the control surface and maximum stress value (51.11 [MPa]) is reached for the connection point of the transmission rods to the transmission parts. It is concluded that the strain and stress values are much below the material limits.

The maximum torque value needed for the servo actuator actuates the upper surface of the control surface is -105.91 [N-mm] and the maximum torque value needed for the servo actuator actuates the lower surface of the control surface is -210.55 [N-mm]. It can be concluded that the reaction moment results are below the servo actuator torque limits.

After ensuring that the designed hybrid trailing edge control surface is safe enough to morph from NACA 6510 profile to NACA 9510 profile, it is decided to find its lower deflection limits. And for that, control surface is checked at 20 [mm], 25 [mm] and 30 [mm] transverse tip deflection.

5.2.1.2 Deflection of NACA 6510 Profile by 20 [mm] in Transverse Direction

In order to deflect the tip of the hybrid trailing edge control surface 20 [mm] in vertical direction, rotation angles around y axis are defined +24.5 [deg] at the rotation center of the moment arm which actuate the upper part of the control surface and -12 [deg] rotation angles around y axis are defined at the center of the moment arm which actuate the lower part of the control surface.

The z directional displacement of the control surface is shown in Figure 64. Equivalent elastic stress and strain of the control surface are shown in Figure 65 and Figure 66 respectively. Maximum combined beam stress of the moment arms and transmission rods is given in Figure 67.
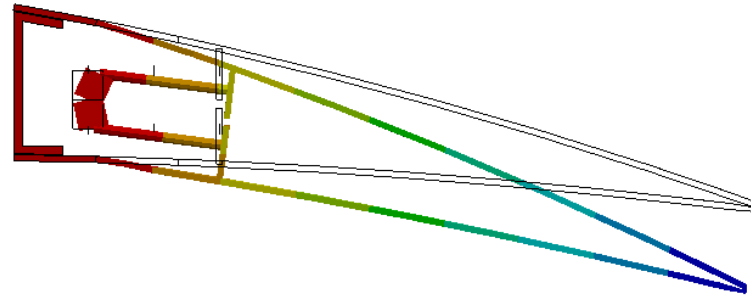
Figure 64: Z Directional Displacement Contours of the Control Surface – 20 [mm] Downward Deflected – Servo Actuators inside the Control Surface –without Pre-Twist – Maximum 20.041 [mm]
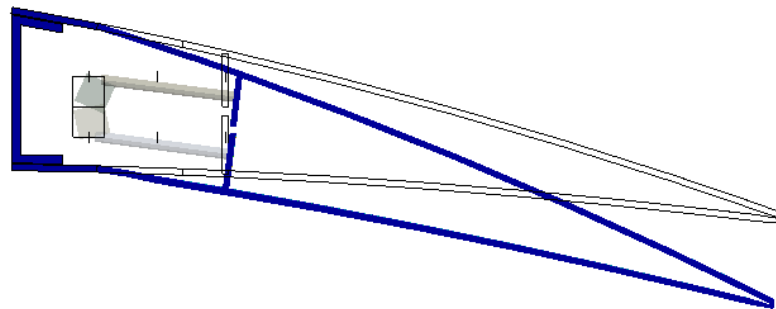
Figure 65: Equivalent Elastic Stress of the Control Surface 20 [mm] Downward Deflected – Servo Actuators inside the Control Surface – without Pre-Twist – Maximum 42.441 [MPa]
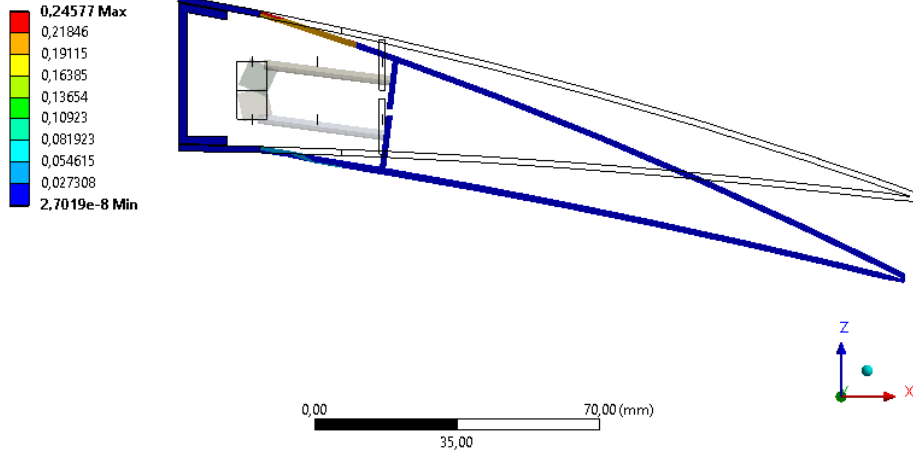
Figure 66: Equivalent Elastic Strain of the Control Surface 20 [mm] Downward Deflected – Servo Actuators inside the Control Surface – without Pre-Twist – Maximum 0.24577 [mm/mm]
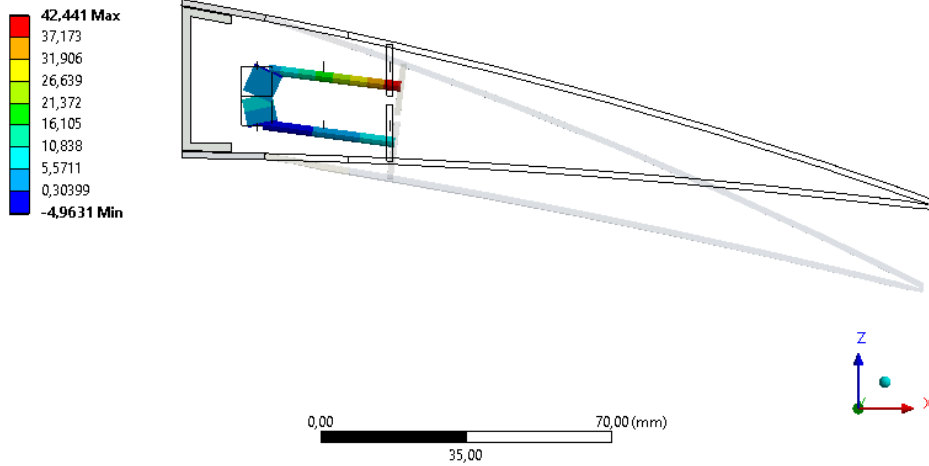
Figure 67: Maximum Combined Beam Stress of the Control Surface 20 [mm] Downward Deflected – Servo Actuators inside the Control Surface – without Pre-Twist – Maximum 42.441 [MPa]

The maximum torque value needed for the servo actuator actuates the upper surface of the control surface is -89.89 [N-mm] and the maximum torque value needed for the servo actuator actuates the lower surface of the control surface is -191.90 [N-mm]. It can be concluded that the reaction moment results are below the servo actuator torque limits.

5.2.1.3 Deflection of NACA 6510 Profile by 25 [mm] in Transverse Direction

In order to deflect the tip of the hybrid trailing edge control surface 25 [mm] in vertical direction, rotation angles around y axis are defined +28.05 [deg] at the rotation center of the moment arm which actuate the upper part of the control surface and -12 [deg] rotation angles around y axis are defined at the center of the moment arm which actuate the lower part of the control surface.

The z directional displacement of the control surface is shown in Figure 68. Equivalent elastic stress and strain of the control surface are shown in Figure 69 and Figure 70 respectively. Maximum combined beam stress of the moment arms and transmission rods is given in Figure 71.

Figure 68: Z Directional Displacement Contours of the Control Surface – 25 [mm] Downward Deflected – Servo Actuators inside the Control Surface –without Pre-Twist – Maximum 25.055 [mm]

58
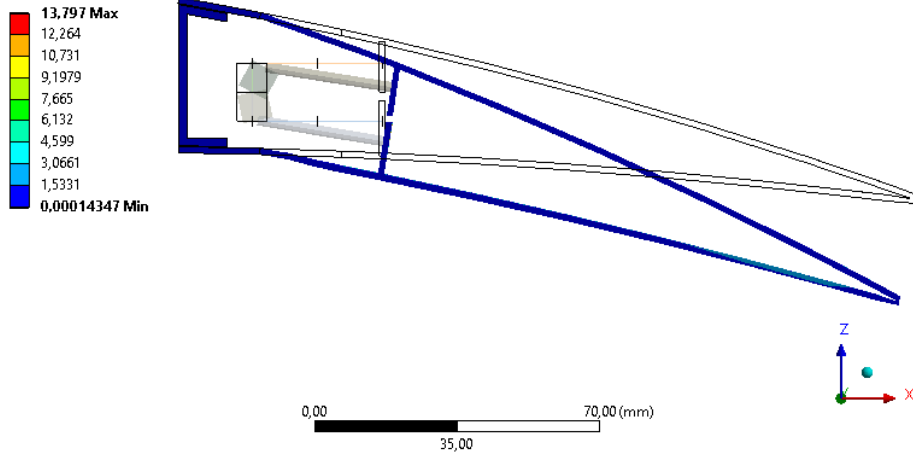
Figure 69: Equivalent Elastic Stress of the Control Surface 25 [mm]
Downward Deflected – Servo Actuators inside the Control Surface – without Pre-
Twist – Maximum 13.797 [MPa]
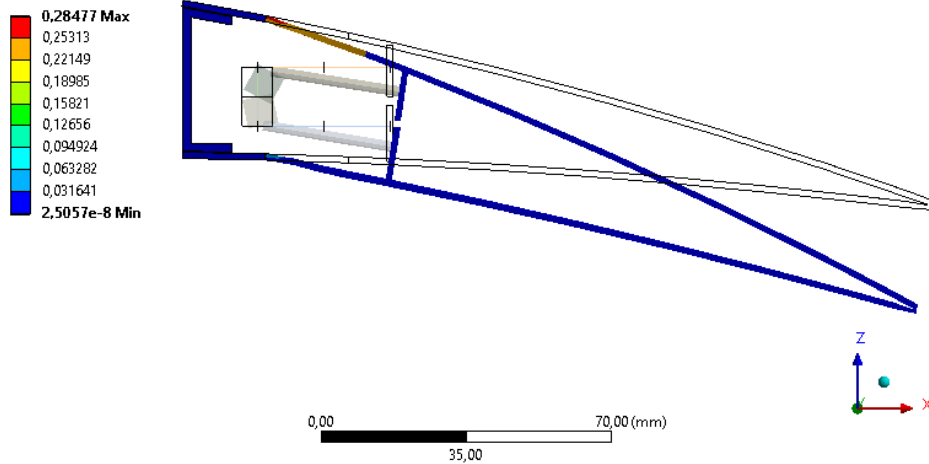
Figure 70: Equivalent Elastic Strain of the Control Surface 25 [mm]
Downward Deflected – Servo Actuators inside the Control Surface – without Pre-
Twist – Maximum 0.28477 [mm/mm]
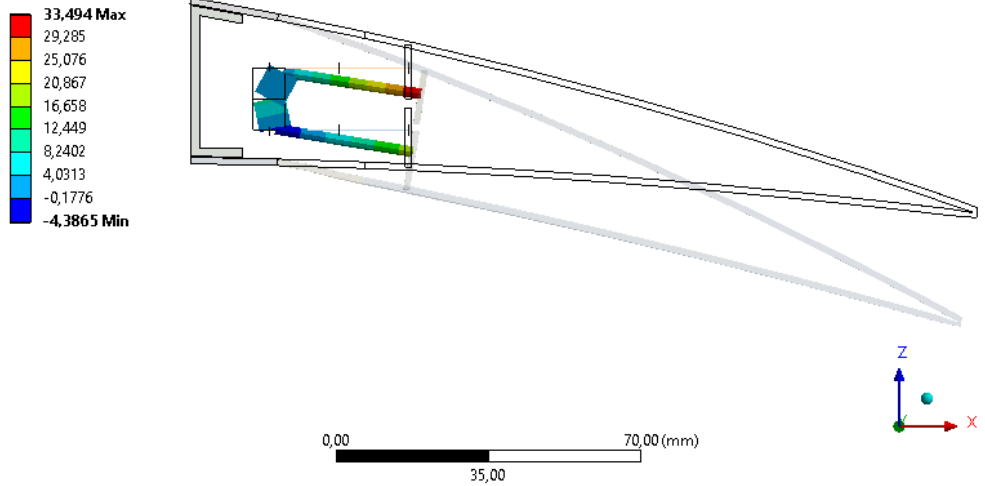
Figure 71: Maximum Combined Beam Stress of the Control Surface 25 [mm] Downward Deflected – Servo Actuators inside the Control Surface – without Pre-Twist – Maximum 33.494 [MPa]

The maximum torque value needed for the servo actuator actuates the upper surface of the control surface is -74.15 [N-mm] and the maximum torque value needed for the servo actuator actuates the lower surface of the control surface is -173.42 [N-mm]. It can be concluded that the reaction moment results are below the servo actuator torque limits.

5.2.1.4 Deflection of NACA 6510 Profile by 30 [mm] in Transverse Direction

In order to deflect the tip of the hybrid trailing edge control surface 30 [mm] in vertical direction, rotation angles around y axis are defined +31.6 [deg] at the rotation center of the moment arm which actuate the upper part of the control surface and -12 [deg] rotation angles around y axis are defined at the center of the moment arm which actuate the lower part of the control surface.

The z directional displacement of the control surface is shown in Figure 72. Equivalent elastic stress and strain of the control surface are shown in Figure 73 and

Figure 74 respectively. Maximum combined beam stress of the moment arms and transmission rods is given in Figure 75.
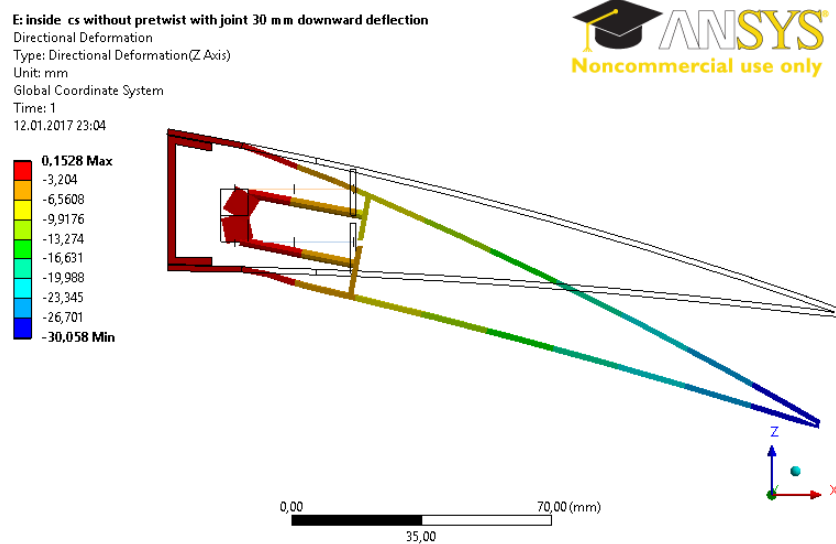
Figure 72: Z Directional Displacement Contours of the Control Surface – 30 [mm] Downward Deflected – Servo Actuators inside the Control Surface –without Pre-Twist – Maximum 30.058 [mm]
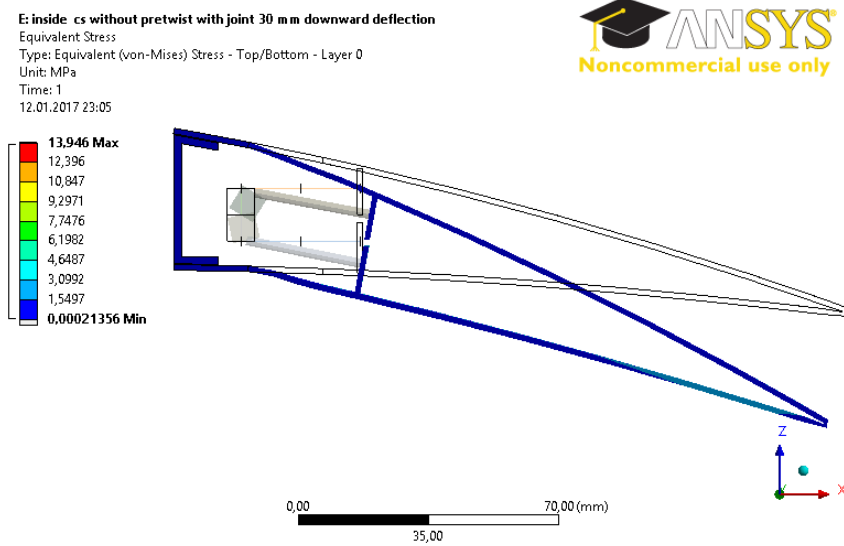
Figure 73: Equivalent Elastic Stress of the Control Surface 30 [mm] Downward Deflected – Servo Actuators inside the Control Surface – without Pre-Twist – Maximum 13.946 [MPa]

Figure 74: Equivalent Elastic Strain of the Control Surface 30 [mm] Downward Deflected – Servo Actuators inside the Control Surface – without Pre-Twist – Maximum 0.32242 [mm/mm]

Figure 75: Maximum Combined Beam Stress of the Control Surface 30 [mm] Downward Deflected – Servo Actuators inside the Control Surface – without Pre-Twist – Maximum 29.093 [MPa]

The maximum torque value needed for the servo actuator actuates the upper surface of the control surface is -59.27 [N-mm] and the maximum torque value needed for the servo actuator actuates the lower surface of the control surface is -159.01 [N-mm]. It can be concluded that the reaction moment results are below the servo actuator torque limits.

5.2.1.5 Discussion and Conclusion

The von Mises yield criteria is used for the failure analysis of the rigid part since this criteria is suitable for isotropic ductile material such as aluminum. Different failure criteria exist for different structures and materials [34]. For the beams of this study, the maximum combined beam stresses are checked. Maximum combined beam stresses mean the summation of both axial stress and bending stress on the beam. For compliant part, although the material had to be a fully anisotropic one, in the study it is assumed as isotropic and hence again von Mises yield criteria is used.

The maximum von Mises strain results of the all the downward deflection cases are tabulated in Table 9. Maximum von Mises strains are expected to occur at the upper complaint part since it is a soft material and exposed to large deflection. According to the results shown, as the deflection increases, the maximum von Mises strain also increases.

Table 9: Maximum von Mises Strain Comparison

	Maximum von Mises Strain [mm/mm]*
15.2 [mm] Deflection Case	0.20688
20.0 [mm] Deflection Case	0.24577
25.0 [mm] Deflection Case	0.28477
30.0 [mm] Deflection Case	0.32242

* Maximum von Misses Strain is observed for the compliant part and its strain limit must be smaller than 1.

The results of maximum von Mises stress, maximum combined beam stresses and required servo actuator torques to actuate upper and lower surface of the trailing edge control surface are given in Table 10, Table 11, Table 12 and Table 13 respectively. Indicated values are safe in terms of yield stress and strain values of the material used and servo torque limit capability.

Table 10: Maximum von Mises Stress Comparison

	Maximum von Mises Stress [MPa]*
15.2 [mm] Deflection Case	13.841
20.0 [mm] Deflection Case	13.765
25.0 [mm] Deflection Case	13.797
30.0 [mm] Deflection Case	13.946

* Maximum von Misses Stress is observed for the transmission parts and their yield stress is 280 [MPa]

Table 11: Maximum Combined Beam Stress

	Maximum Combined Beam Stress [MPa]*
15.2 [mm] Deflection Case	51.112
20.0 [mm] Deflection Case	42.441
25.0 [mm] Deflection Case	33.494
30.0 [mm] Deflection Case	29.093

*Aluminum is used for beams and its yield point is 280 [MPa]

Table 12: Servo Actuator Torque Required to Actuate the Upper Surface of the Control Surface

	Servo Actuate Upper Surface [N-mm]*
15.2 [mm] Deflection Case	-105.91
20.0 [mm] Deflection Case	-89.894
25.0 [mm] Deflection Case	-74.149
30.0 [mm] Deflection Case	-59.274

*Servo actuator torque capacity is 600 [Nmm]

Table 13: Servo Actuator Torque Required to Actuate the Lower Surface of the Control Surface

	Servo Actuate Lower Surface [N-mm]*
15.2 [mm] Deflection Case	-210.55
20.0 [mm] Deflection Case	-191.9
25.0 [mm] Deflection Case	-173.42
30.0 [mm] Deflection Case	-159.01

*Servo actuator torque capacity is 600 [Nmm]

According to the results shown in the above tables, the hybrid trailing edge control surface is capable of performing downward deflection up to 30 [mm] without any problem.

In order to keep the control surface in the desired position, the servo actuator torques should always balance the torque created by the gravitational force and the torque created by the inplane force occurring in the compliant part due to the strain in the plane of the compliant part. Since, initially the compliant material is neither in tension nor in compression, then the servo actuators are just balancing the weight of

the control surface. As the downward deflection increases, the compliant part starts to elongate and work against the gravitational force, which is nearly constant. Up to a certain deflection value, the magnitude of the torque created by the gravitational force is larger than the magnitude of the torque created by the force in the compliant part. Therefore, the servo actuator torques are the net torque of the one created by the weight minus that of created by the compliant part. This effectively means that there is an actuator torque which starts from a value and then progressively becomes smaller in magnitude. As the downward deflection further increases, the torque magnitude created by the compliant part surpasses the torque created by the gravity; and the resultant torque changes its sign and increases in magnitude. This reflects itself by changing the sign of the servo actuator torque values in order to balance the system. As servo actuators torque value decreases in magnitude, the beam stress values also decrease. Therefore, during the deflection of the control surface, the beam stresses are decreasing up to a certain value and then they increase. If the gravity is not considered during the analyses, it is expected that the combined beam stress will always increase along with the increasing downward deflection. In order to study that, the analyses are performed without using the gravity and the results are shown in Table 14. It can be seen that, as the downward deflection increases, the maximum combined beam stress values also increase.

Table 14: Maximum Combined Beam Stress for the Case without Gravity

	Maximum Combined Beam Stress [MPa] without considering the gravity
15.2 [mm] Deflection Case	44.928
20.0 [mm] Deflection Case	54.046
25.0 [mm] Deflection Case	63.467
30.0 [mm] Deflection Case	73.033

Final check of the control surface while performing downward deflection is the checking whether the upper surface of the control surface touches the upper edge part of the servo actuators or not. There is no risk for touching the upper surface of the control surface to the upper edge part of the servo actuators. This is shown in Figure 76.
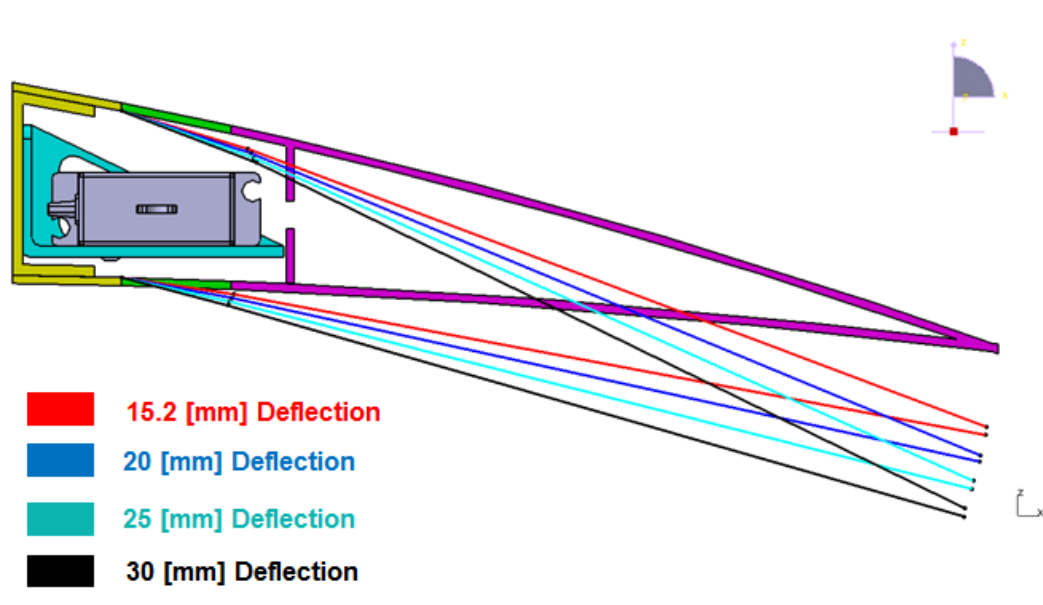
Figure 76: Contact Check between Servo Actuators and Upper Surface of the Control Surface

For the 30 [mm] downward deflection case, the minimum distance between the upper edge point of servo actuator and upper surface of the control surface is measured as 1.8 [mm]. This distance is considered as clearance during the motion of the control surface. But further deflection of the control surface beyond 30 [mm] downward deflection is also checked. For 32 [mm] of downward deflection, 1.5 [mm] of clearance is measured. Beyond that limit, there exists some convergence problem related with the compliant material.

5.2.2 Investigation of Twist Capability of the Hybrid Trailing Edge Control Surface

In this section, twist capability of the hybrid trailing edge control surface is examined.

In order to twist the hybrid trailing edge control surface, the angles of 6 [deg], 10 [deg] and 14 [deg] are defined at the outboard, middle and inboard upper servo actuators respectively. Also the angles of -1 [deg] and -3 [deg] are defined at the outboard and inboard lower servo actuators respectively.

The z directional displacement of the control surface is shown in Figure 77. Equivalent elastic stress and strain of the control surface are shown in Figure 78 and Figure 79 respectively. Maximum combined beam stress of the moment arms and transmission rods is given in Figure 80.
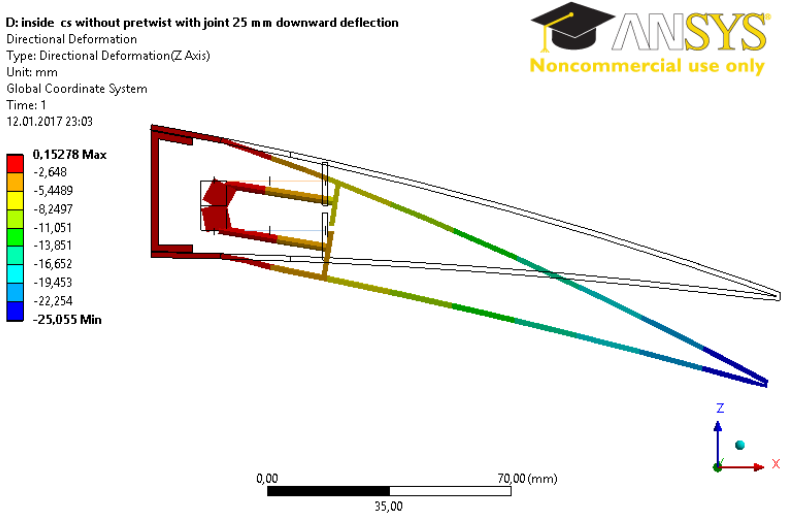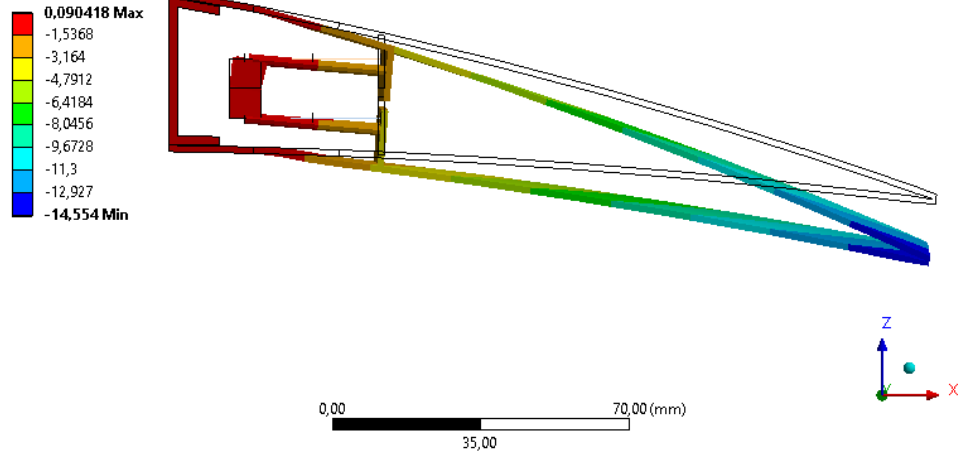
Figure 77: Z Directional Displacement Contours of the Control Surface –
Twist Investigation – Servo Actuators inside the Control Surface – without Pre-Twist
– Maximum 14.554 [mm]
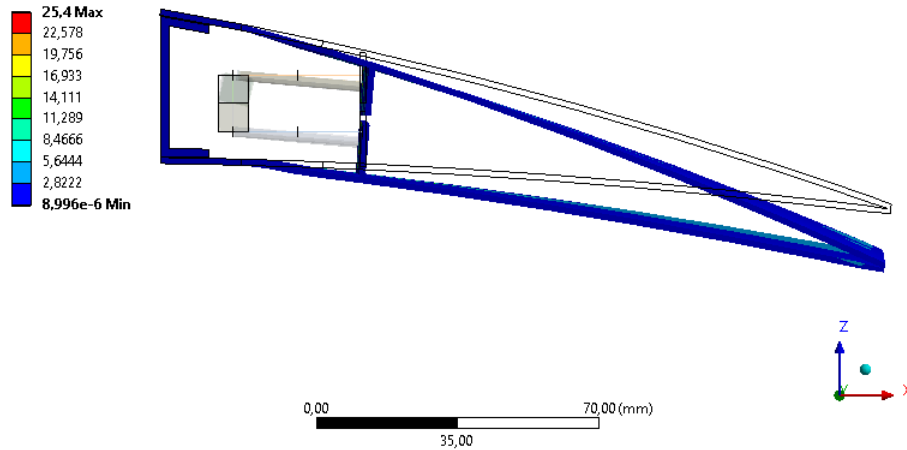
Figure 78: Equivalent Elastic Stress of the Control – Twist Investigation –
Servo Actuators inside the Control Surface – without Pre-Twist – Maximum 25.4
[MPa]
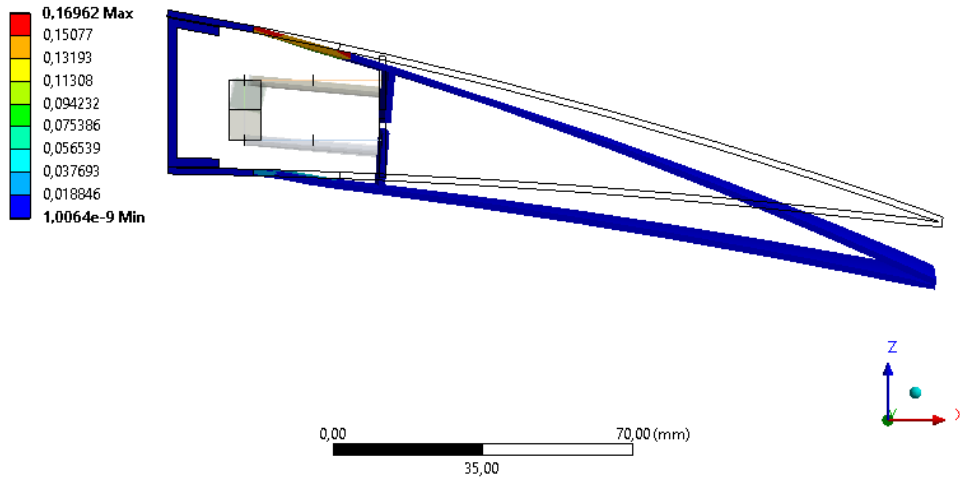
Figure 79: Equivalent Elastic Strain of the Control – Twist Investigation – Servo Actuators inside the Control Surface – without Pre-Twist – Maximum 0.16962 [mm/mm]
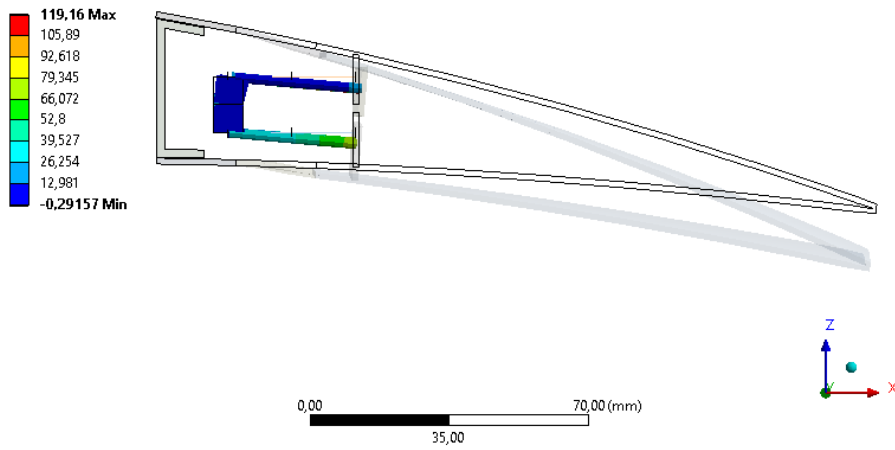
Figure 80: Maximum Combined Beam Stress of the Control – Twist Investigation – Servo Actuators inside the Control Surface – without Pre-Twist – Maximum 119.16 [MPa]

The values shown in Figure 78, Figure 79 and Figure 80 are safe in terms of yield stress and strain values of the material used.

The z directional displacements of the inboard and outboard edge point of the trailing edge control are shown in Figure 81. There is a 3.289 [mm] z directional difference between these edge points which gives an idea about the twist of the trailing edge control surface.
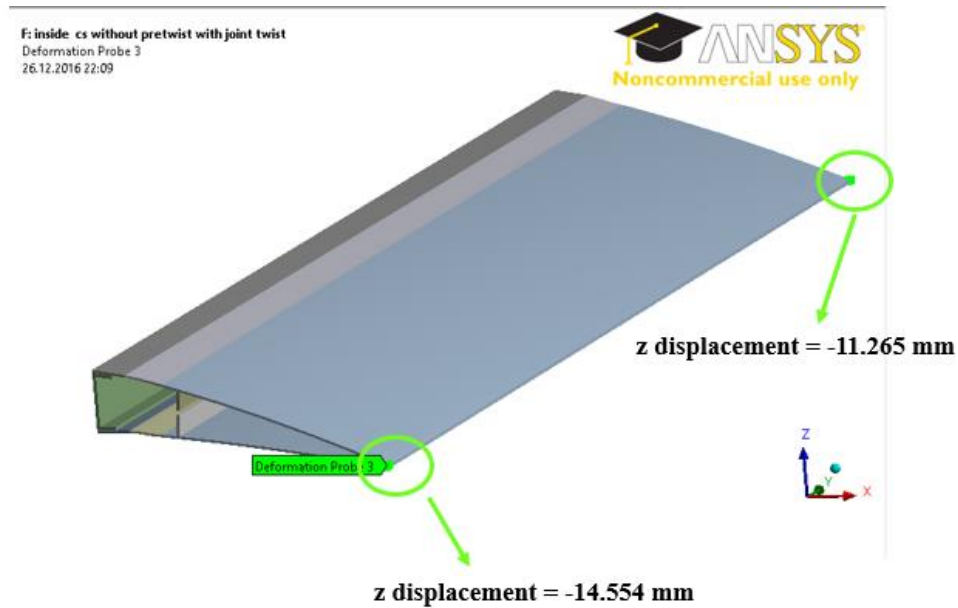
Figure 81: Inboard and Outboard Edge Point of the Trailing Edge Control Surface

The maximum torque value needed for the servo actuator actuates the upper surface of the control surface is -339.68 [N-mm] and the maximum torque value needed for the servo actuator actuates the lower surface of the control surface is -548.92 [N-mm]. It can be concluded that the reaction moment results are below the servo actuator torque limits.

5.3 Control Surface with Pre-Twist Configuration

5.3.1 Downward Deflection of the Hybrid Trailing Edge Control Surface

In this section, downward deflection of the hybrid trailing edge control surface without pre-twist configuration is studied. The limit of the downward deflection is determined. The baseline airfoil profile is selected as NACA 6510. Therefore all the downward deflection analyses starts from the baseline airfoil.

5.3.1.1 Deflection of NACA 6510 Profile by 15.2 [mm] in Transverse Direction

In order to deflect the tip of the hybrid trailing edge control surface 15.2 [mm] in vertical direction, rotation angles around y axis are defined +13.47 [deg] at the rotation center of the moment arms which actuate the upper part of the control surface and -3 [deg] rotation angles around y axis are defined at the center of the moment arms which actuate the lower part of the control surface.

The z directional displacement of the control surface is shown in Figure 82. Equivalent elastic stress and strain of the control surface are shown in Figure 83 and Figure 84 respectively. Maximum combined beam stress of the moment arms and transmission rods is given in Figure 85.
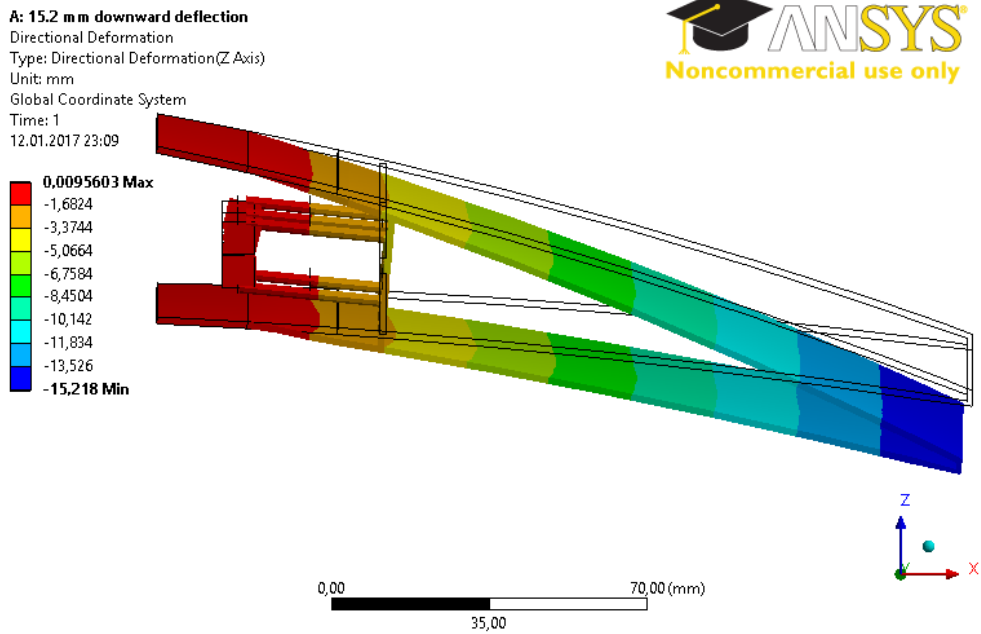
Figure 82: Z Directional Displacement Contours of the Control Surface –
15.2 [mm] Downward Deflected – Servo Actuators inside the Control Surface –with
Pre-Twist – Maximum 15.218 [mm]
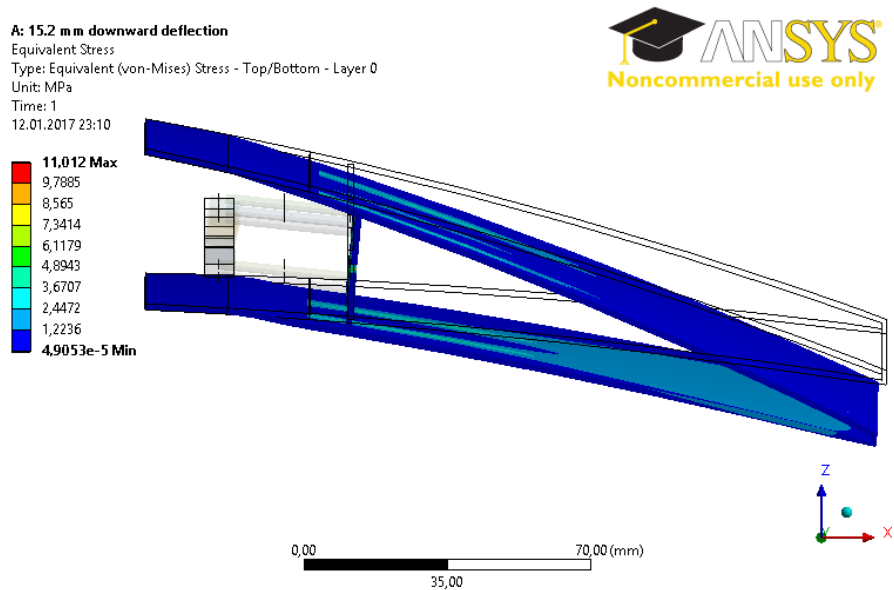
Figure 83: Equivalent Elastic Stress of the Control Surface 15.2 [mm]
Downward Deflected – Servo Actuators inside the Control Surface – with Pre-Twist
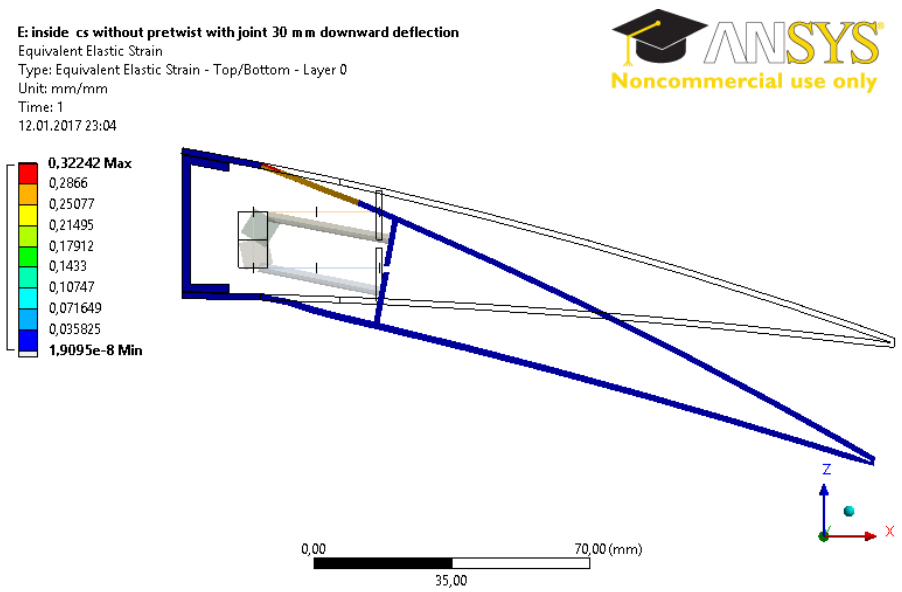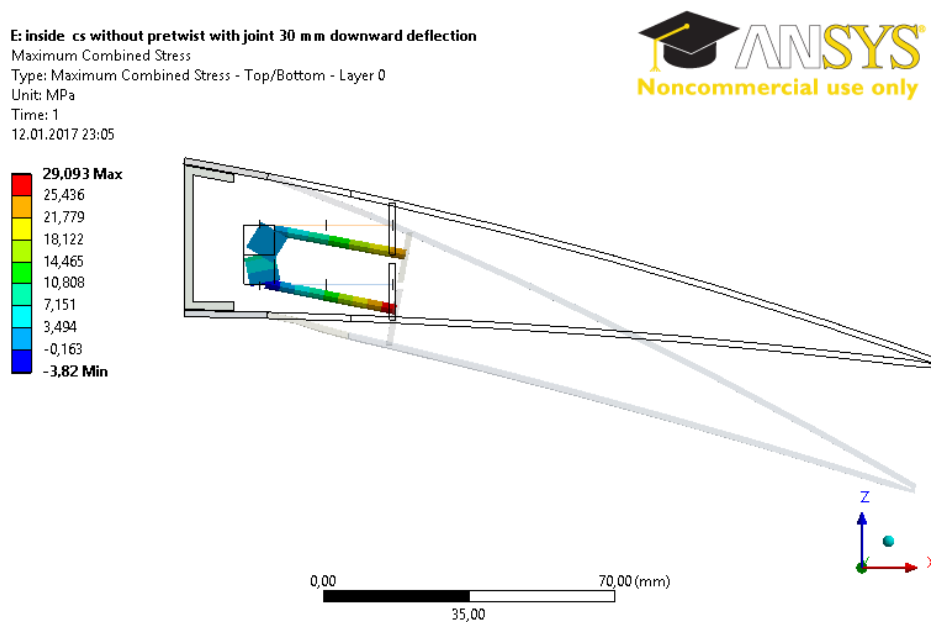– Maximum 11.012 [MPa]

73
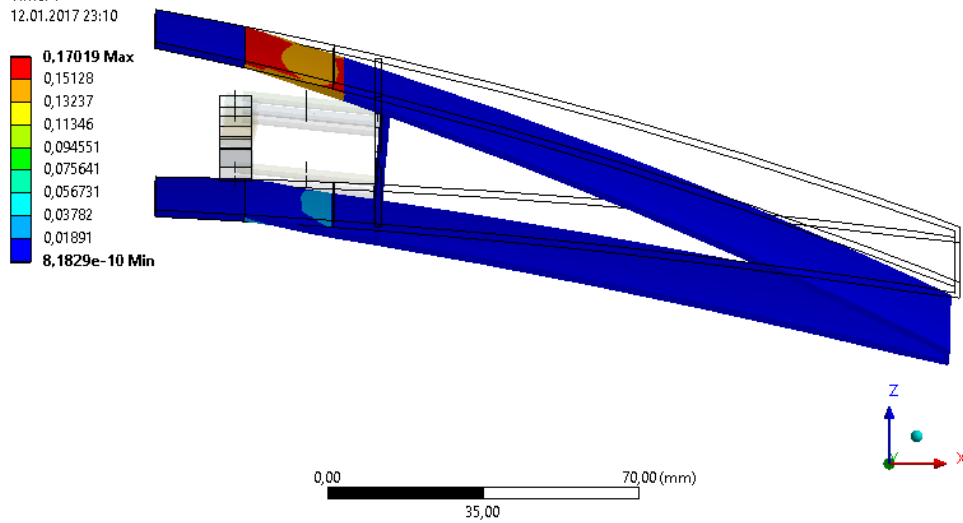
Figure 84: Equivalent Elastic Strain of the Control Surface 15.2 [mm] Downward Deflected – Servo Actuators inside the Control Surface – with Pre-Twist – Maximum 0.17019 [mm/mm]
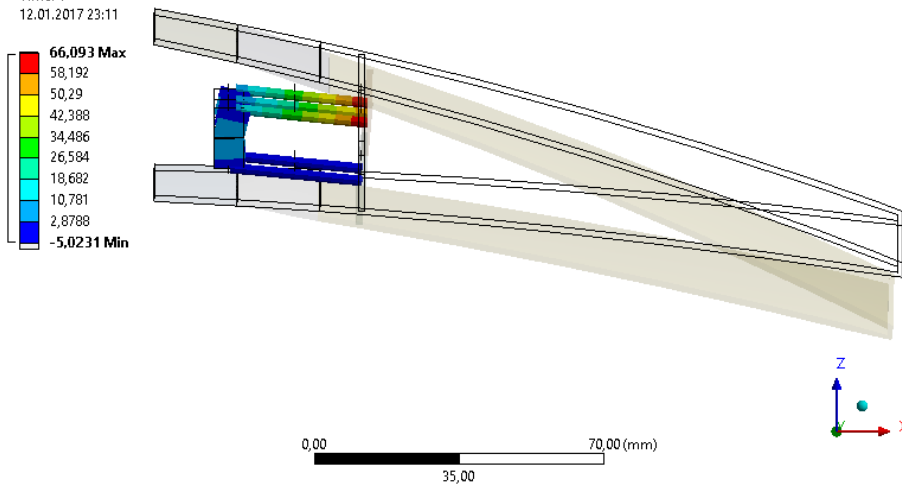
Figure 85: Maximum Combined Beam Stress of the Control Surface 15.2 [mm] Downward Deflected – Servo Actuators inside the Control Surface – with Pre-Twist – Maximum 66.093 [MPa]

The maximum torque value needed for the servo actuator actuates the upper surface of the control surface is -124.62 [N-mm] and the maximum torque value needed for the servo actuator actuates the lower surface of the control surface is -173.79 [N-mm]. It can be concluded that the reaction moment results are below the servo actuator torque limits.

5.3.1.2 Deflection of NACA 6510 Profile by 20 [mm] in Transverse Direction

In order to deflect the tip of the hybrid trailing edge control surface 20 [mm] in vertical direction, rotation angles around y axis are defined +17.3 [deg] at the rotation center of the moment arm which actuate the upper part of the control surface and -3 [deg] rotation angles around y axis are defined at the center of the moment arm which actuate the lower part of the control surface.

The z directional displacement of the control surface is shown in Figure 86. Equivalent elastic stress and strain of the control surface are shown in Figure 87 and Figure 88 respectively. Maximum combined beam stress of the moment arms and transmission rods is given in Figure 89.

Figure 86: Z Directional Displacement Contours of the Control Surface – 20 [mm] Downward Deflected – Servo Actuators inside the Control Surface –with Pre-Twist – Maximum 20.119 [mm]
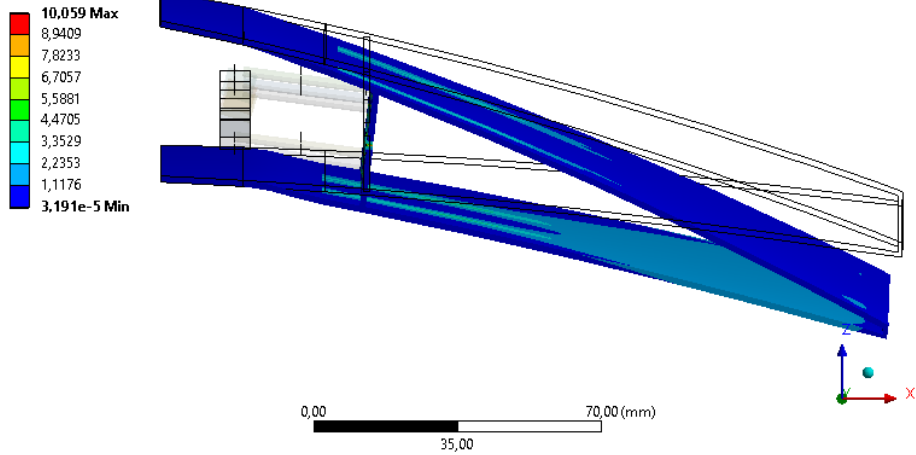
Figure 87: Equivalent Elastic Stress of the Control Surface 20 [mm] Downward Deflected – Servo Actuators inside the Control Surface – with Pre-Twist – Maximum 10.059 [MPa]
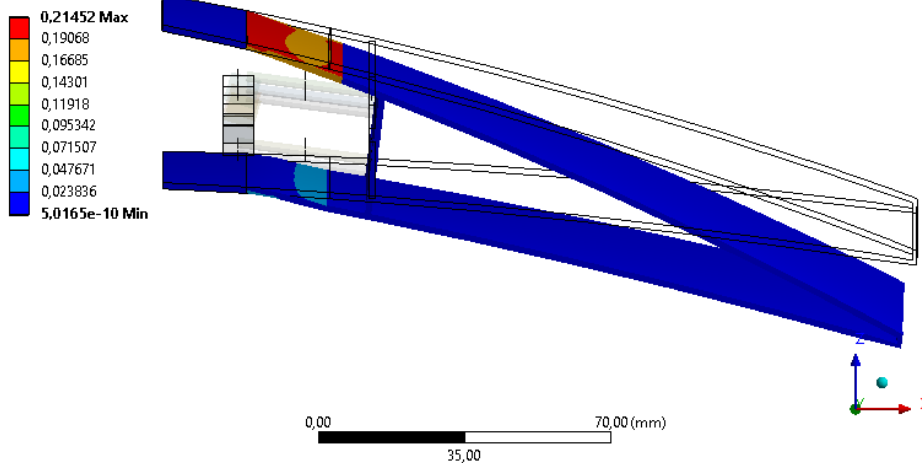
Figure 88: Equivalent Elastic Strain of the Control Surface 20 [mm] Downward Deflected – Servo Actuators inside the Control Surface – with Pre-Twist – Maximum 0.21452 [mm/mm]
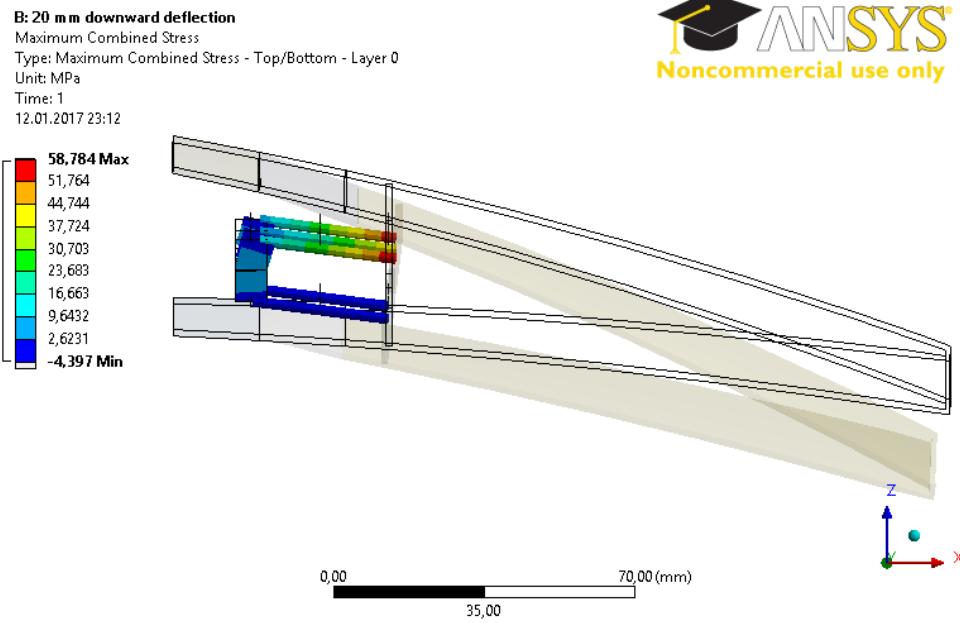
Figure 89: Maximum Combined Beam Stress of the Control Surface 20 [mm] Downward Deflected – Servo Actuators inside the Control Surface – with Pre-Twist – Maximum 58.784 [MPa]

The maximum torque value needed for the servo actuator actuates the upper surface of the control surface is -122.59 [N-mm] and the maximum torque value needed for the servo actuator actuates the lower surface of the control surface is -157.54 [N-mm]. It can be concluded that the reaction moment results are below the servo actuator torque limits.

5.3.1.3 Deflection of NACA 6510 Profile by 25 [mm] in Transverse Direction

In order to deflect the tip of the hybrid trailing edge control surface 25 [mm] in vertical direction, rotation angles around y axis are defined +21.3 [deg] at the rotation center of the moment arm which actuate the upper part of the control surface and -3 [deg] rotation angles around y axis are defined at the center of the moment arm which actuate the lower part of the control surface.

The z directional displacement of the control surface is shown in Figure 90. Equivalent elastic stress and strain of the control surface are shown in Figure 91 and

Figure 92 respectively. Maximum combined beam stress of the moment arms and transmission rods is given in Figure 93.
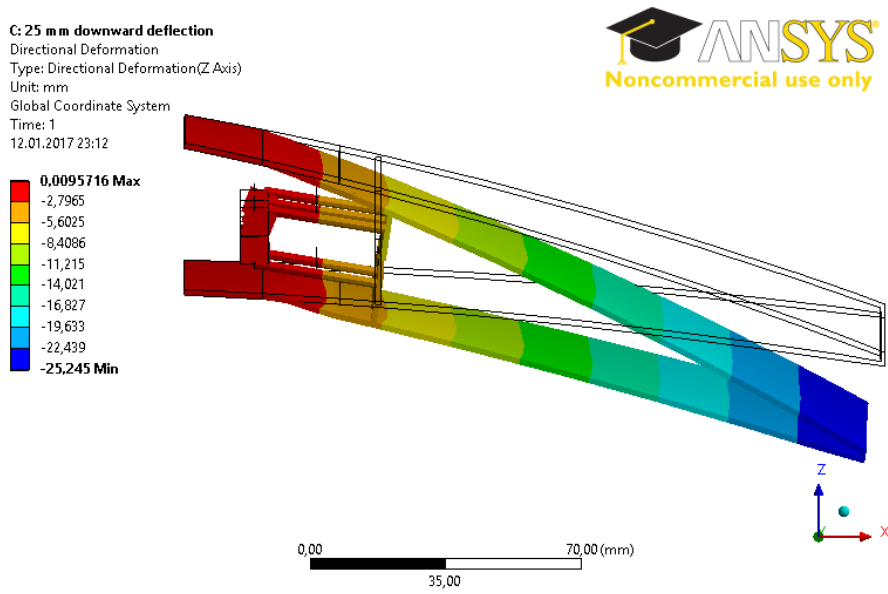
Figure 90: Z Directional Displacement Contours of the Control Surface – 25 [mm] Downward Deflected – Servo Actuators inside the Control Surface –with Pre-Twist – Maximum 25.245 [mm]
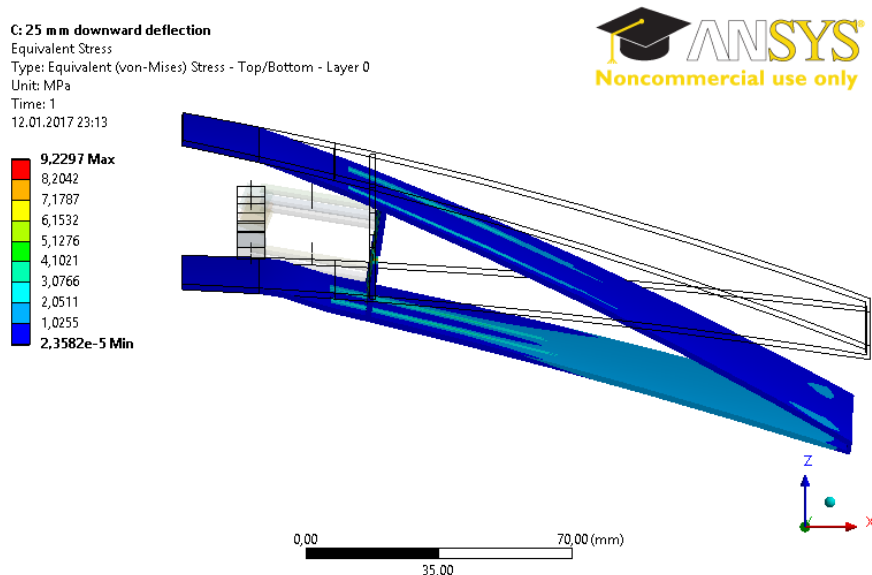
Figure 91: Equivalent Elastic Stress of the Control Surface 25 [mm] Downward Deflected – Servo Actuators inside the Control Surface – with Pre-Twist – Maximum 9.2297 [MPa]
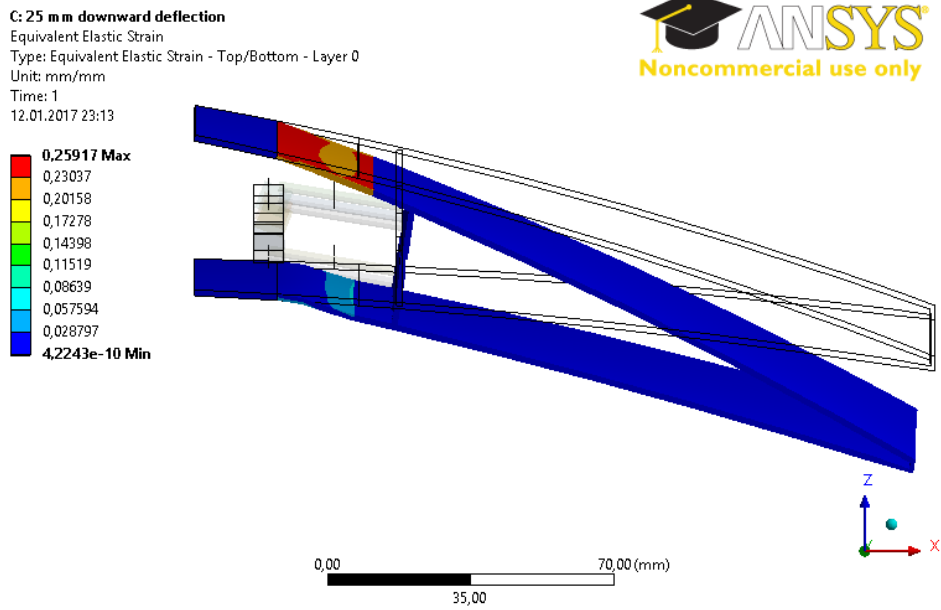
Figure 92: Equivalent Elastic Strain of the Control Surface 25 [mm]
Downward Deflected – Servo Actuators inside the Control Surface – with Pre-Twist
– Maximum 0.25917 [mm/mm]
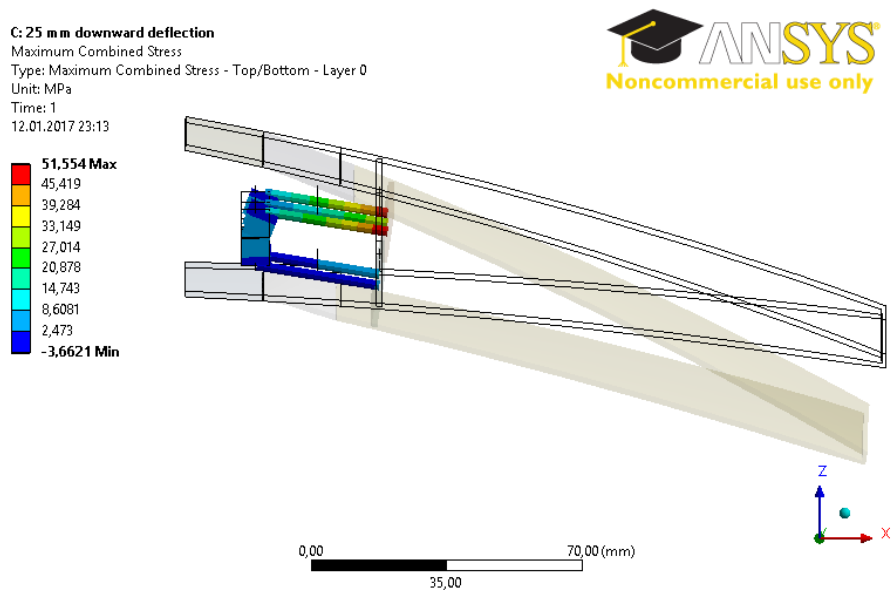
Figure 93: Maximum Combined Beam Stress of the Control Surface 25 [mm]
Downward Deflected – Servo Actuators inside the Control Surface – with Pre-Twist
– Maximum 51.554 [MPa]

The maximum torque value needed for the servo actuator actuates the upper surface of the control surface is -121.86 [N-mm] and the maximum torque value needed for the servo actuator actuates the lower surface of the control surface is -143.20 [N-mm]. It can be concluded that the reaction moment results are below the servo actuator torque limits.

5.3.1.4 Deflection of NACA 6510 Profile by 30 [mm] in Transverse Direction

In order to deflect the tip of the hybrid trailing edge control surface 30 [mm] in vertical direction, rotation angles around y axis are defined +25 [deg] at the rotation center of the moment arm which actuate the upper part of the control surface and -3 [deg] rotation angles around y axis are defined at the center of the moment arm which actuate the lower part of the control surface.

The z directional displacement of the control surface is shown in Figure 94. Equivalent elastic stress and strain of the control surface are shown in Figure 95 and Figure 96 respectively. Maximum combined beam stress of the moment arms and transmission rods is given in Figure 97.
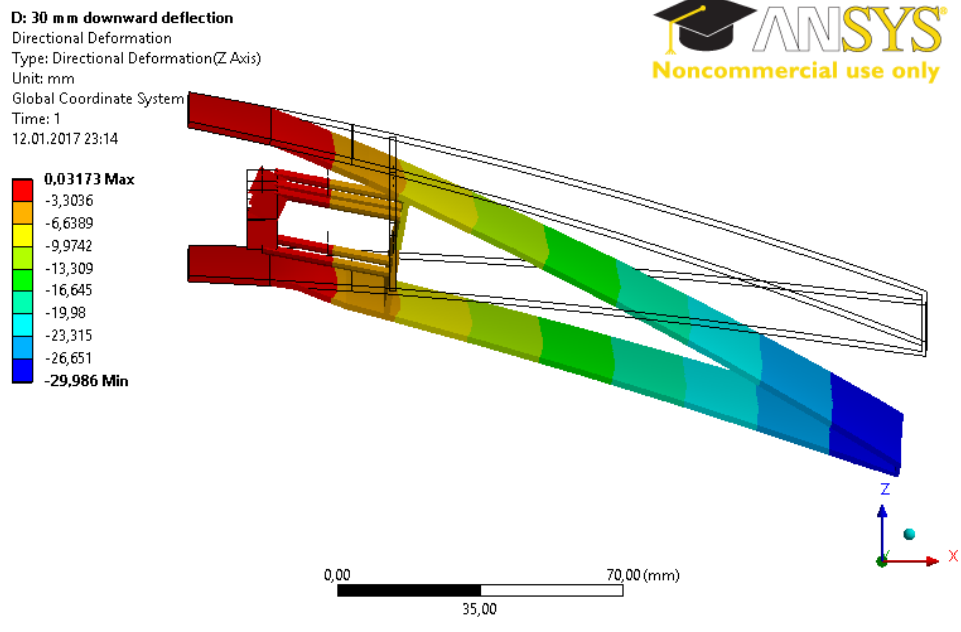
Figure 94: Z Directional Displacement Contours of the Control Surface – 30 [mm] Downward Deflected – Servo Actuators inside the Control Surface –with Pre-Twist – Maximum 29.986 [mm]
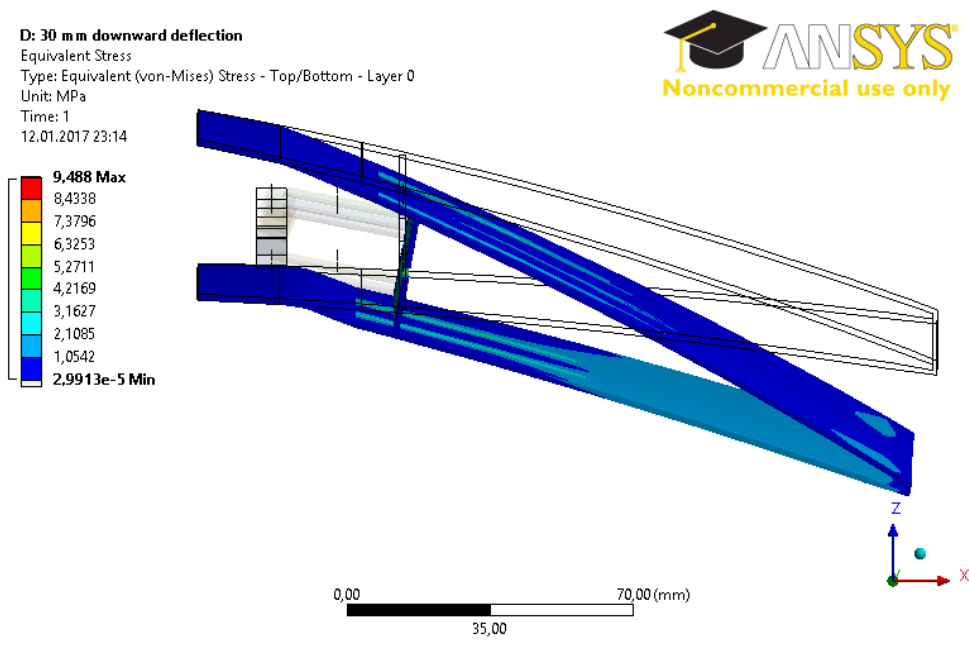
Figure 95: Equivalent Elastic Stress of the Control Surface 30 [mm] Downward Deflected – Servo Actuators inside the Control Surface – with Pre-Twist – Maximum 9.488 [MPa]
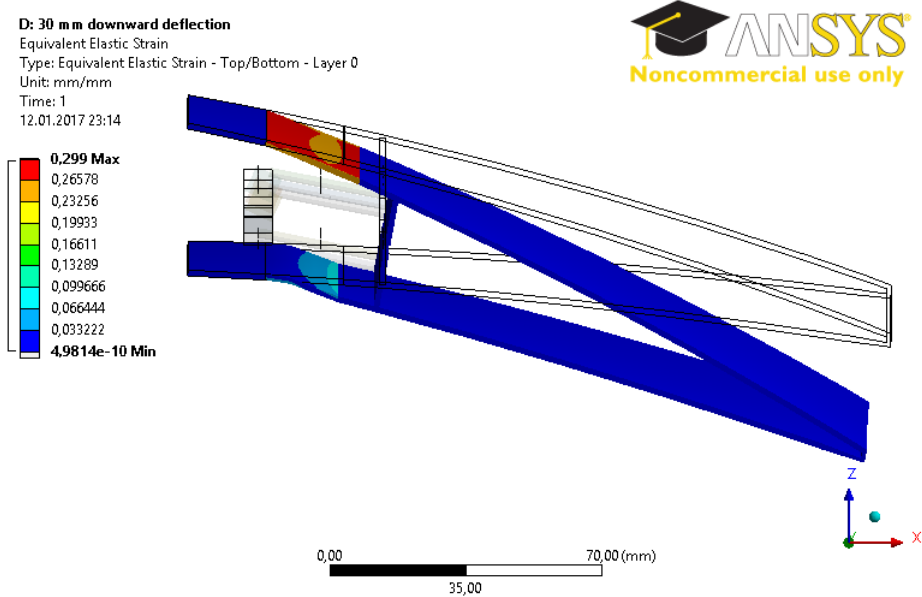
Figure 96: Equivalent Elastic Strain of the Control Surface 30 [mm]
Downward Deflected – Servo Actuators inside the Control Surface – with Pre-Twist
– Maximum 0.299 [mm/mm]
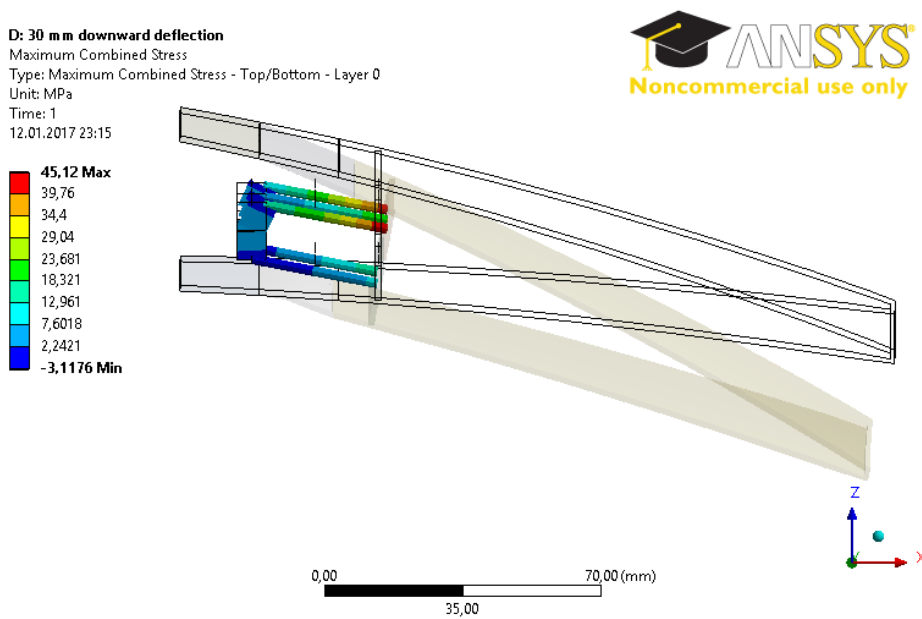
Figure 97: Maximum Combined Beam Stress of the Control Surface 30 [mm]
Downward Deflected – Servo Actuators inside the Control Surface – with Pre-Twist
– Maximum 45.12 [MPa]

The maximum torque value needed for the servo actuator actuates the upper surface of the control surface is -122.22 [N-mm] and the maximum torque value needed for the servo actuator actuates the lower surface of the control surface is -132.62 [N-mm]. It can be concluded that the reaction moment results are below the servo actuator torque limits.

5.3.1.5 Discussion and Conclusion

The maximum von Mises strain results of the all the downward deflection cases are tabulated in Table 15.

Table 15: Maximum von Mises Strain Comparison

	Maximum von Mises Strain [mm/mm]*
15.2 [mm] Deflection Case	0.17019
20.0 [mm] Deflection Case	0.21452
25.0 [mm] Deflection Case	0.25917
30.0 [mm] Deflection Case	0.299

* Maximum von Misses Strain is observed for the compliant part and its strain limit must be smaller than 1.

The results of maximum von Mises stress, maximum combined beam stresses and required servo actuator torques to actuate upper and lower surface of the trailing edge control surface are given in Table 16, Table 17, Table 18 and Table 19 respectively. Indicated values are safe in terms of yield stress and strain values of the material used and servo torque limit capability.

Table 16: Maximum von Mises Stress Comparison

	Maximum von Mises Stress [MPa]*
15.2 [mm] Deflection Case	11.012
20.0 [mm] Deflection Case	10.059
25.0 [mm] Deflection Case	9.2297
30.0 [mm] Deflection Case	9.488

* Maximum von Misses Stress is observed for the transmission parts and their yield stress is 280 [MPa]

Table 17: Maximum Combined Beam Stress

	Maximum Combined Beam Stress [MPa]*
15.2 [mm] Deflection Case	66.093
20.0 [mm] Deflection Case	58.784
25.0 [mm] Deflection Case	51.554
30.0 [mm] Deflection Case	45.12

*Aluminum is used for beams and its yield point is 280 [MPa]

Table 18: Servo Actuator Torque Required to Actuate the Upper Surface of the Control Surface

	Servo Actuate Upper Surface [N-mm]*
15.2 [mm] Deflection Case	-124.62
20.0 [mm] Deflection Case	-122.59
25.0 [mm] Deflection Case	-121.86
30.0 [mm] Deflection Case	-122.22

*Servo actuator torque capacity is 600 [Nmm]

Table 19: Servo Actuator Torque Required to Actuate the Lower Surface of the Control Surface

	Servo Actuate Lower Surface [N-mm]*
15.2 [mm] Deflection Case	-173.79
20.0 [mm] Deflection Case	-157.54
25.0 [mm] Deflection Case	-143.2
30.0 [mm] Deflection Case	-132.62

*Servo actuator torque capacity is 600 [Nmm]

5.3.2 Investigation of Twist Capability of the Hybrid Trailing Edge Control Surface

In order to twist the hybrid trailing edge control surface, the angles of 6 [deg], 10 [deg] and 15.3 [deg] are defined at the outboard, middle and inboard upper servo actuators respectively. Also the angles of -1 [deg] and -3 [deg] are defined at the outboard and inboard lower servo actuators respectively.

The z directional displacement of the control surface is shown in Figure 98. Equivalent elastic stress and strain of the control surface are shown in Figure 99 and Figure 100 respectively. Maximum combined beam stress of the moment arms and transmission rods is given in Figure 101.
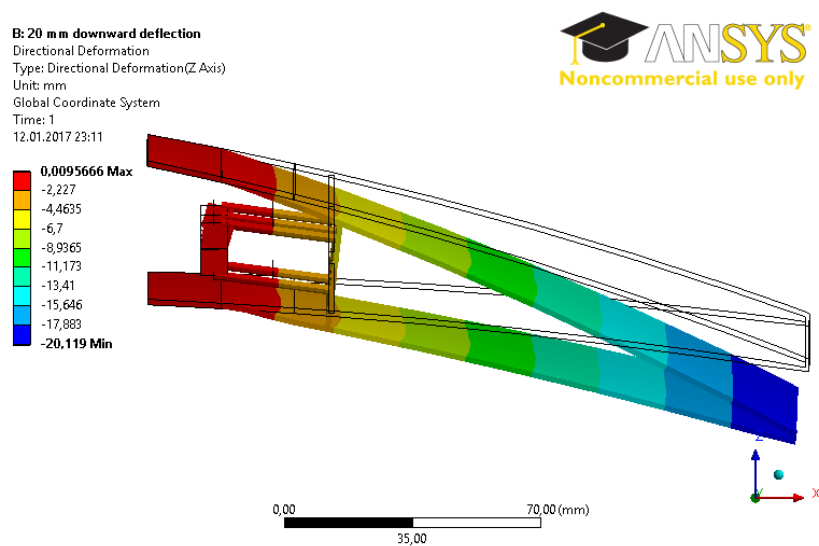

Figure 98: Z Directional Displacement Contours of the Control Surface – Twist Investigation – Servo Actuators inside the Control Surface – with Pre-Twist – Maximum 14.395 [mm]
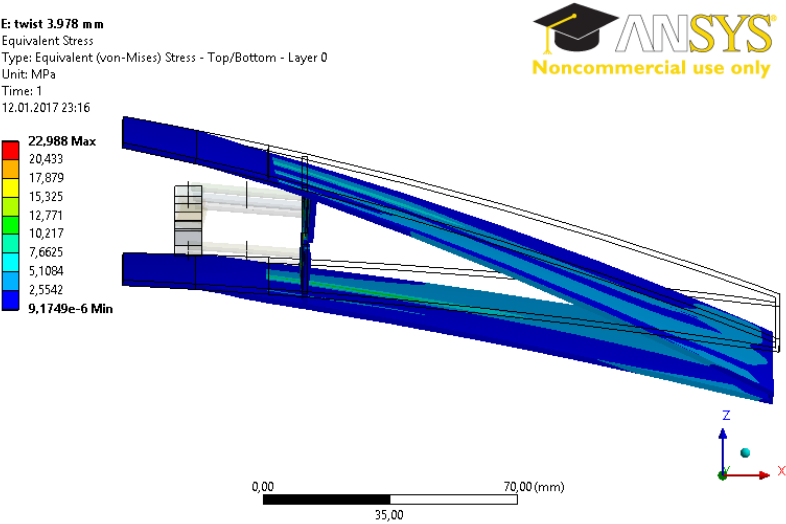
Figure 99: Equivalent Elastic Stress of the Control – Twist Investigation – Servo Actuators inside the Control Surface – with Pre-Twist – Maximum 22.988 [MPa]

86
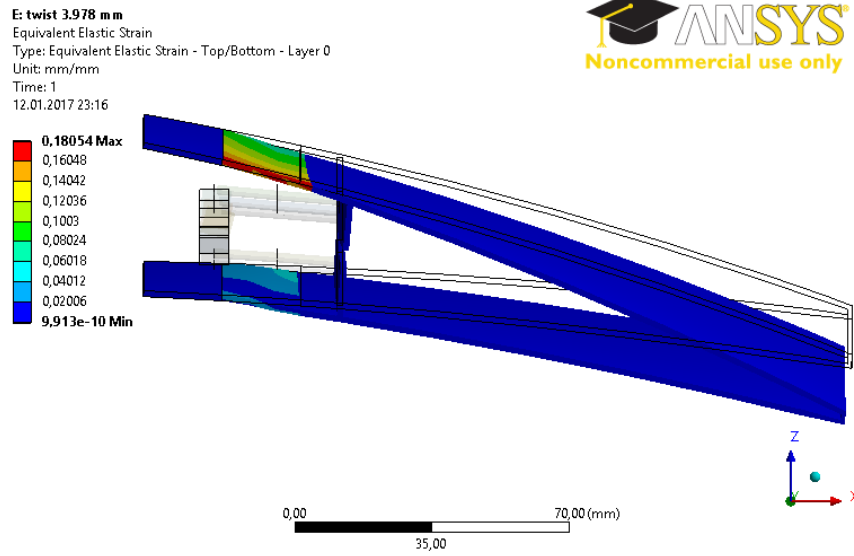
Figure 100: Equivalent Elastic Strain of the Control – Twist Investigation –
Servo Actuators inside the Control Surface – with Pre-Twist – Maximum 0.18054
[mm/mm]
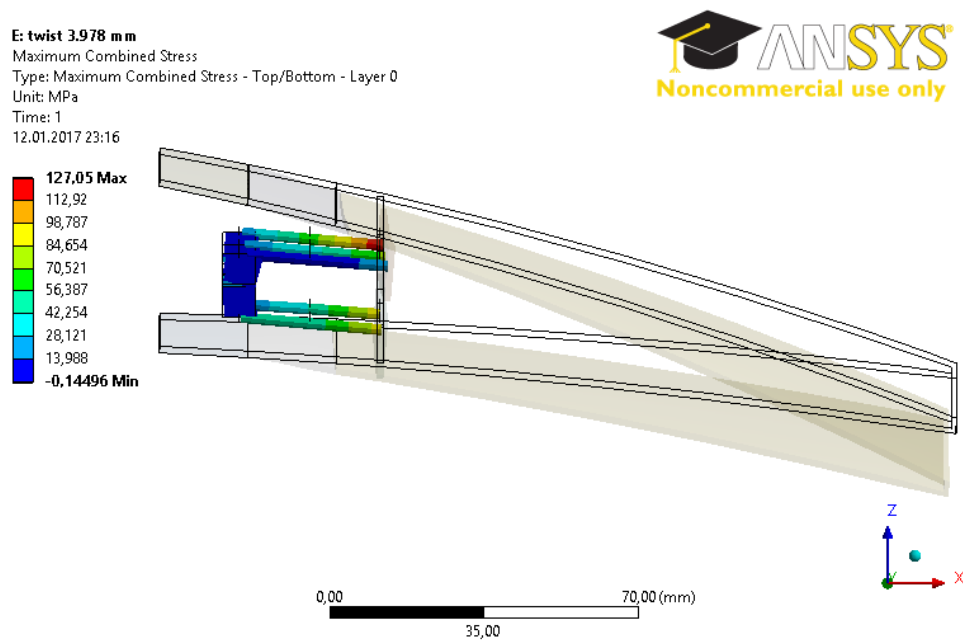
Figure 101: Maximum Combined Beam Stress of the Control – Twist
Investigation – Servo Actuators inside the Control Surface – with Pre-Twist –
Maximum 127.05 [MPa]

The values shown in Figure 99, Figure 100 and Figure 101 are safe in terms of yield stress and strain values of the material used.

The z directional displacements of the inboard and outboard edge point of the trailing edge control are shown in Figure 102. There is a 3.978 [mm] z directional difference between these edge points which gives an idea about the twist of the trailing edge control surface.
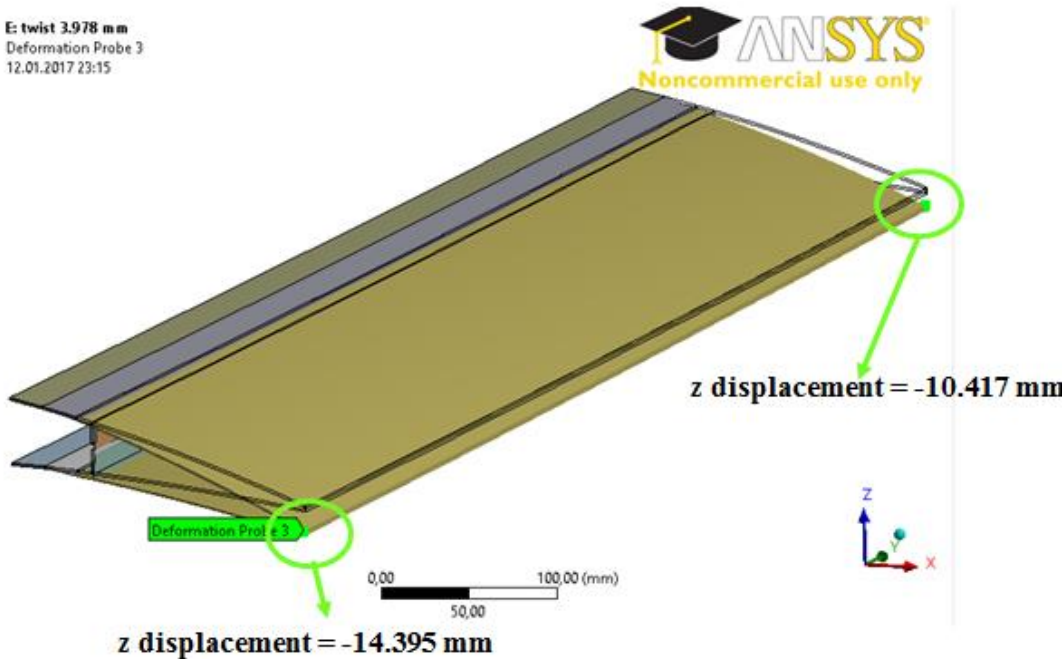
Figure 102: Inboard and Outboard Edge Point of the Trailing Edge Control Surface

The maximum torque value needed for the servo actuator actuates the upper surface of the control surface is -301.04 [N-mm] and the maximum torque value needed for the servo actuator actuates the lower surface of the control surface is -599.46 [N-mm]. It can be concluded that the reaction moment results are below the servo actuator torque limits.

5.4 Discussion and Conclusion

In this chapter, static structural finite element analyses of the hybrid trailing edge control surface which have servo actuators inside the control surface volume are performed in in-vacuo condition. Both control surface with and without pre-twist conditions are considered. Only downward deflection of the control surface is analyzed. After proving the ability of downward deflection up to NACA 9510 profile, the limits of the downward deflection is examined. Finally, the twist capability of the trailing edge control surface is proved.

According to the results, both configurations can perform downward deflection up to 30 [mm] and twisting motion without exceeding the torque capacity of the servo actuators or material limits.

Note that, as the downward deflection increases, the servo actuators loads tend to decrease towards zero. This is an expected result. Initially, servo actuators torque sign are negative. In other words, they are trying to hold the control surface against gravity. But as the compliant part stretches, it consumes some power of servo actuators and the absolute value of the torque is decreases. If we further stretch the compliant part, servo actuator torque sign will become positive and both servo actuators and gravity will try to balance the compliant part.

CHAPTER 6

STRUCTURAL ANALYSIS OF THE HYBRID TRAILING EDGE CONTROL SURFACE WITH THE ACTATORS INSIDE THE TORQUE BOX VOLUME IN IN-VACUO CONDITION

6.1 Introduction

In this chapter, finite element analysis of the hybrid trailing edge control surface with the servo actuator inside the torque box volume is performed in in-vacuo condition. Both control surfaces with pre-twist and without pre-twist are analyzed. Static Structural module of ANSYS v14.0 program is used for finite element analyses. Only downward deflection of the control surface is examined. First of all, the downward deflection of the airfoil profile from NACA 6510 to NACA 9510 profile is tested. If the trailing edge control surface is capable of this morphing, further deflection of the control surface is also studied. The camber deflection limit of the control surface is determined. Finally, twist capability of the designed control surface is studied. Since the available volume for servo actuators in the torque box is greater than the available volume in control surface, servo actuators inside the torque box are stronger than the servo actuators inside the control surface volume. Also during downward deflection of the control surface; there is no risk for servo actuators to touch the upper surface of the control surface. As a result, more deflection of the control surface with the servo actuators inside the torque box is expected with compared to the control surface inside the control surface volume.

6.2 Control Surface without Pre-Twist Configuration

6.2.1 Downward Deflection of the Hybrid Trailing Edge Control Surface

In this section, downward deflection of the hybrid trailing edge control surface is studied. The limit of the downward deflection is determined. The baseline airfoil profile is selected as NACA 6510. Therefore all the downward deflection analyses starts from the baseline airfoil.

6.2.1.1 Deflection of NACA 6510 Profile by 15.2 [mm] in Transverse Direction

In section 5.2.1.1, it was shown that the around 15.2 [mm] transverse tip deflection of the trailing edge control surface is needed in order to morph from NACA 6510 profile to NACA 9510 profile. This morphing is tried to be achieved with the control surface having the servo actuators inside the torque box volume.

In order to deflect the tip of the hybrid trailing edge control surface 15.2 [mm] in vertical direction, rotation angles around y axis are defined +18.35 [deg] at the rotation center of the moment arms which actuate the upper part of the control surface and -10.7 [deg] rotation angles around y axis are defined at the center of the moment arms which actuate the lower part of the control surface.

The z directional displacement of the control surface is shown in Figure 103. Equivalent elastic stress and strain of the control surface are shown in Figure 104 and Figure 105 respectively. Maximum combined beam stress of the moment arms and transmission rods is given in Figure 106.

Figure 103: Z Directional Displacement Contours of the Control Surface –
15.2 [mm] Downward Deflected – Servo Actuators inside the Torque Box Volume –
without Pre-Twist – Maximum 15.217 [mm]

Figure 104: Equivalent Elastic Stress of the Control Surface 15.2 [mm]
Downward Deflected – Servo Actuators inside the Torque Box Volume – without
Pre-Twist – Maximum 26.917 [MPa]

Figure 105: Equivalent Elastic Strain of the Control Surface 15.2 [mm] Downward Deflected – Servo Actuators inside the Torque Box Volume – without Pre-Twist – Maximum 0.3453 [mm/mm]

Figure 106: Maximum Combined Beam Stress of the Control Surface 15.2 [mm] Downward Deflected – Servo Actuators inside the Torque Box Volume – without Pre-Twist – Maximum 47.756 [MPa]

The maximum torque value needed for the servo actuator actuates the upper surface of the control surface is -99.08 [N-mm] and the maximum torque value needed for the servo actuator actuates the lower surface of the control surface is -269.08 [N-mm]. It can be concluded that the reaction moment results are below the servo actuator torque limits.

6.2.1.2 Deflection of NACA 6510 Profile by 20 [mm] in Transverse Direction

In order to deflect the tip of the hybrid trailing edge control surface 20 [mm] in vertical direction, rotation angles around y axis are defined +21.4 [deg] at the rotation center of the moment arm which actuate the upper part of the control surface and -10.7 [deg] rotation angles around y axis are defined at the center of the moment arm which actuate the lower part of the control surface.

The z directional displacement of the control surface is shown in Figure 107. Equivalent elastic stress and strain of the control surface are shown in Figure 108 and Figure 109 respectively. Maximum combined beam stress of the moment arms and transmission rods is given in Figure 110.
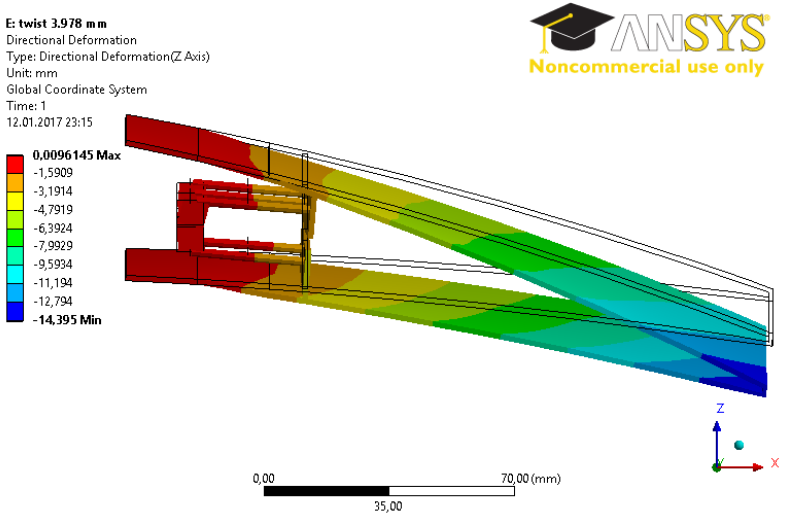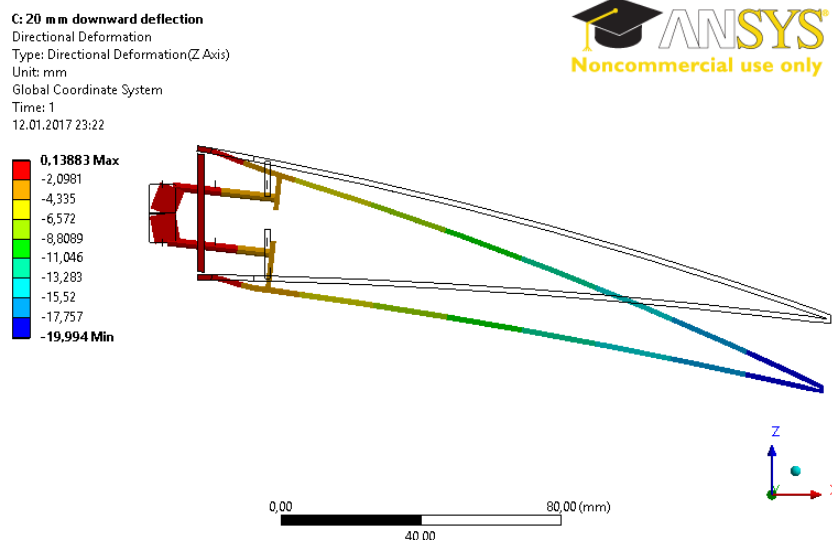

Figure 107: Z Directional Displacement Contours of the Control Surface – 20 [mm] Downward Deflected – Servo Actuators inside the Torque Box Volume – without Pre-Twist – Maximum 19.994 [mm]

95
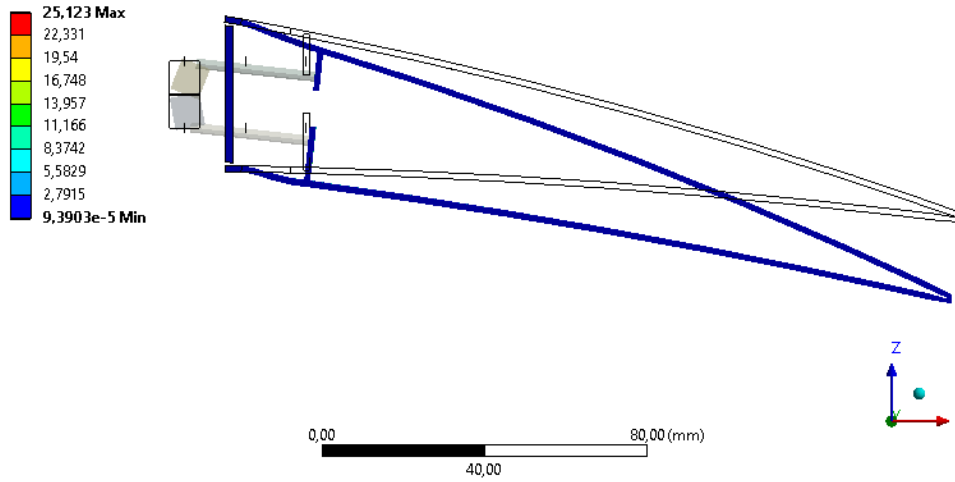
Figure 108: Equivalent Elastic Stress of the Control Surface 20 [mm] Downward Deflected – Servo Actuators inside the Torque Box Volume – without Pre-Twist – Maximum 25.123 [MPa]
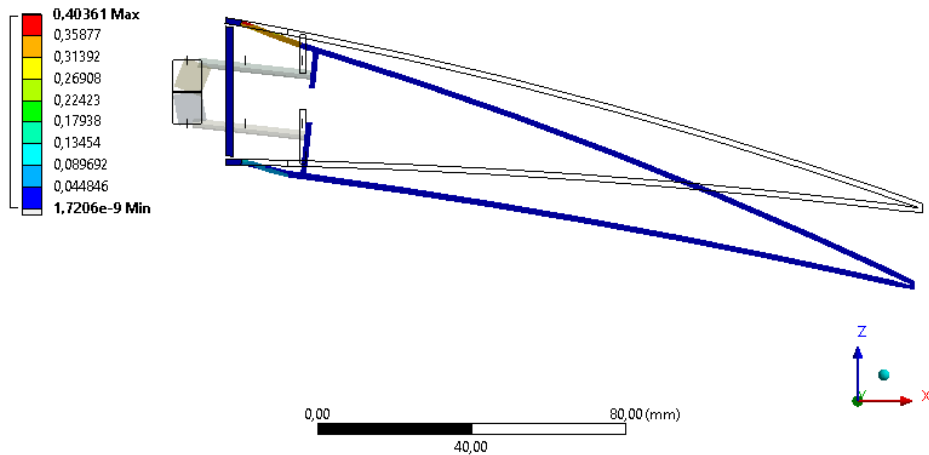
Figure 109: Equivalent Elastic Strain of the Control Surface 20 [mm] Downward Deflected – Servo Actuators inside the Torque Box Volume – without Pre-Twist – Maximum 0.40361 [mm/mm]
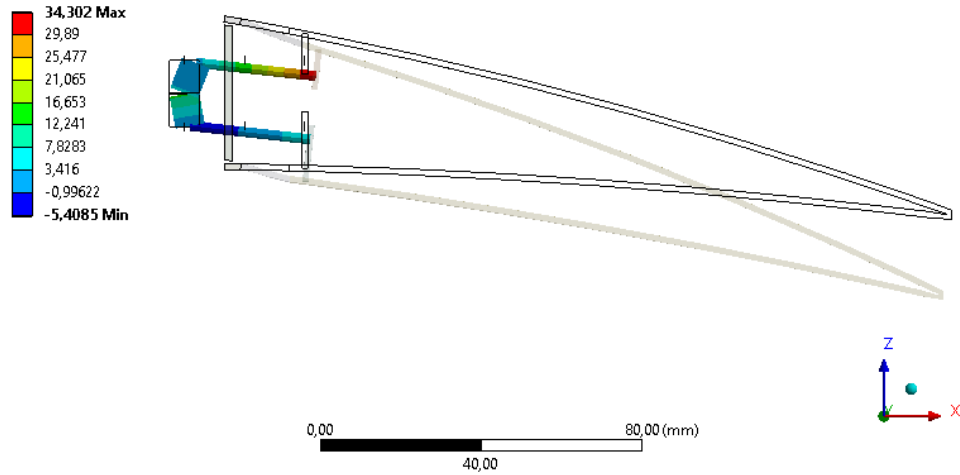
Figure 110: Maximum Combined Beam Stress of the Control Surface 20 [mm] Downward Deflected – Servo Actuators inside the Torque Box Volume – without Pre-Twist – Maximum 34.302 [MPa]

The maximum torque value needed for the servo actuator actuates the upper surface of the control surface is 71.84 [N-mm] and the maximum torque value needed for the servo actuator actuates the lower surface of the control surface is 238.95 [N-mm]. It can be concluded that the reaction moment results are below the servo actuator torque limits.

6.2.1.3 Deflection of NACA 6510 Profile by 25 [mm] in Transverse Direction

In order to deflect the tip of the hybrid trailing edge control surface 25 [mm] in vertical direction, rotation angles around y axis are defined +24.6 [deg] at the rotation center of the moment arm which actuate the upper part of the control surface and -10.7 [deg] rotation angles around y axis are defined at the center of the moment arm which actuate the lower part of the control surface.

The z directional displacement of the control surface is shown in Figure 111. Equivalent elastic stress and strain of the control surface are shown in Figure 112 and

Figure 113 respectively. Maximum combined beam stress of the moment arms and transmission rods is given in Figure 114.

Figure 111: Z Directional Displacement Contours of the Control Surface – 25 [mm] Downward Deflected – Servo Actuators inside the Torque Box Volume – without Pre-Twist – Maximum 25.009 [mm]
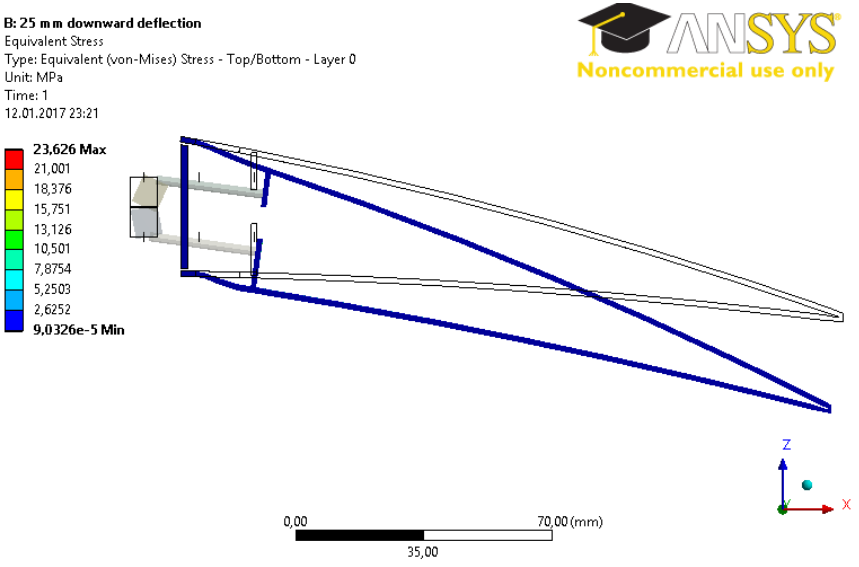
Figure 112: Equivalent Elastic Stress of the Control Surface 25 [mm] Downward Deflected – Servo Actuators inside the Torque Box Volume – without Pre-Twist – Maximum 23.626 [MPa]

98
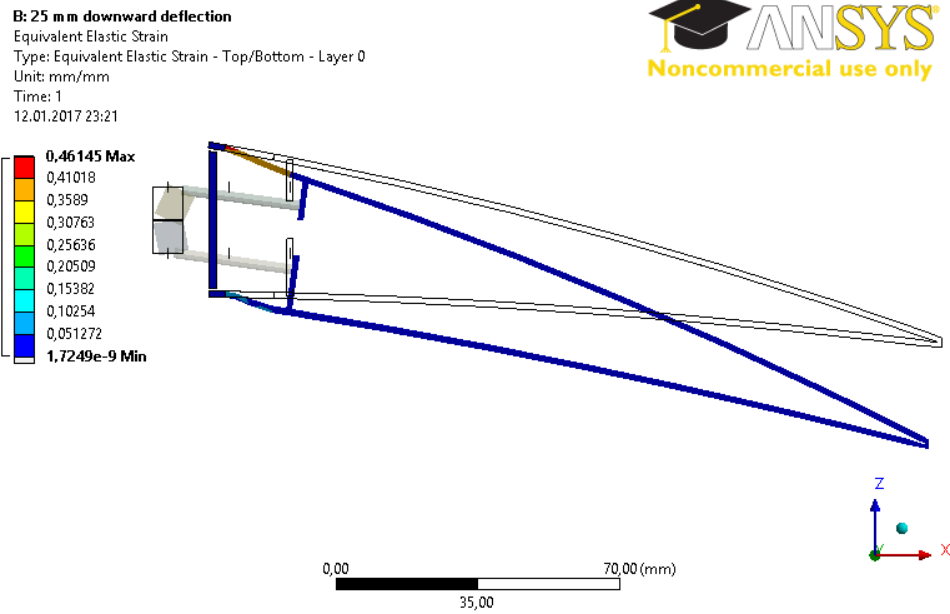
Figure 113: Equivalent Elastic Strain of the Control Surface 25 [mm] Downward Deflected – Servo Actuators inside the Torque Box Volume – without Pre-Twist – Maximum 0.46145 [mm/mm]
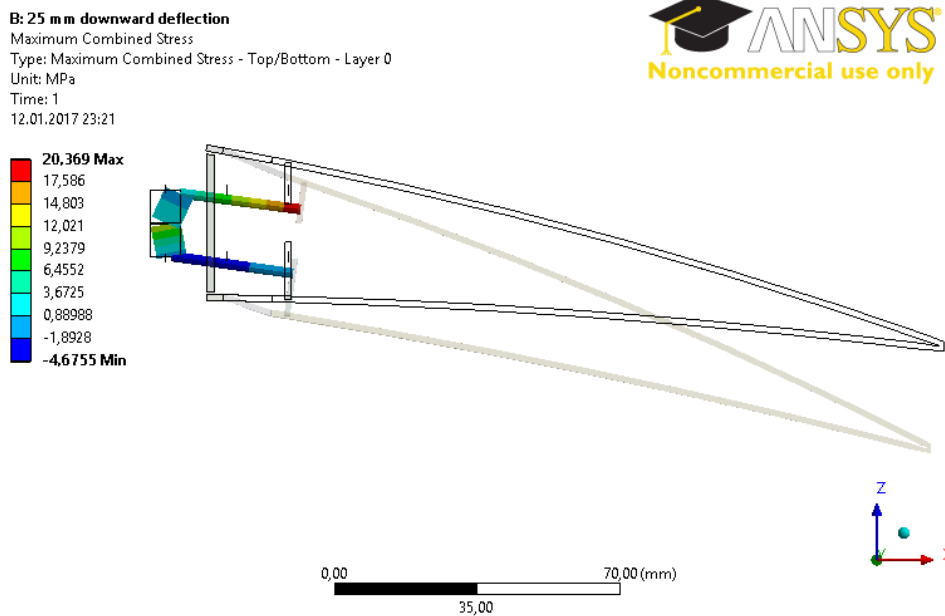
Figure 114: Maximum Combined Beam Stress of the Control Surface 25 [mm] Downward Deflected – Servo Actuators inside the Torque Box Volume – without Pre-Twist – Maximum 20.369 [MPa]

99

The maximum torque value needed for the servo actuator actuates the upper surface of the control surface is -44.83 [N-mm] and the maximum torque value needed for the servo actuator actuates the lower surface of the control surface is -209.66 [N-mm]. It can be concluded that the reaction moment results are below the servo actuator torque limits.

6.2.1.4 Deflection of NACA 6510 Profile by 30 [mm] in Transverse Direction

In order to deflect the tip of the hybrid trailing edge control surface 30 [mm] in vertical direction, rotation angles around y axis are defined +28 [deg] at the rotation center of the moment arm which actuate the upper part of the control surface and -10.7 [deg] rotation angles around y axis are defined at the center of the moment arm which actuate the lower part of the control surface.

The z directional displacement of the control surface is shown in Figure 115. Equivalent elastic stress and strain of the control surface are shown in Figure 116 and Figure 117 respectively. Maximum combined beam stress of the moment arms and transmission rods is given in Figure 118.
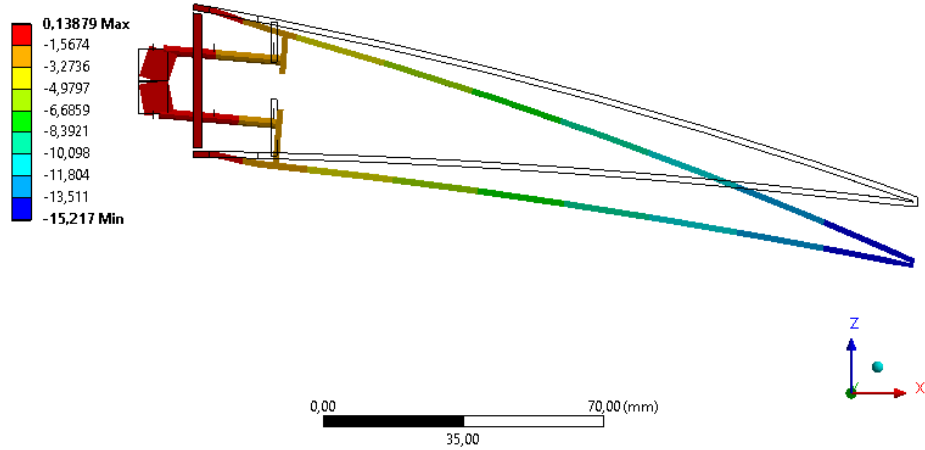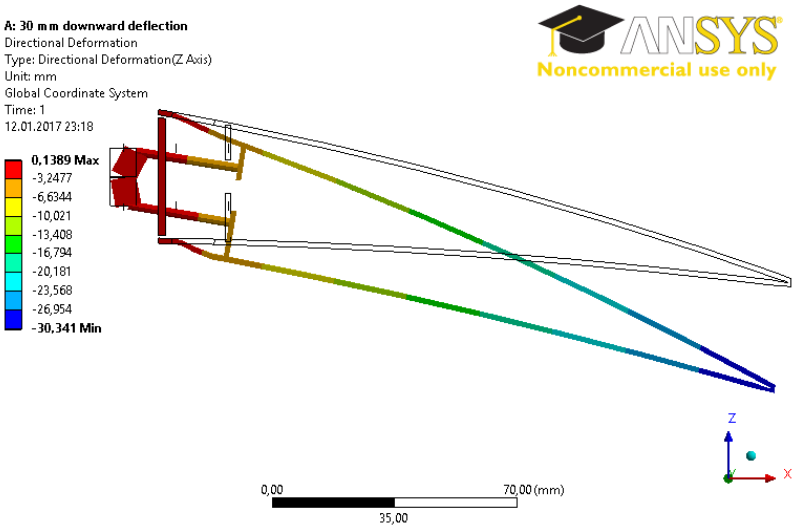

Figure 115: Z Directional Displacement Contours of the Control Surface – 30 [mm] Downward Deflected – Servo Actuators inside the Torque Box Volume – without Pre-Twist – Maximum 30.341 [mm]
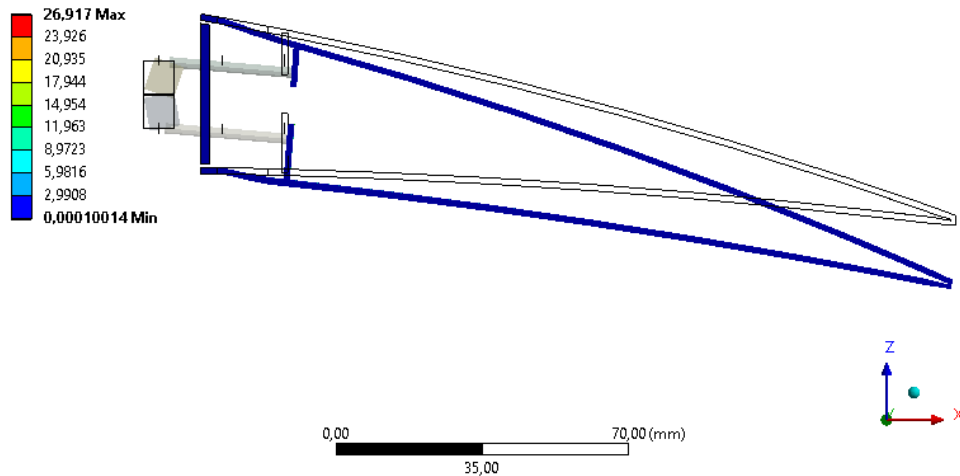
100
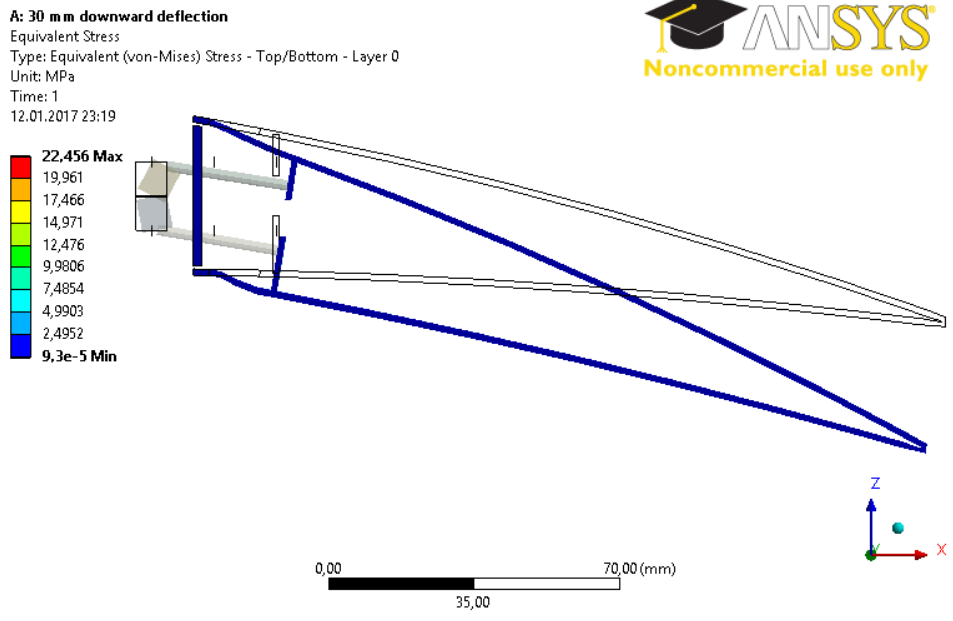
Figure 116: Equivalent Elastic Stress of the Control Surface 30 [mm] Downward Deflected – Servo Actuators inside the Torque Box Volume – without Pre-Twist – Maximum 22.456 [MPa]
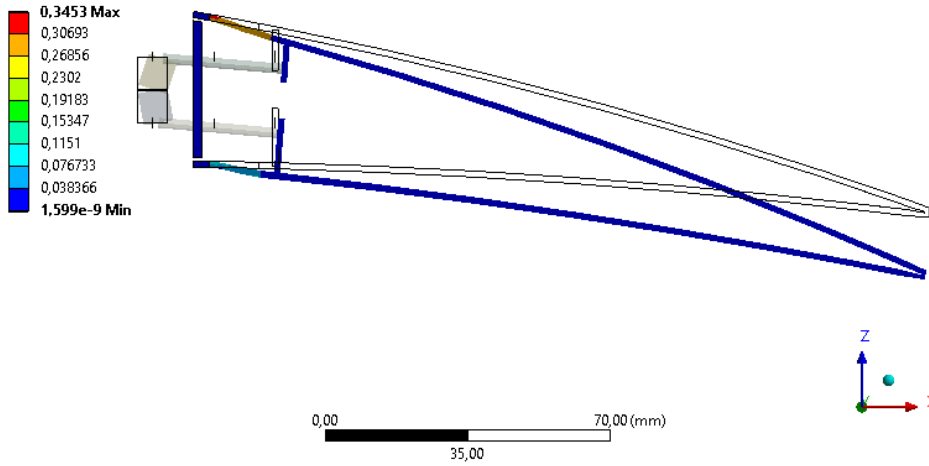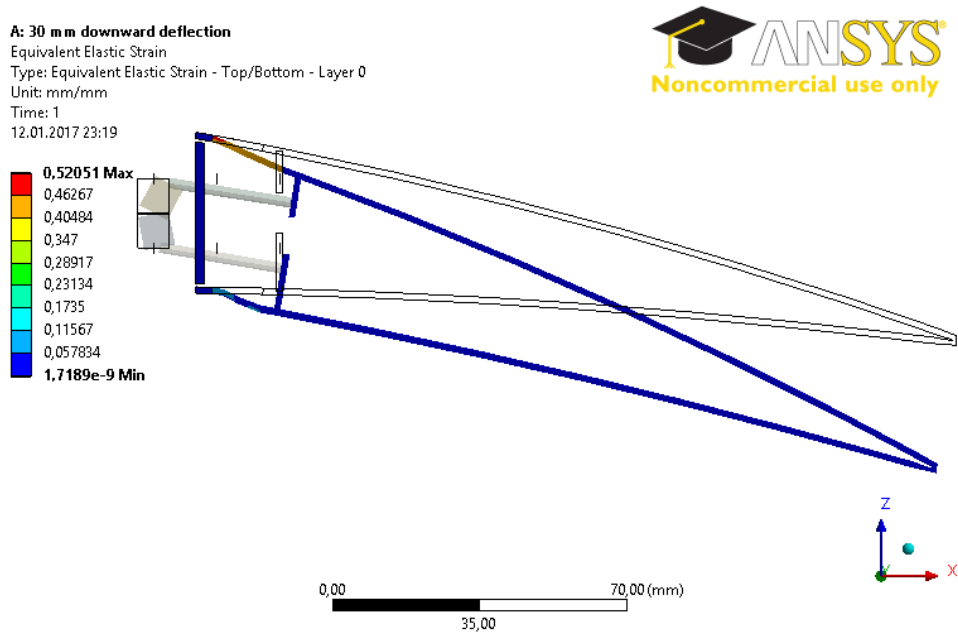

Figure 117: Equivalent Elastic Strain of the Control Surface 30 [mm] Downward Deflected – Servo Actuators inside the Torque Box Volume – without Pre-Twist – Maximum 0.52051 [mm/mm]
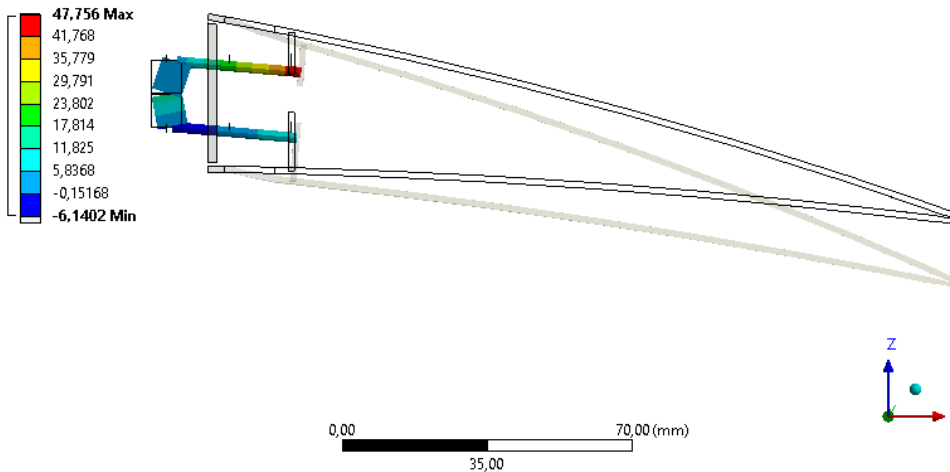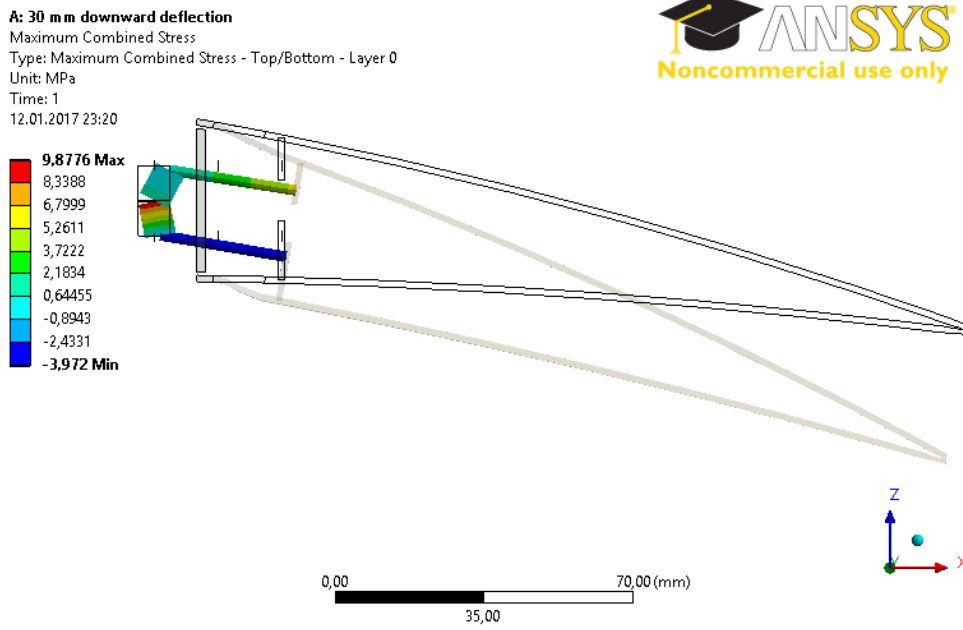
Figure 118: Maximum Combined Beam Stress of the Control Surface 30 [mm] Downward Deflected – Servo Actuators inside the Torque Box Volume – without Pre-Twist – Maximum 9.8776 [MPa]

The maximum torque value needed for the servo actuator actuates the upper surface of the control surface is -17.85 [N-mm] and the maximum torque value needed for the servo actuator actuates the lower surface of the control surface is -181.54 [N-mm]. It can be concluded that the reaction moment results are below the servo actuator torque limits.

6.2.1.5 Discussion and Conclusion

The maximum von Mises strain results of all the downward deflection cases are tabulated in Table 20. According to the results shown, as the deflections increase, the maximum von Mises strain also increases. Note that, the strain values obtained for the configuration having the servo actuators inside the torque box volume are greater than the strain values of the configuration having the servo actuators inside the control surface volume. This is an expected result since the initial length of the

compliant part is smaller for the case which the servo actuators are inside the torque box.

Table 20: Maximum von Mises Strain Comparison

	Maximum von Mises Strain [mm/mm]*
15.2 [mm] Deflection Case	0.3453
20.0 [mm] Deflection Case	0.40361
25.0 [mm] Deflection Case	0.46145
30.0 [mm] Deflection Case	0.52051

* Maximum von Misses Strain is observed for the compliant part and its strain limit must be smaller than 1.

The results of maximum von Mises stress, maximum combined beam stresses and required servo actuator torques to actuate upper and lower surface of the trailing edge control surface are given in Table 21, Table 22, Table 23 and Table 24, respectively. Indicated values are safe in terms of yield stress and strain values of the material used and servo torque limit capability.

Table 21: Maximum von Mises Stress Comparison

	Maximum von Mises Stress [MPa]*
15.2 [mm] Deflection Case	26.917
20.0 [mm] Deflection Case	25.123
25.0 [mm] Deflection Case	23.626
30.0 [mm] Deflection Case	22.456

* Maximum von Misses Stress is observed for the transmission parts and their yield stress is 280 [MPa]

Table 22: Maximum Combined Beam Stress

	Maximum Combined Beam Stress [MPa]*
15.2 [mm] Deflection Case	47.756
20.0 [mm] Deflection Case	34.302
25.0 [mm] Deflection Case	20.369
30.0 [mm] Deflection Case	9.8776

*Aluminum is used for beams and its yield point is 280 [MPa]

Table 23: Servo Actuator Torque Required to Actuate the Upper Surface of the Control Surface

	Servo Actuate Upper Surface [N-mm]*
15.2 [mm] Deflection Case	-99.081
20.0 [mm] Deflection Case	-71.84
25.0 [mm] Deflection Case	-44.829
30.0 [mm] Deflection Case	-17.846

*Servo actuator torque capacity is 19.6 [kg cm]

Table 24: Servo Actuator Torque Required to Actuate the Lower Surface of
the Control Surface

	Servo Actuate Lower Surface [N-mm]*
15.2 [mm] Deflection Case	-269.08
20.0 [mm] Deflection Case	-238.96
25.0 [mm] Deflection Case	-209.66
30.0 [mm] Deflection Case	-181.54

*Servo actuator torque capacity is 19.6 [kg cm]

6.2.2 Investigation of Twist Capability of the Hybrid Trailing Edge Control Surface

In this section, the twist capability of the hybrid trailing edge control surface without pre-twist and having the servo actuators inside the torque box volume is examined. The control surface consists of five servo actuators three of which actuates the upper surface of the control surface and remaining two actuates the lower surface of the control surface. The configuration detail is explained in Chapter 3.

In order to twist the hybrid trailing edge control surface, the angles of 6 [deg], 10 [deg] and 25 [deg] are defined at the outboard, middle and inboard upper servo actuators respectively. Also the angles of -1 [deg] and -3 [deg] are defined at the outboard and inboard lower servo actuators respectively.

The z directional displacement of the control surface is shown in Figure 119. Equivalent elastic stress and strain of the control surface are shown in Figure 120 and Figure 121 respectively. Maximum combined beam stress of the moment arms and transmission rods is given in Figure 122.
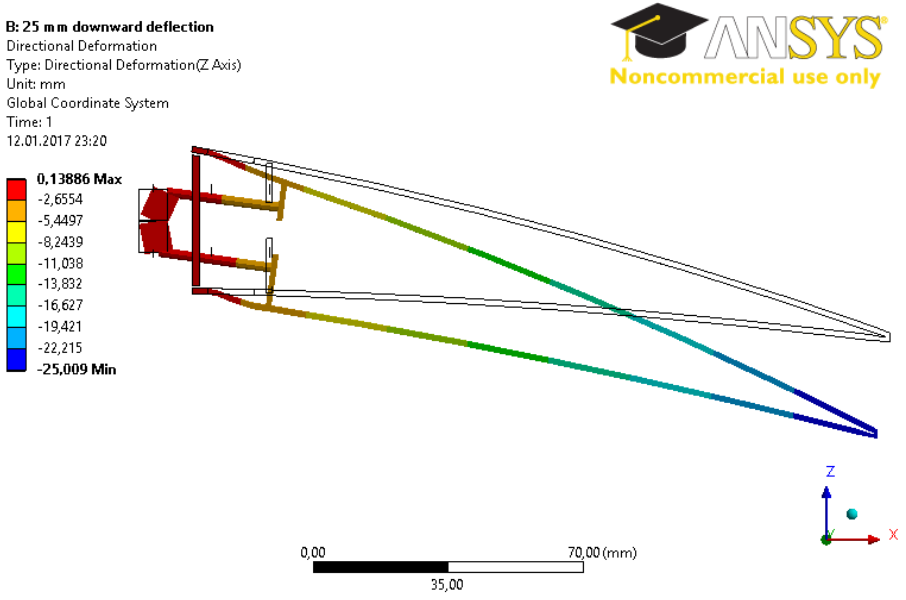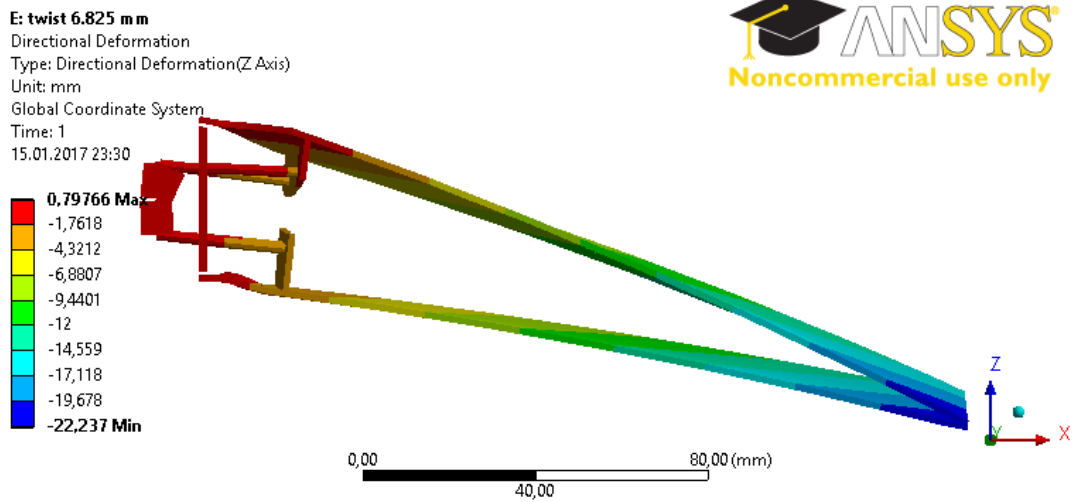
Figure 119: Z Directional Displacement Contours of the Control Surface –
Twist Investigation – Servo Actuators inside the Torque Box Volume – without Pre-
Twist – Maximum 22.237 [mm]
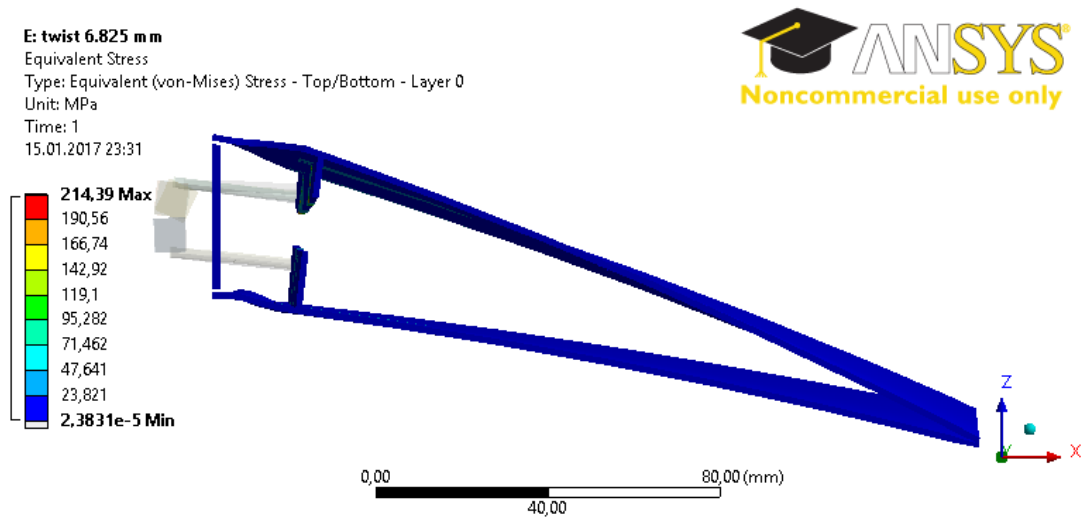
Figure 120: Equivalent Elastic Stress of the Control – Twist Investigation –
Servo Actuators inside the Torque Box Volume – without Pre-Twist – Maximum
214.39 [MPa]
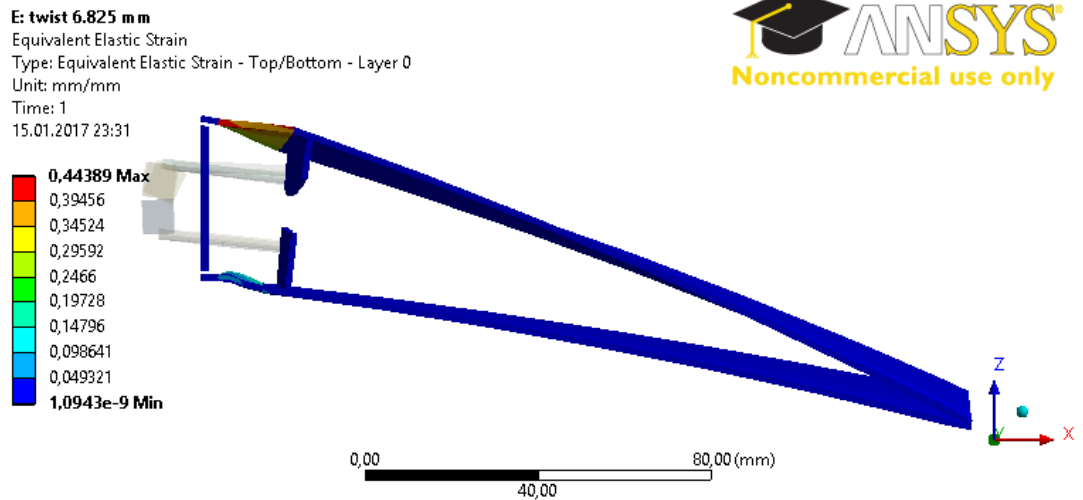
Figure 121: Equivalent Elastic Strain of the Control – Twist Investigation – Servo Actuators inside the Torque Box Volume – without Pre-Twist – Maximum 0.44389 [mm/mm]
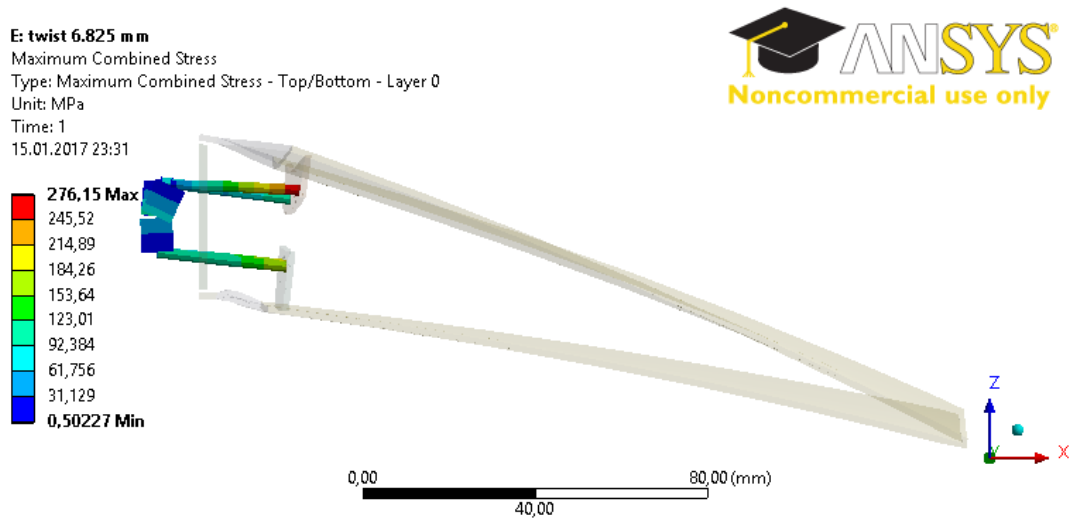
Figure 122: Maximum Combined Beam Stress of the Control – Twist Investigation – Servo Actuators inside the Torque Box Volume – without Pre-Twist – Maximum 276.15 [MPa]

The values shown in Figure 120, Figure 121 and Figure 122 are safe in terms of yield stress and strain values of the material used.

The z directional displacements of the inboard and outboard edge point of the trailing edge control are shown in Figure 123. There is a 6.825 [mm] z directional

difference between these edge points which gives an idea about the twist of the trailing edge control surface.
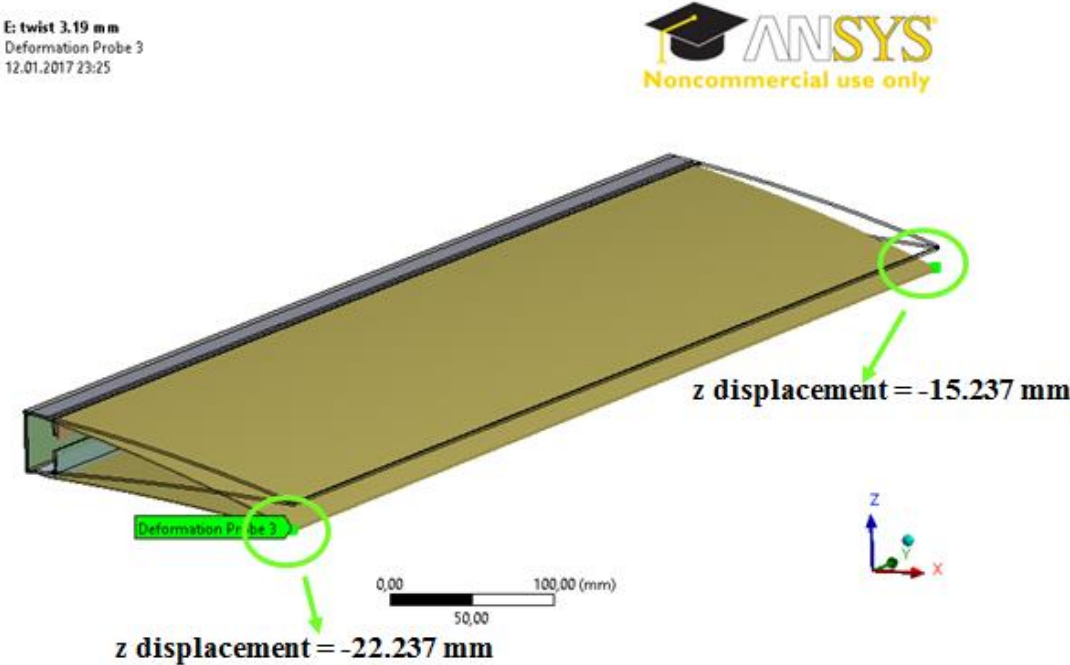
Figure 123: Inboard and Outboard Edge Point of the Trailing Edge Control Surface

The maximum torque value needed for the servo actuator actuates the upper surface of the control surface is -1869.50 [N-mm] and the maximum torque value needed for the servo actuator actuates the lower surface of the control surface is -1224.40 [N-mm]. It can be concluded that the reaction moment results are below the servo actuator torque limits.

6.3 Control Surface with Pre-Twist Configuration

6.3.1 Downward Deflection of the Hybrid Trailing Edge Control Surface

In this section, downward deflection of the hybrid trailing edge control surface with pre-twist configuration is studied. The limit of the downward deflection

is determined. The baseline airfoil profile is selected as NACA 6510. Therefore all the downward deflection analyses starts from the baseline airfoil.

6.3.1.1 Deflection of NACA 6510 Profile by 15.2 [mm] in Transverse Direction

In order to deflect the tip of the hybrid trailing edge control surface 15.2 [mm] in vertical direction, rotation angles around y axis are defined +20.05 [deg] at the rotation center of the moment arms which actuate the upper part of the control surface and –11.85 [deg] rotation angles around y axis are defined at the center of the moment arms which actuate the lower part of the control surface.

The z directional displacement of the control surface is shown in Figure 124. Equivalent elastic stress and strain of the control surface are shown in Figure 125 and Figure 126 respectively. Maximum combined beam stress of the moment arms and transmission rods is given in Figure 127.

Figure 124: Z Directional Displacement Contours of the Control Surface –
15.2 [mm] Downward Deflected – Servo Actuators inside the Torque Box Volume –
with Pre-Twist – Maximum 15.231 [mm]

109

Figure 125: Equivalent Elastic Stress of the Control Surface 15.2 [mm] Downward Deflected – Servo Actuators inside the Torque Box Volume – with Pre-Twist – Maximum 24.817 [MPa]

Figure 126: Equivalent Elastic Strain of the Control Surface 15.2 [mm] Downward Deflected – Servo Actuators inside the Torque Box Volume – with Pre-Twist – Maximum 0.36499 [mm/mm]

Figure 127: Maximum Combined Beam Stress of the Control Surface 15.2 [mm] Downward Deflected – Servo Actuators inside the Torque Box Volume – with Pre-Twist – Maximum 46.818 [MPa]

The maximum torque value needed for the servo actuator actuates the upper surface of the control surface is -103.55 [N-mm] and the maximum torque value needed for the servo actuator actuates the lower surface of the control surface is -257.48 [N-mm]. It can be concluded that the reaction moment results are below the servo actuator torque limits.

6.3.1.2 Deflection of NACA 6510 Profile by 20 [mm] in Transverse Direction

In order to deflect the tip of the hybrid trailing edge control surface 20 [mm] in vertical direction, rotation angles around y axis are defined +23.28 [deg] at the rotation center of the moment arms which actuate the upper part of the control surface and -11.85 [deg] rotation angles around y axis are defined at the center of the moment arms which actuate the lower part of the control surface.

The z directional displacement of the control surface is shown in Figure 128. Equivalent elastic stress and strain of the control surface are shown in Figure 129 and

Figure 130 respectively. Maximum combined beam stress of the moment arms and transmission rods is given in Figure 131.

Figure 128: Z Directional Displacement Contours of the Control Surface – 20 [mm] Downward Deflected – Servo Actuators inside the Torque Box Volume –with Pre-Twist – Maximum 20.03 [mm]

Figure 129: Equivalent Elastic Stress of the Control Surface 20 [mm] Downward Deflected – Servo Actuators inside the Torque Box Volume – with Pre-Twist – Maximum 23.504 [MPa]

Figure 130: Equivalent Elastic Strain of the Control Surface 20 [mm]
Downward Deflected – Servo Actuators inside the Torque Box Volume – with Pre-
Twist – Maximum 0.42531 [mm/mm]

Figure 131: Maximum Combined Beam Stress of the Control Surface 20
[mm] Downward Deflected – Servo Actuators inside the Torque Box Volume – with
Pre-Twist – Maximum 31.992 [MPa]

The maximum torque value needed for the servo actuator actuates the upper surface of the control surface is -86.85 [N-mm] and the maximum torque value needed for the servo actuator actuates the lower surface of the control surface is -230.18 [N-mm]. It can be concluded that the reaction moment results are below the servo actuator torque limits.

6.3.1.3 Deflection of NACA 6510 Profile by 25 [mm] in Transverse Direction

In order to deflect the tip of the hybrid trailing edge control surface 25 [mm] in vertical direction, rotation angles around y axis are defined +26.62 [deg] at the rotation center of the moment arms which actuate the upper part of the control surface and -11.85 [deg] rotation angles around y axis are defined at the center of the moment arms which actuate the lower part of the control surface.

The z directional displacement of the control surface is shown in Figure 132. Equivalent elastic stress and strain of the control surface are shown in Figure 133 and Figure 134 respectively. Maximum combined beam stress of the moment arms and transmission rods is given in Figure 135.
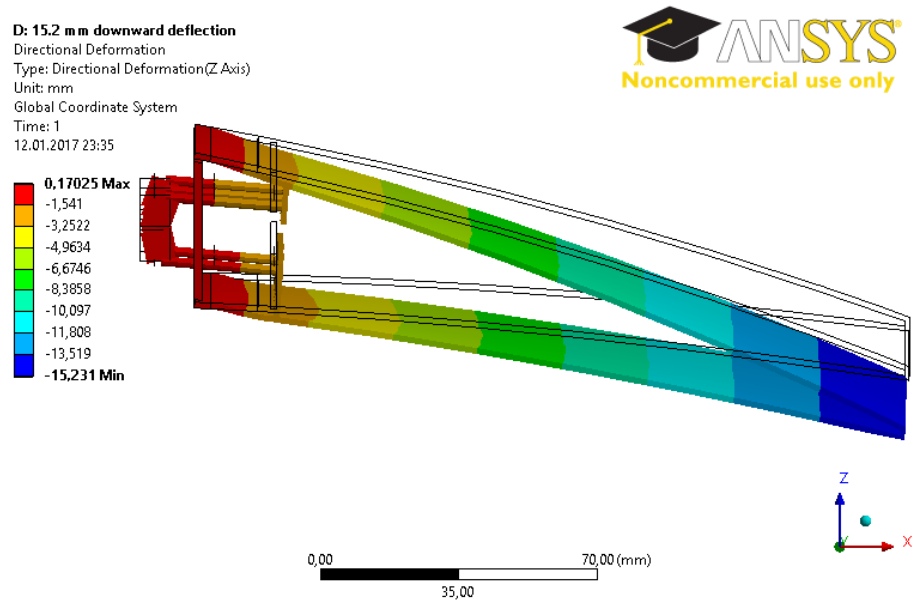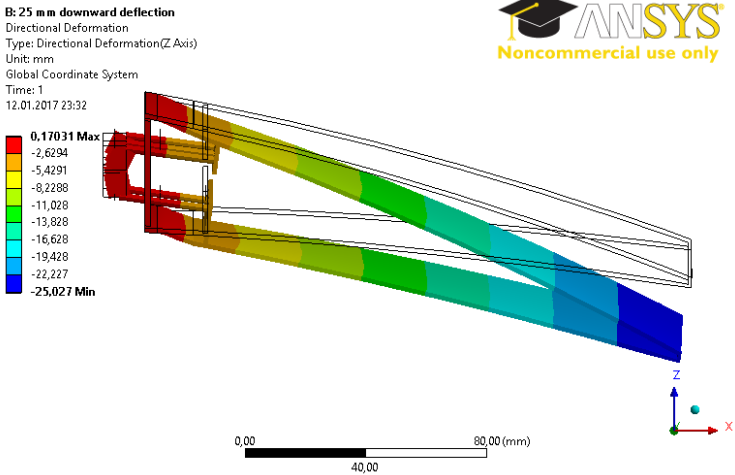

Figure 132: Z Directional Displacement Contours of the Control Surface – 25 [mm] Downward Deflected – Servo Actuators inside the Torque Box Volume –with Pre-Twist – Maximum 25.027 [mm]
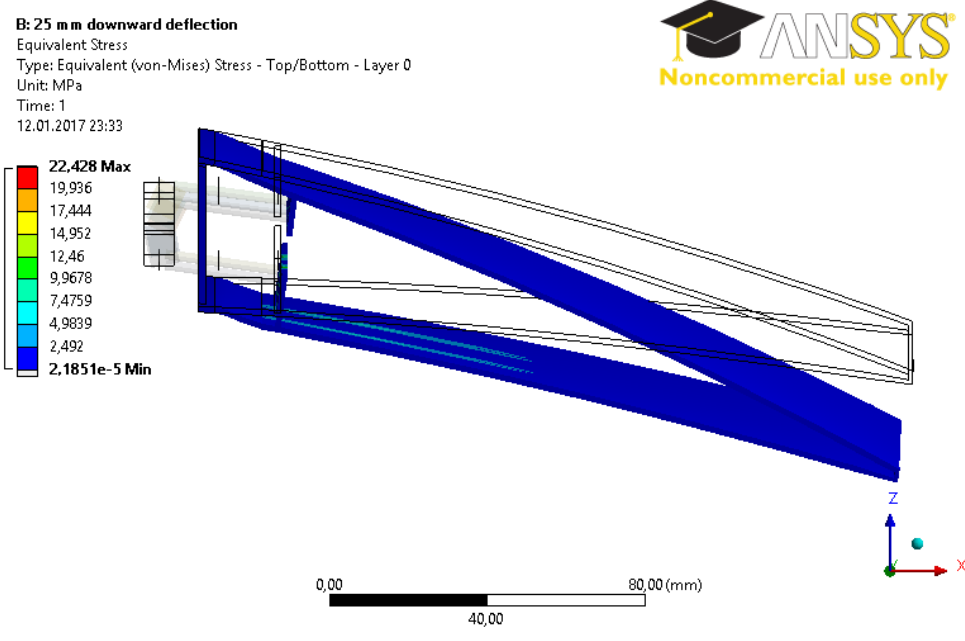
Figure 133: Equivalent Elastic Stress of the Control Surface 25 [mm] Downward Deflected – Servo Actuators inside the Torque Box Volume – with Pre-Twist – Maximum 22.428 [MPa]
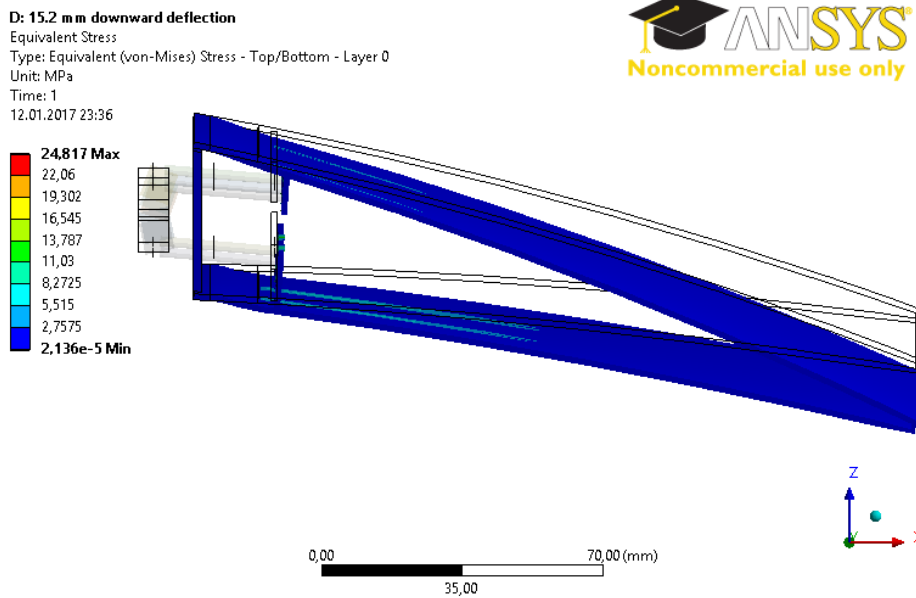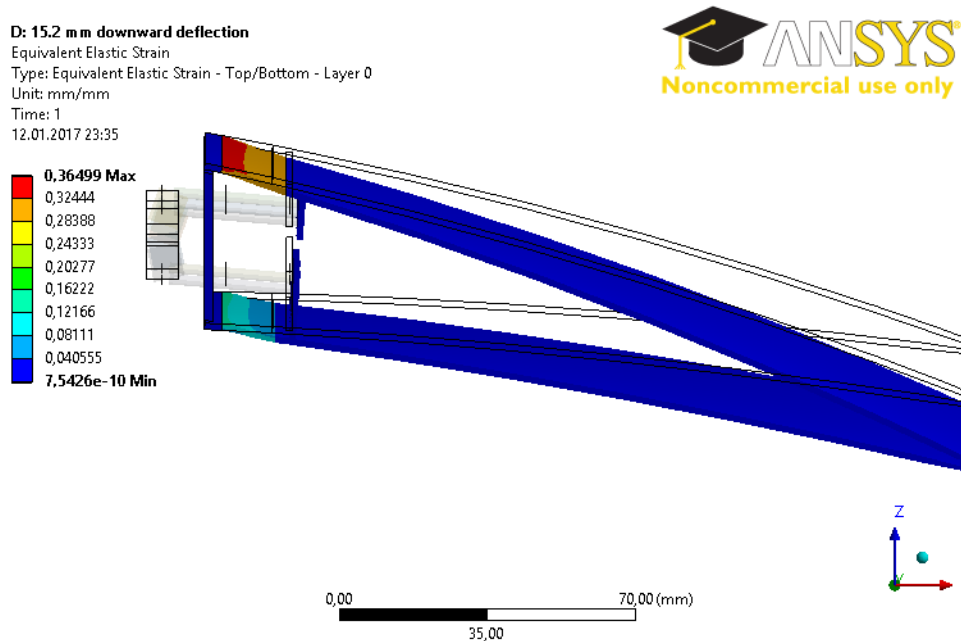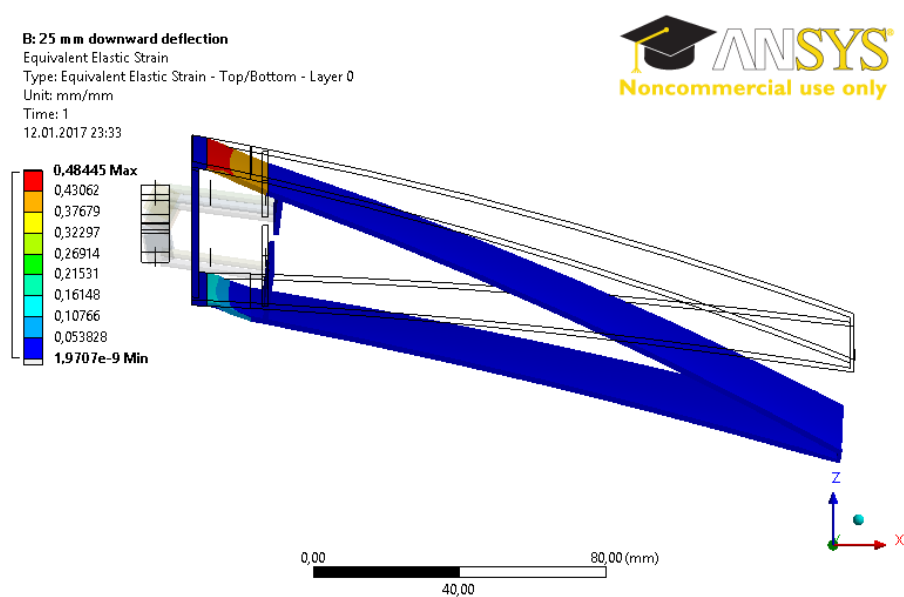

Figure 134: Equivalent Elastic Strain of the Control Surface 25 [mm] Downward Deflected – Servo Actuators inside the Torque Box Volume – with Pre-Twist – Maximum 0.48445 [mm/mm]
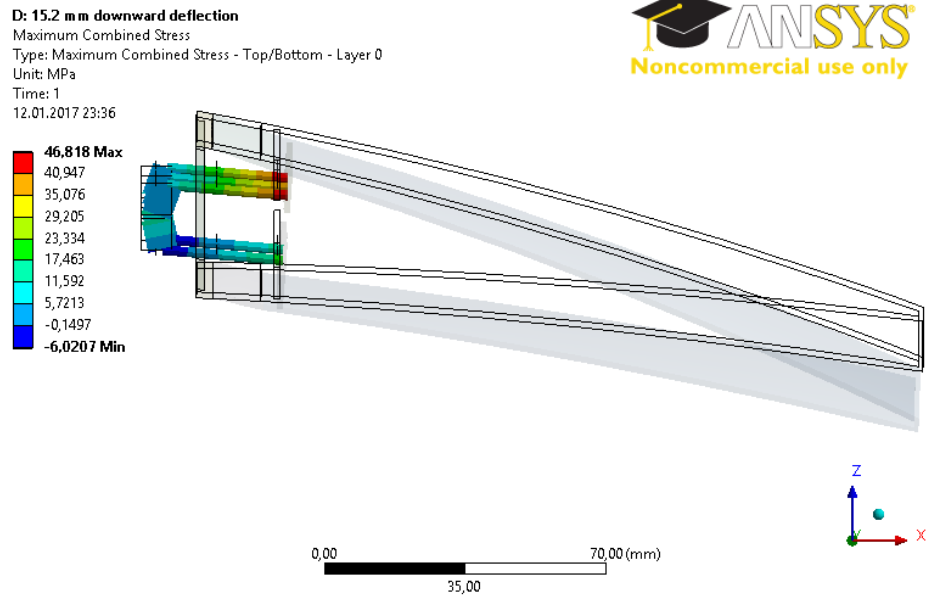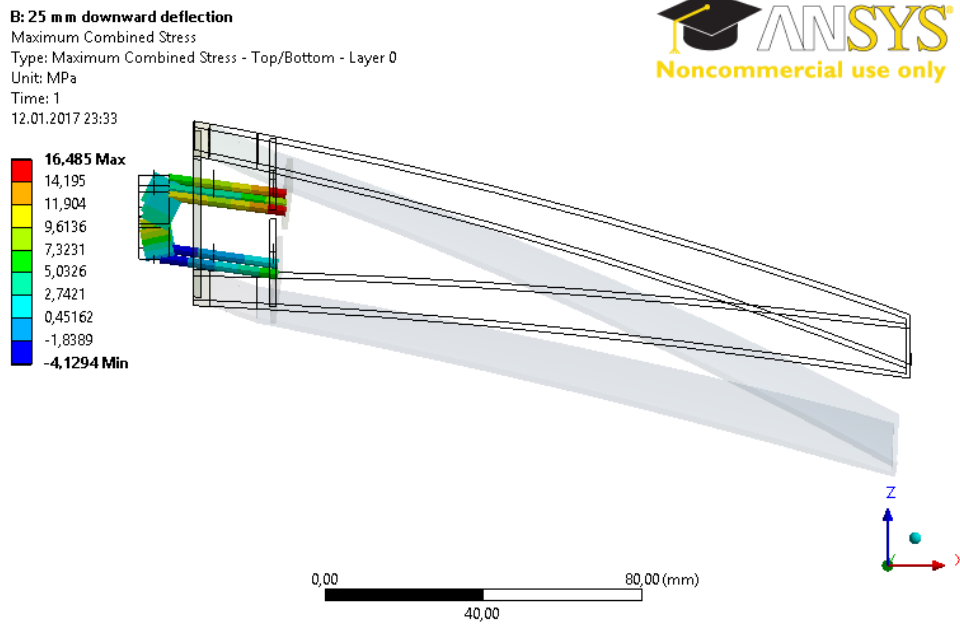
Figure 135: Maximum Combined Beam Stress of the Control Surface 25 [mm] Downward Deflected – Servo Actuators inside the Torque Box Volume – with Pre-Twist – Maximum 16.485 [MPa]

The maximum torque value needed for the servo actuator actuates the upper surface of the control surface is -71.10 [N-mm] and the maximum torque value needed for the servo actuator actuates the lower surface of the control surface is -204.12 [N-mm]. It can be concluded that the reaction moment results are below the servo actuator torque limits.

6.3.1.4 Deflection of NACA 6510 Profile by 30 [mm] in Transverse Direction

In order to deflect the tip of the hybrid trailing edge control surface 30 [mm] in vertical direction, rotation angles around y axis are defined +30 [deg] at the rotation center of the moment arms which actuate the upper part of the control surface and -11.85 [deg] rotation angles around y axis are defined at the center of the moment arms which actuate the lower part of the control surface.

The z directional displacement of the control surface is shown in Figure 136. Equivalent elastic stress and strain of the control surface are shown in Figure 137 and

Figure 138 respectively. Maximum combined beam stress of the moment arms and transmission rods is given in Figure 139.
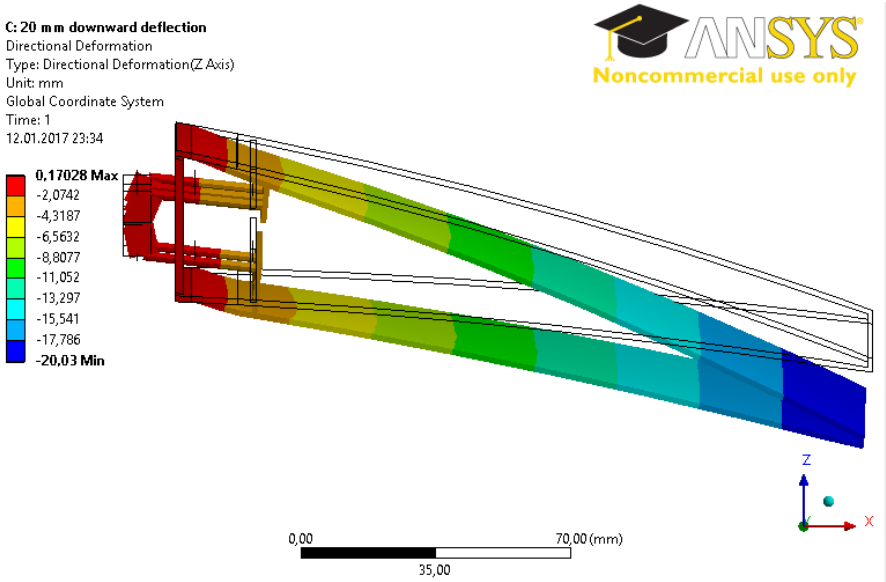

Figure 136: Z Directional Displacement Contours of the Control Surface – 30 [mm] Downward Deflected – Servo Actuators inside the Torque Box Volume –with Pre-Twist – Maximum 29.997 [mm]
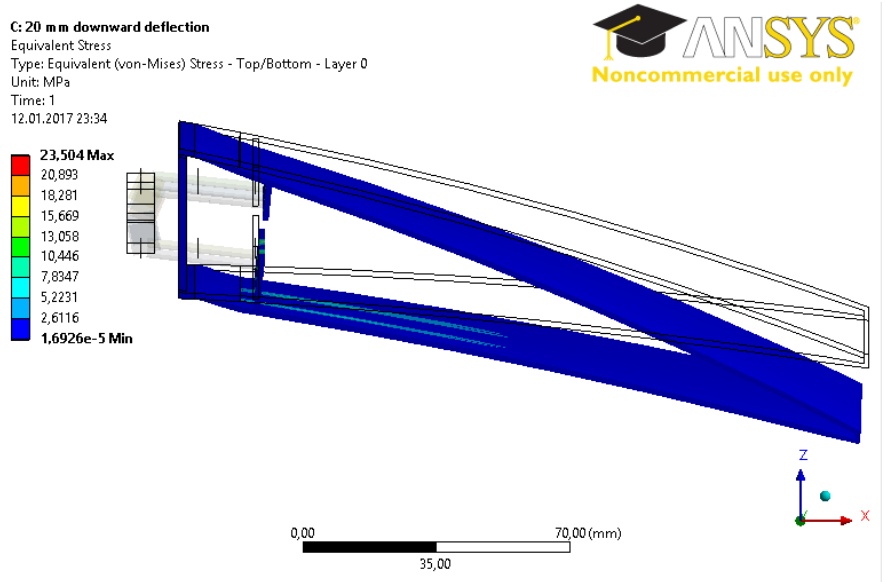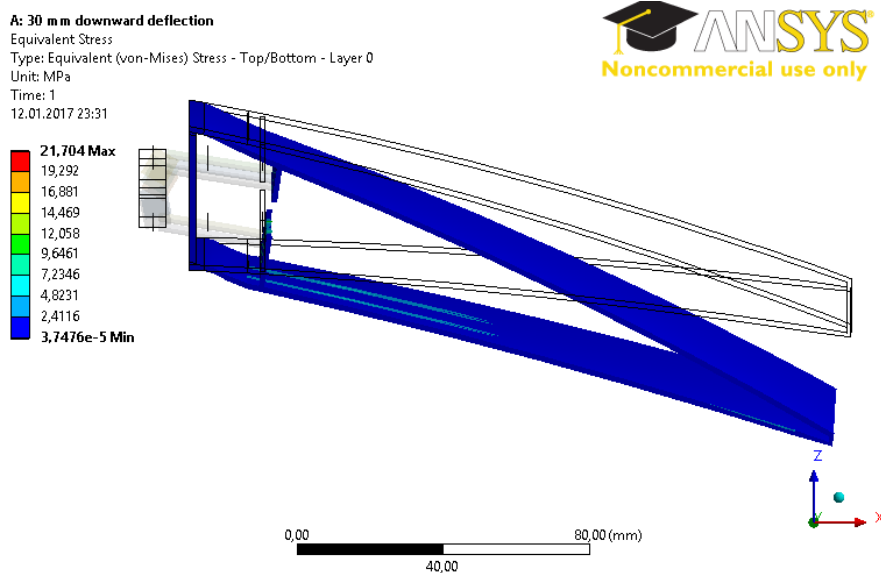

Figure 137: Equivalent Elastic Stress of the Control Surface 30 [mm] Downward Deflected – Servo Actuators inside the Torque Box Volume – with Pre-Twist – Maximum 21.704 [MPa]
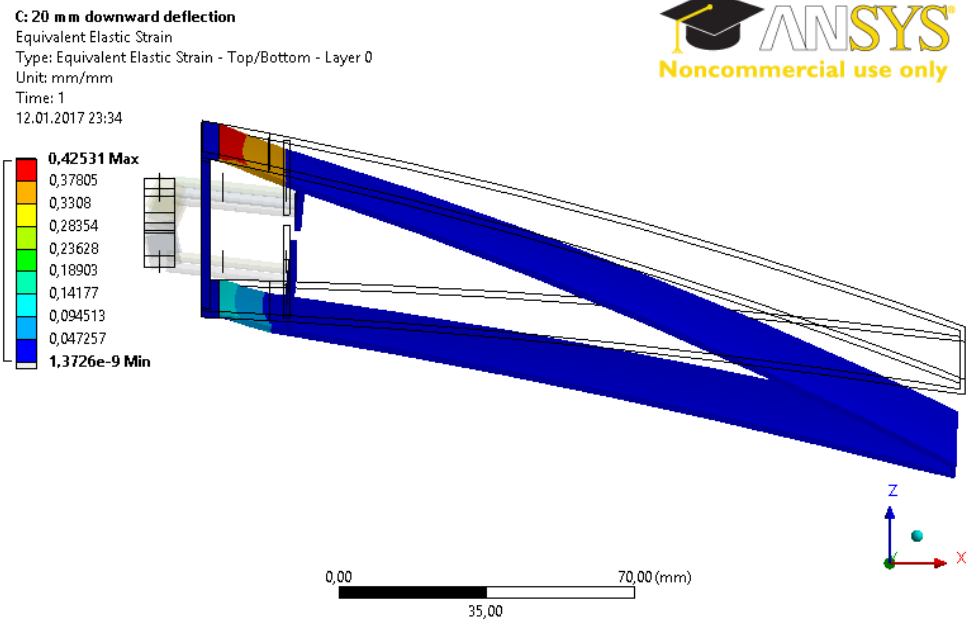
117
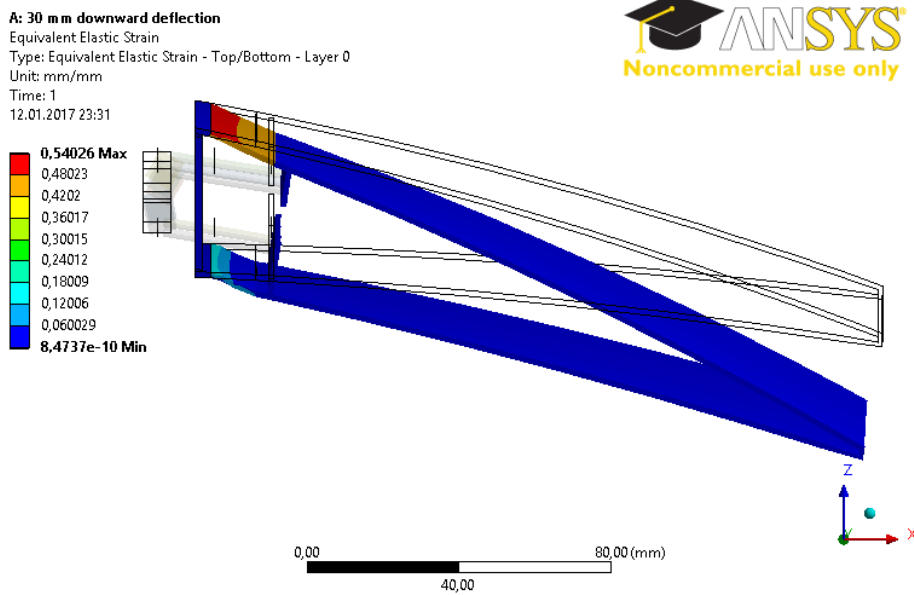
Figure 138: Equivalent Elastic Strain of the Control Surface 30 [mm] Downward Deflected – Servo Actuators inside the Torque Box Volume – with Pre-Twist – Maximum 0.54026 [mm/mm]
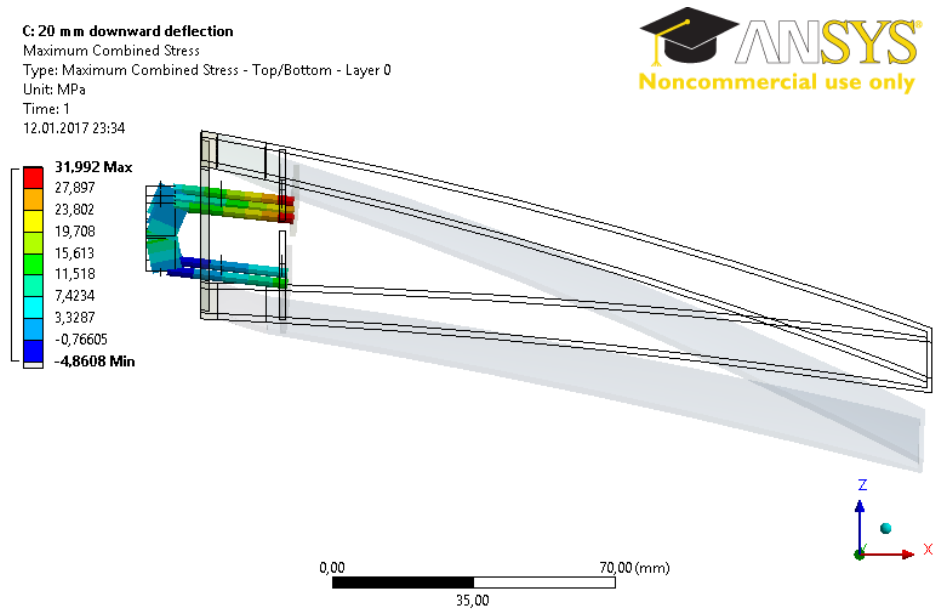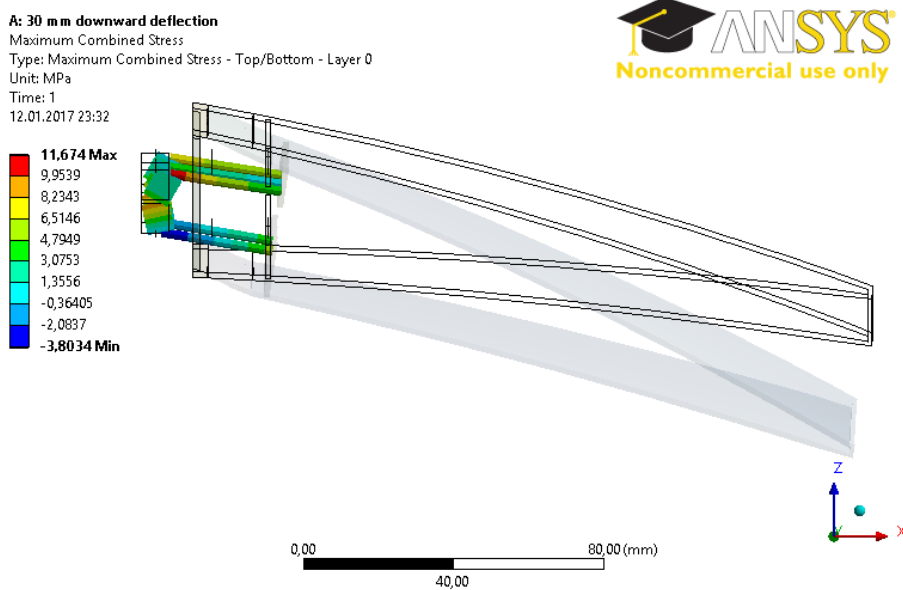

Figure 139: Maximum Combined Beam Stress of the Control Surface 30 [mm] Downward Deflected – Servo Actuators inside the Torque Box Volume – with Pre-Twist – Maximum 11.674 [MPa]

The maximum torque value needed for the servo actuator actuates the upper surface of the control surface is 104.94 [N-mm] and the maximum torque value needed for the servo actuator actuates the lower surface of the control surface is -180.92 [N-mm]. It can be concluded that the reaction moment results are below the servo actuator torque limits.

6.3.1.5 Discussion and Conclusion

The maximum von Mises strain results of the all the downward deflection cases are tabulated in Table 25.

Table 25: Maximum von Mises Strain Comparison

	Maximum von Mises Strain [mm/mm]*
15.2 [mm] Deflection Case	0.36499
20.0 [mm] Deflection Case	0.42531
25.0 [mm] Deflection Case	0.48445
30.0 [mm] Deflection Case	0.54026

* Maximum von Misses Strain is observed for the compliant part and its strain limit must be smaller than 1.

The results of maximum von Mises stress, maximum combined beam stresses and required servo actuator torques to actuate upper and lower surface of the trailing edge control surface are given in Table 26, Table 27, Table 28 and Table 29 respectively. Indicated values are safe in terms of yield stress and strain values of the material used and servo torque limit capability.

Table 26: Maximum von Mises Stress Comparison

	Maximum von Mises Stress [MPa]*
15.2 [mm] Deflection Case	24.817
20.0 [mm] Deflection Case	23.504
25.0 [mm] Deflection Case	22.428
30.0 [mm] Deflection Case	21.704

* Maximum von Misses Stress is observed for the transmission parts and their yield stress is 280 [MPa]

Table 27: Maximum Combined Beam Stress

	Maximum Combined Beam Stress [MPa]*
15.2 [mm] Deflection Case	46.818
20.0 [mm] Deflection Case	31.992
25.0 [mm] Deflection Case	16.485
30.0 [mm] Deflection Case	11.674

*Aluminum is used for beams and its yield point is 280 [MPa]

Table 28: Servo Actuator Torque Required to Actuate the Upper Surface of the Control Surface

	Servo Actuate Upper Surface [N-mm]*
15.2 [mm] Deflection Case	-103.55
20.0 [mm] Deflection Case	-86.848
25.0 [mm] Deflection Case	-71.099
30.0 [mm] Deflection Case	104.94

*Servo actuator torque capacity is 19.6 [kg cm]

Table 29: Servo Actuator Torque Required to Actuate the Lower Surface of the Control Surface

	Servo Actuate Lower Surface [N-mm]*
15.2 [mm] Deflection Case	-257.48
20.0 [mm] Deflection Case	-230.18
25.0 [mm] Deflection Case	-204.12
30.0 [mm] Deflection Case	-180.92

*Servo actuator torque capacity is 19.6 [kg cm]

6.3.2 Investigation of Twist Capability of the Hybrid Trailing Edge Control Surface

In order to twist the hybrid trailing edge control surface, the angles of 6 [deg], 10 [deg] and 24 [deg] are defined at the outboard, middle and inboard upper servo actuators respectively. Also the angles of -1 [deg] and -3 [deg] are defined at the outboard and inboard lower servo actuators respectively.

The z directional displacement of the control surface is shown in Figure 140. Equivalent elastic stress and strain of the control surface are shown in Figure 141 and Figure 142 respectively. Maximum combined beam stress of the moment arms and transmission rods is given in Figure 143.
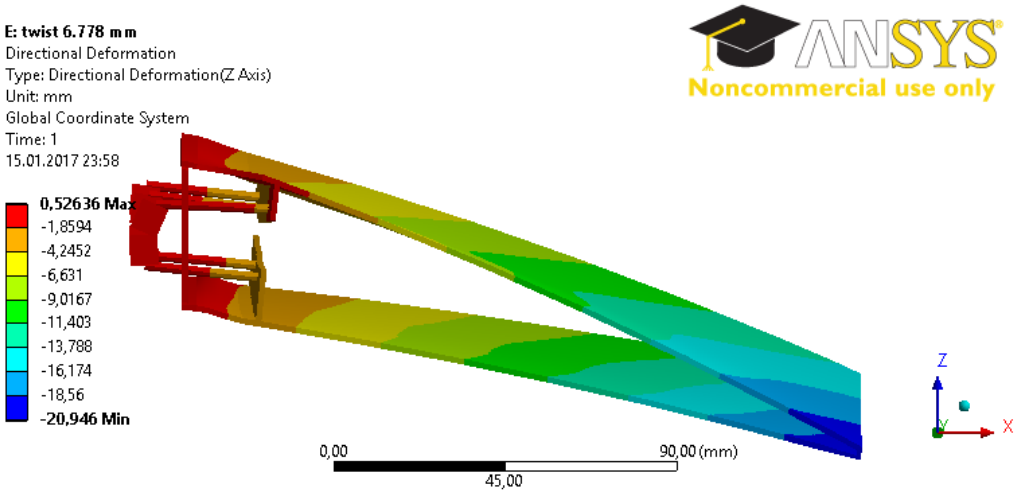
Figure 140: Z Directional Displacement Contours of the Control Surface – Twist Investigation – Servo Actuators inside the Torque Box – with Pre-Twist – Maximum 20.946 [mm]
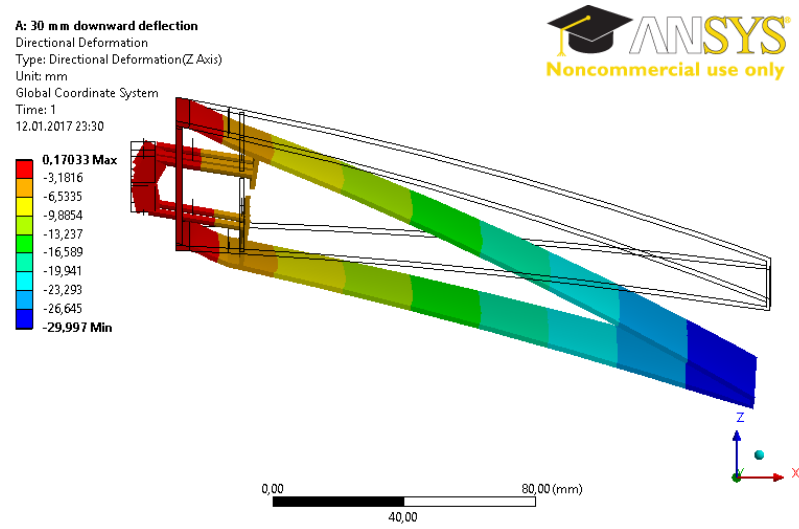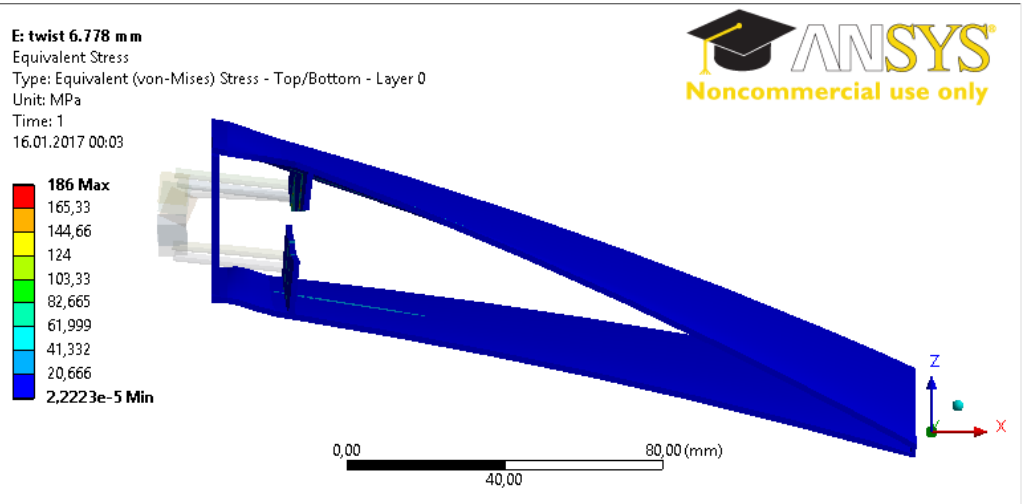

Figure 141: Equivalent Elastic Stress of the Control – Twist Investigation – Servo Actuators inside the Torque Box Volume – with Pre-Twist – Maximum 186 [MPa]
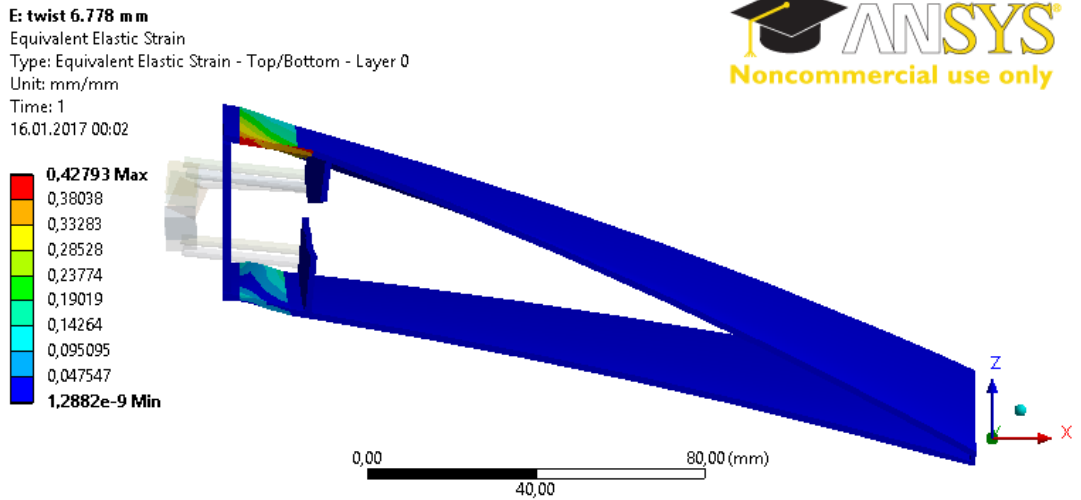
Figure 142: Equivalent Elastic Strain of the Control – Twist Investigation – Servo Actuators inside the Torque Box Volume – with Pre-Twist – Maximum 0.42793 [mm/mm]
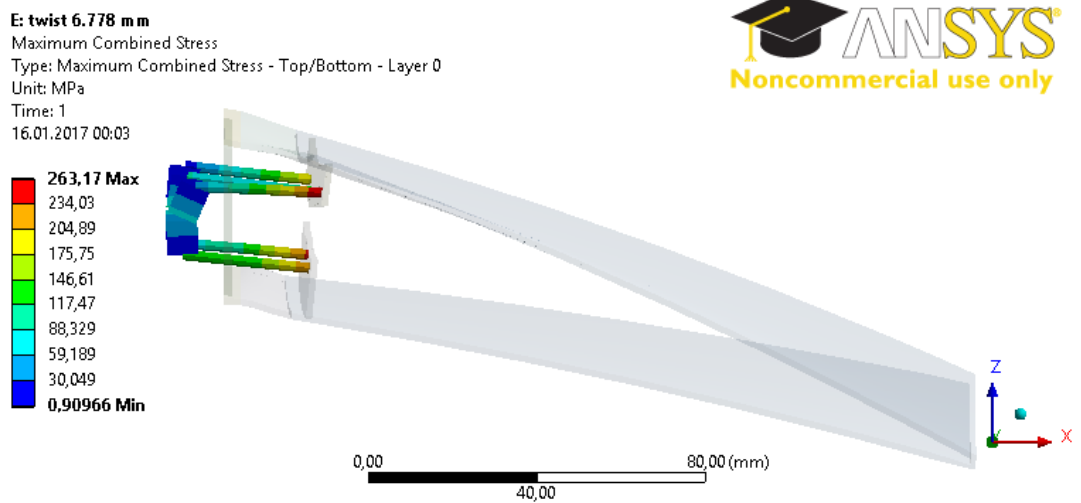
Figure 143: Maximum Combined Beam Stress of the Control – Twist Investigation – Servo Actuators inside the Torque Box Volume – with Pre-Twist – Maximum 263.17 [MPa]

The values shown in Figure 141, Figure 142 and Figure 143 are safe in terms of yield stress and strain values of the material used.

The z directional displacements of the inboard and outboard edge point of the trailing edge control are shown in Figure 144. There is a 6.778 [mm] z directional difference between these edge points which gives an idea about the twist of the trailing edge control surface.
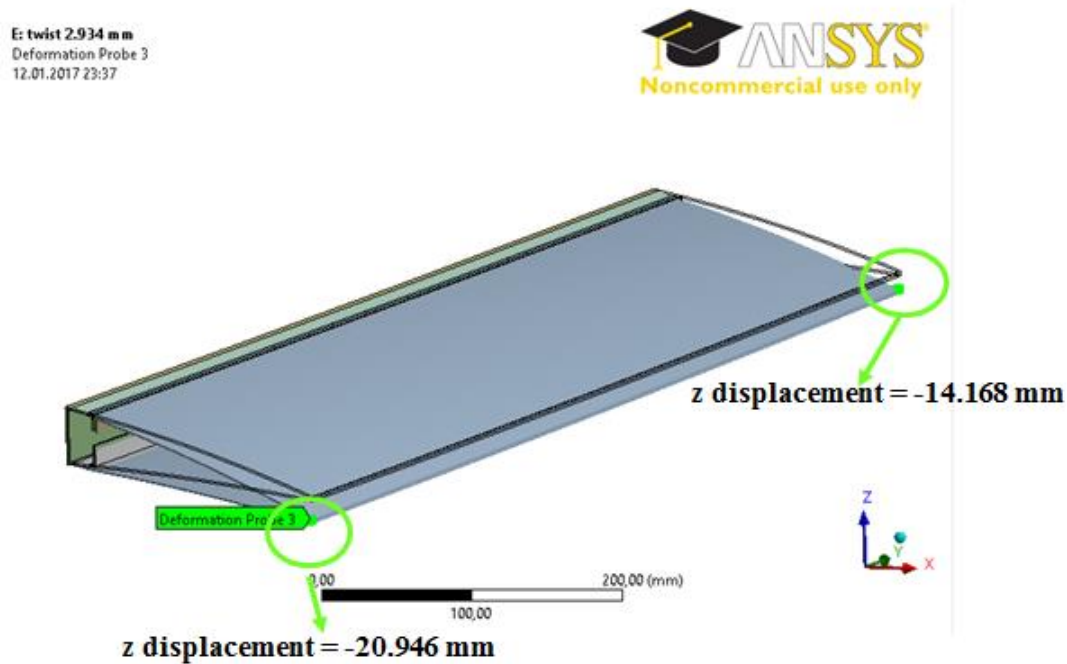
Figure 144: Inboard and Outboard Edge Point of the Trailing Edge Control Surface

The maximum torque value needed for the servo actuator actuates the upper surface of the control surface is -1589.30 [N-mm] and the maximum torque value needed for the servo actuator actuates the lower surface of the control surface is -1209.70 [N-mm]. It can be concluded that the reaction moment results are below the servo actuator torque limits.

6.4 Discussion and Conclusion

In this chapter, the downward deflection of the hybrid trailing edge control surface having the servo actuators inside the torque box volume is performed. Since

the servo actuators of this configuration is stronger and there is no risk for the servo actuators to touch the upper surface of the control surface, more transverse deflection of the control surface can be obtained and therefore more twisting of the control surface can also be achieved.

CHAPTER 7

CONCLUSION

7.1 General Conclusions

In this thesis, structural analyses of fully morphing hybrid trailing edge control surface are performed. The CAD model of the control surface is created by using CATIA V5-6R2012 package software. The finite element analyses are performed by using the ANSYS Workbench v14.0 package software.

Downward deflection of the hybrid trailing edge control surface in in-vacuo condition is investigated. Different configuration of the control surfaces such as

- Control surface without pre-twist configuration and having the actuators inside the control surface volume,
- Control surface with pre-twist configuration and having the actuators inside the control surface volume,
- Control surface without pre-twist configuration and having the actuators inside the torque box volume,
- Control surface with pre-twist configuration and having the actuators inside the torque box volume are tested.

According to the results given in Chapter 5 and Chapter 6, it can be seen that the control surfaces can deflect up to 30 [mm], although not perfectly. For the deflections close to 30 [mm], bumps are determined at the surface of the compliant material and this degrades the aerodynamic efficiency. The deflection values after 30 [mm], 32 [mm] to be precise, were found to give erroneous results and therefore not included in the thesis. Hence this 30 [mm] downward deflection puts a limit to the

system considered. The effects of these bumps on the aerodynamic performance must be checked for the future work.

Also in this thesis, the selection of proper servo actuators for each of the configuration is performed. It is concluded that, there is more space available in the torque box volume. If this space is available for the servo actuators, bigger and stronger servo actuators can be selected. This may results in more deflection of the control surface and also more twisting of the control surface. Also if the servo actuators are put inside the torque box volume, there is no risk for upper surface of the control surface to touch the upper part of the servo actuators which may increase the limit of downward deflection. If the torque box area is occupied by the structures other than the servo actuators, then, the servo actuators can be put inside the control surface volume. This results in selection of the smaller servo actuators which results in decreasing the limits of downward deflection and twisting motion.

7.2 Recommendations for Further Studies

If the aerodynamic loading is considered for the downward deflection cases, aerodynamic loading will result in reduction of servo actuators torque requirements up to some deflection limits. These deflection limits are the points where the servo actuators torque values change sign from negative values to positive values. Beyond these limiting deflection points, aerodynamic loading acts against the servo actuators. But all of these conclusions must be verified for the future work.

Inertial and aerodynamic loads coming from the maneuvers (pull-up, gust, yaw etc.) can be calculated and designed hybrid trailing edge control surface can be evaluated under these loads.

Since the higher load factors may occur during the landing phase, the calculation of landing loads can be done and the structural analyses of the control surface by applying these landing loads can be conducted.

In addition to using the servo actuators, shape memory alloy actuators (SMA actuators) can also be used. But using SMA actuators may bring some extra

complexity to the system such as the heating and cooling requirements of the SMA and extra battery requirement for SMA.

Although in this thesis, the static deflections were considered; the dynamic analysis and fatigue analysis of the designed control surface can also be studied.

REFERENCES

[1]   I. Chopra, "Review of state of art of smart structures and integrated systems," *AIAA J.*, vol. 40, no. 11, pp. 2145–2187, 2002.

[2]   L. Ünlüsoy, "Effects of Morphing on Aeroelastic Behavior of Unmanned Aerial Wings," Middle East Technical University, 2014.

[3]   G. Seber, E. Sakarya, E. T. Insuyu, M. Şahin, S. Ozgen, and Y. Yaman, "Evaluation of a camber morphing concept based on controlled flexibility," in *IFASD2009, International Forum on Aeroelasticity and Structural Dynamics*, 2009.

[4]   G. Seber, E. Sakarya, T. İnsuyu, S. Özgen, M. Şahin, and Y. Yaman, "Structural Modeling and Flutter Analysis of Adaptive Camber Wings," in *5. Ankara International Aerospace Conference*, 2009.

[5]   G. Seber and E. Sakarya, "Nonlinear Modeling and Aeroelastic Analysis of an Adaptive Camber Wing," *J. Aircr.*, vol. 47, no. 6, pp. 2067–2074, 2010.

[6]   "CHANGE FP7 Project." [Online]. Available: http://change.tekever.com. [Accessed: 01-Jan-2017].

[7]   D. S. Körpe, "Aerodynamic Modeling and Optimization of Morphing Wings," Middle East Technical University, 2014.

[8]   P. Arslan, U. Kalkan, H. Tıraş, İ. O. Tunçöz, Y. Yang, E. Gürses, M. Şahin, S. Özgen, and Y. Yaman, "A Hybrid Trailing Edge Control Surface Concept," in *DeMEASS VI Conference*, 2014.

[9]   P. Arslan, U. Kalkan, H. Tıraş, İ. O. Tunçöz, E. Gürses, M. Şahin, S. Özgen, Y. Yaman, and İ. O. Tunçöz, "Structural Analysis of an Unconventional Hybrid Control Surface of a Morphing Wing," *Proc. ICAST 2014*, pp. 1–12, 2014.

[10]   E. Gürses, İ. O. Tunçöz, Y. Yang, P. Arslan, U. Kalkan, H. Tıraş, M. Şahin, S. Özgen, and Y. Yaman, "Structural and aerodynamic analyses of a hybrid trailing edge control surface of a fully morphing wing," *J. Intell. Mater. Syst.*

Struct., 2016.

[11]   Y. Yaman, İ. Tunçöz, Y. Yang, P. Arslan, U. Kalkan, H. Tıraş, E. Gürses, M. Şahin, and S. Özgen, "Decamber Morphing Concepts by Using a Hybrid Trailing Edge Control Surface," *Aerospace*, vol. 2, no. 3, pp. 482–504, 2015.

[12]   T. Oktay, M. Konar, M. A. Mohamed, M. Aydin, F. Sal, M. Onay, and M. Soylak, "Autonomous Flight Performance Improvement of Load-Carrying Unmanned Aerial Vehicles by Active Morphing," vol. 10, no. 1, pp. 123–132, 2016.

[13]   P. Weiss, "Wings of Change – Shape-shifting aircraft may ply future skyways," *Science News*, pp. 359–367, 2003.

[14]   "1899 Write Kite." [Online]. Available: https://airandspace.si.edu/exhibitions/wright-brothers/online/fly/1899/kite.cfm. [Accessed: 02-Jan-2017].

[15]   T. Weisshaar, "Morphing aircraft technology-new shapes for aircraft design," *Multifunct. Struct. / Integr. Sensors Antennas*, pp. O1-1 – O1-20, 2006.

[16]   E. F. Gallaudet, "Aeroplane US 1145013 A." [Online]. Available: https://www.google.ch/patents/US1145013. [Accessed: 02-Jan-2017].

[17]   "Westland Pterodactyl IV." [Online]. Available: http://www.aviastar.org/air/england/west_pterodactyl4.php. [Accessed: 02-Jan-2017].

[18]   "Makhonine Mak.10." [Online]. Available: http://aviadejavu.ru/Site/Crafts/Craft30899.htm. [Accessed: 02-Jan-2017].

[19]   R. D. Love, "An Experimentally-Based Procedure for Aeroservoelastic Model Identification and Control Synthesis for Morphing and Flapping Wings," University of Florida, 2011.

[20]   "General Dynamics F-111A." [Online]. Available: http://www.nationalmuseum.af.mil/Upcoming/Photos.aspx?igphoto=2000541535. [Accessed: 02-Jan-2017].

[21]   S. Barbarino, O. Bilgen, R. M. Ajaj, M. I. Friswell, and D. J. Inman, "A Review of Morphing Aircraft," *J. Intell. Mater. Syst. Struct.*, vol. 22, no. 9, pp.

823–877, 2011.

[22] B. W. McCormik, *Aeronautics and Flight Mechanics*, no. 2. 1995.

[23] M. Khoshlahjeh, E. S. Bae, and F. Gandhi, "Helicopter Performance Improvement with Variable Chord Morphing Rotors," *36th Eur. Rotorcr. Forum*, p. 12, 2010.

[24] G. D. Miller, "Active Flexible Wing (AFW) Technology," 1988.

[25] A. Shelton, A. Tomar, J. Prasad, M. Smith, and N. Komerath, "Active Multiple Winglets for Improved Unmanned-Aerial-Vehicle Performance," *J. Aircr.*, vol. 43, no. 1, pp. 110–116, 2006.

[26] A. Y. N. Sofla, S. A. Meguid, K. T. Tan, and W. K. Yeo, "Shape morphing of aircraft wing: Status and challenges," *Mater. Des.*, vol. 31, no. 3, pp. 1284–1292, 2010.

[27] J. Spillman, "The Use of Variable Camber to Reduce Drag, Weight and Costs of Transport Aircraf," *Aeronaut. J.*, vol. 96, pp. 1–9, 1992.

[28] S. Gano and J. Renaud, "Optimized Unmanned Aerial Vehicle with Wing Morphing for Extended Range and Endurance," *9th AIAA/ISSMO Symp. Multidiscip. Anal. Optim.*, no. September, pp. 1–9, 2002.

[29] O. Tunçöz, "Design and Analysis of a Hybrid Trailing Edge Control Surface of a Fully Morphing Unmanned Aerial Vehicle Wing," 2015.

[30] M. Kintscher, M. Wiedemann, H. P. Monner, and T. Kühn, "Design of a Smart Leading Edge Device for Low Speed Wind Tunnel Tests in the European Project SADE," in *2nd EASN Workshop on Flight Physics and Propulsion*, 2012.

[31] "Cambridge University Materials Data Book." [Online]. Available: http://www-mdp.eng.cam.ac.uk/web/library/enginfo/cueddatabooks/materials.pdf. [Accessed: 02-Jan-2017].

[32] "Volz Servos." [Online]. Available: http://www.volz-servos.com/English/13mmClass/.

[33] "Ansys Workbench v14.0 Help." .

[34] Özlem O. "Validation of Structural Model of a Layered Structure with Elastomeric Components", 2010